CHALMERS
UNIVERSITY OF TECHNOLOGY

Functional Coatings through Axial Thermal Spraying of Powder-Suspension Feedstocks

New generation coatings through HVAF, APS and SPS Powder-Suspension Feedstocks

Master's thesis in Materials Chemistry

LOUISE ÖRNFELDT

DEPARTMENT OF INDUSTRIAL AND MATERIALS SCIENCE

CHALMERS UNIVERSITY OF TECHNOLOGY
Gothenburg, Sweden 2020
www.chalmers.se

DEPARTMENT OF INDUSTRIAL AND
MATERIALS SCIENCE
CHALMERS UNIVERSITY OF TECHNOLOGY
Gothenburg, Sweden
www.chalmers.se

Functional Coatings through Axial Thermal Spraying of Powder-Suspension Feedstocks

New generation coatings through HVAF, APS and SPS Powder-Suspension Feedstocks

Louise Örnfeldt

Göteborg, Sweden, 2020

Chalmers University of Technologies
SE- 41296 Göteborg
Sweden
www.chalmers.se

Functional Coatings through Axial Thermal Spraying of Powder-Suspension Feedstocks **-** *New generation coatings through HVAF, APS and SPS Powder-Suspension Feedstocks*

Louise Örnfeldt
Department of Industrial and Materials Science
Chalmers University of Technology

Abstract

Thermal spraying is a widespread method for applying coatings on top of a material to enhance, protect or add certain properties. As the standard has been to use one feedstock, often in powder form, an interesting area to explore is the effect of adding a supplementary feed during the coating process. Recent studies have also shown several advantages when axial loading has been used. Thus, this thesis has studied the influence of a simultaneously sprayed hybrid powder-suspension as well as premixing two different suspension feeds before spraying. Additionally, the influence of the spray distance on the coating and the effect of adding different amounts of hBN wt% in suspension feed have also been examined. HVAF and APS in an axial setup were the applied coating techniques with NiCr-Cr_3C_2, Cr_2O_3, water and hBN used as the feedstocks.

Results show that when spraying NiCr-Cr_3C_2 powder together with either a water or hBN suspension feed in a HVAF setting, more delaminations occur. There are also more particles with sharper edges embedded into the coating when a liquid feed has been added to the spraying process. Different Ni-Cr and Cr-C phases are produced in all of the NiCr-Cr_3C_2 containing coatings, a Ni-rich phase and a Cr-rich phase. All NiCr-Cr_3C_2 sprayed coatings show a homogeneous distribution of the phases with both fine and globular pores in the coating. Cracks in the different phases can also be seen, especially in the Cr-rich phase.

SEM imaging of Cr_2O_3 coatings sprayed together with a 5% hBN suspension in an APS setup reveals that varying the spray distance between 100 – 130 mm influences topography and microstructure of the coating. When a shorter distance is used, bulges on top of the coating are formed with a higher pore content underneath them as well as larger vertical or diagonal cracks in the coating. All Cr_2O_3 sprayed coatings show a homogeneous distribution with a laminar microstructure containing a mixture of fine and globular pores embedded into the coating. Moreover, all Cr_2O_3 coatings showed splats that they were prone to cracking. For most of the hBN sprayed coatings, only small amounts of hBN could be detected by SEM-EDS.

Keywords: Thermal spraying, coating, hybrid powder-suspension, HVAF, APS, SPS, NiCr-Cr_3C_2, Cr_2O_3, hBN.

Acknowledgements

First and foremost, I would like to thank my examiner and supervisor Prof. Uta Klement who have helped and guided me with her immense knowledge and support during this period. It has been a privilege to have been your student and to have worked with you. Thank you for your teachings and for taking care of me during this research!

I would also like to express my sincere gratitude to Dr. Yiming Yao and Ms. Adrianna Lozinko who have taught me the practical skills I have needed to execute this master´s thesis. Thank you for your patience and the opportunity to learn from you.

I also want to acknowledge Mr. Roger Sagdahl who have helped me with all sorts of practical problems that have shown up during the research. Thanks to Prof. Shrikant Joshi for the collaboration and your valuable impute during this master´s thesis.

Louise Örnfeldt
26th of May 2020, Göteborg

CONTENT PAGES

1. Background

Thermal spraying is a widespread coating technique used in the industry to apply coatings on various products in order to protect and enhance certain properties of a material. The name thermal spraying is often used as an overall term to describe a variety of coating techniques with similar process schemes. What mainly differentiates them are the in-flight conditions such as the process temperature, velocity, feedstock type and how the feed is introduced into the plasma jet. This gives the coatings their unique features that provides them with different properties. By altering the process technique and parameters, a large variety of coatings with dissimilar microstructures can be produced. [1]–[5]

As the spraying process primarily only affects the surface of the substrate, it can often be used to coat more sensitive materials while causing minimal damage to the product itself. It is a cost-effective and flexible technique that can apply coatings on complex structures while being able to use virtually any material as a feedstock as high temperature heating sources can be applied. This enables a large spectrum of different types of coatings and with diverse properties. However, since it is a line-of-sight technique, hidden areas or undercuts that are shielded by other structures are difficult to coat. [2]

In applications where there are rotating or moving parts involved, it is important to have materials with good tribological performances. Thermal spraying is a technique used to improve these properties where a coating is applied to reduce the wear losses and improve the friction coefficient of a component. [5], [6] Wear of a material primarily occurs when surfaces are in contact with each other, such as when a solid is in contact with either another solid or liquid. For solid-solid interactions, wear mainly happens due to adhesion and abrasion either during a sliding or rolling interaction, and the material properties play a big role in how quickly the component deteriorates and the removal of material. The friction coefficient for a material is also an important aspect to consider as this will have a large impact on the energy losses during a process and thus has a direct economic effect. [6]

By choosing appropriate constituents, together with a suitable surface treatment, properties such as wear loss and frictional coefficients can be improved. [6] NiCr-Cr_3C_2 is one material mixture with good wear and corrosion resistance that can be applied to a substrate to enhance the tribological performance. This is due to the inherent thermal stability and oxidation resistance properties of the constituents up to temperatures around 800 °C. The NiCr matrix acts as an alloy binder and has corrosion resisting qualities while Cr_3C_2 provides hardness and wear resistance to the material. [7] [8] Another established hard, wear resistant compound with good tribological performance is plasma sprayed Cr_2O_3. [9]

To improve the frictional properties of these hard materials, solid lubricants can be added into coatings. Hexagonal boron nitride (hBN) is one such lubricant where the structural formation of the hexagonal rings allows for sliding of the atomic planes. Their inherently weaker π-bonding makes it easier to glide along the atomic planes and can thus improve the friction properties. [10]

The phases existing in a given compound are an important aspect to take in consideration as they will affect the performance and characteristics of the compound. Depending on the element compositions, temperature and pressure, different phases will be more stable in a given alloy.

Knowing the characteristics of a given phase can help to determine suitable application areas for a material. [11] Figure 1 show the phase diagrams of Ni-Cr, Cr-C and Cr-O.

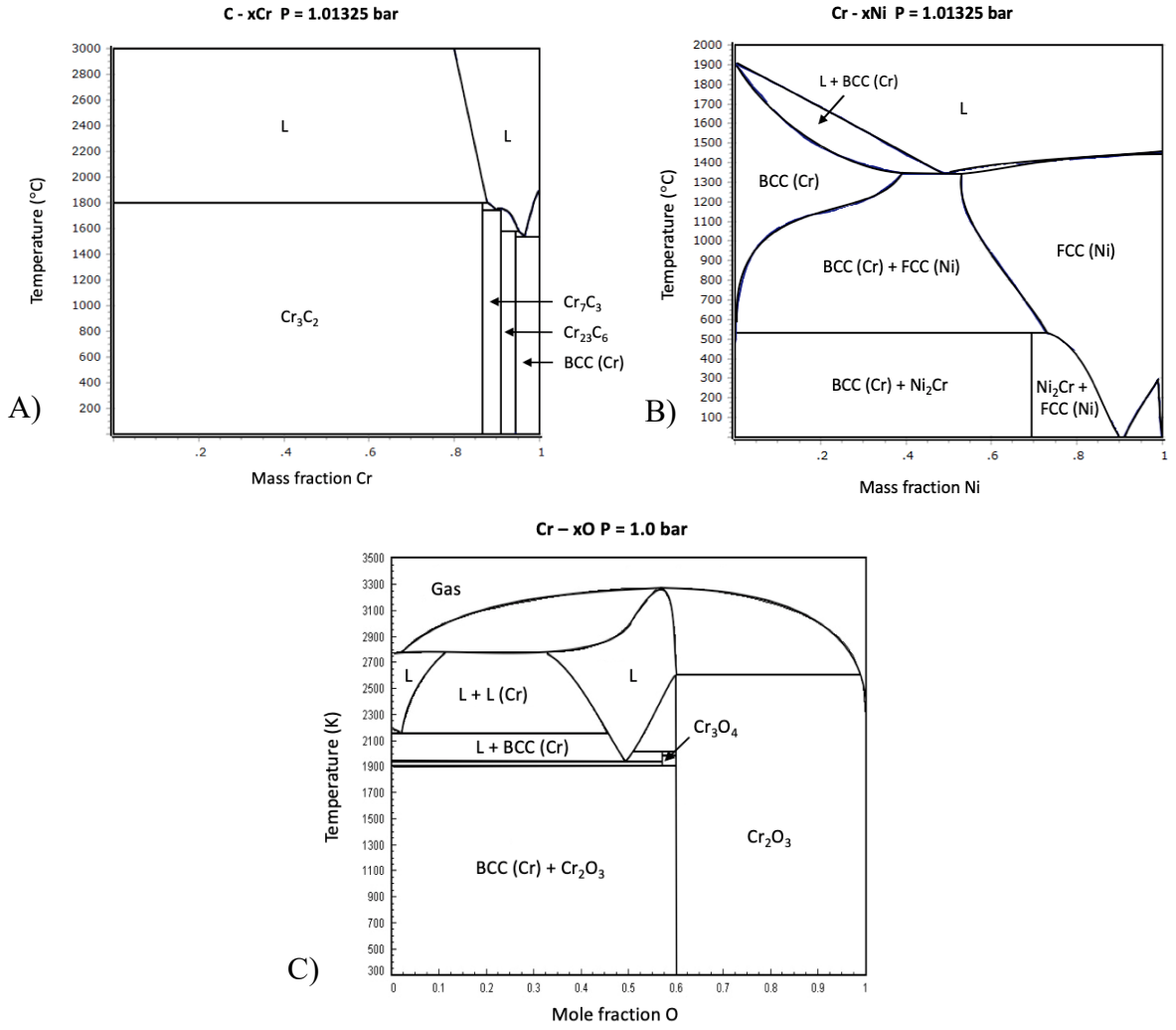

Figure 1. Binary phase diagrams of A) Cr-C, B) Ni-Cr and C) Cr-O. The Cr-C phase diagram is adapted from [12], [13]*, Ni-Cr from* [14]–[16] *and Cr-O from* [17], [18].

2. General outline of the thermal spraying process

The typical outline of a thermal spray process is that raw material, often in the form of powder, rod, wire or suspension, is guided into a spray gun. The feedstock is then subsequently accelerated and heated in a gas stream where the particles are melted into a molten or semi-molten state. Upon contact with the substrate, the molten droplets are flattened, forming splats that are bonded to the surface through rapid solidification and quenching. As more splats are deposited on the surface, a coating is built up that can have various properties depending on the morphology of the surface, microstructure, material composition and so forth. Figure 2 is a schematic illustration of the general thermal spraying process and important factors that influence the coating. [1]–[3]

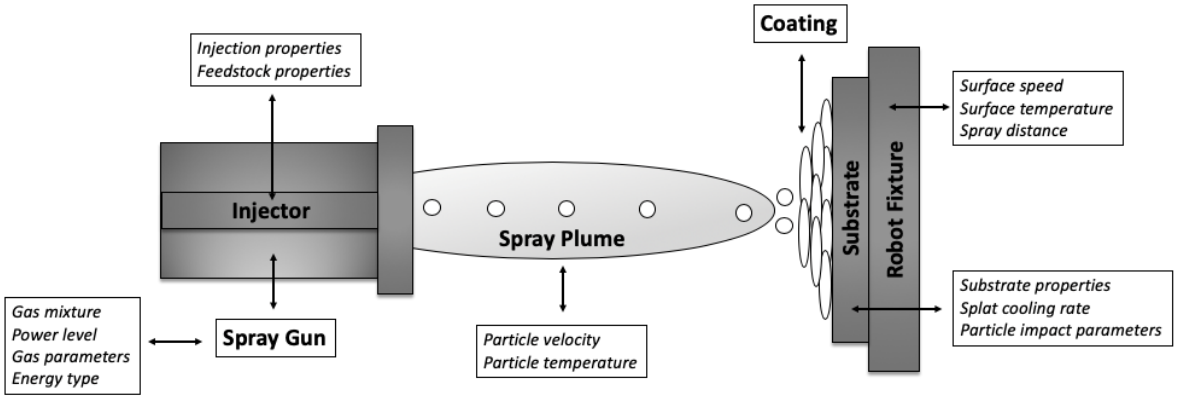

Figure 2. Schematic illustration of a general thermal spray process in an axial setup and corresponding important parameters. Adapted from A. Ganvir [2]

There are several factors that are important when adjusting the parameters in thermal spraying process and some of them are illustrated in Figure 2. [2]

The position and angle of the injection system into the plasma plume are factors that will influence the coating. The most common position of the injection system in industry is perpendicular to the spray plume. However, radial loading limits the size range of the feedstock. If the particle is too small, then the momentum of it will not be large enough to enter the spray plume and may instead also risk reentering the injection system that can cause possible clogging in the feed tube. If the particle is too large, however, it might instead pass through the heat source and be incorporated into the coating as unmolten particles due to poor heat treatment. [2]

The size difference of the feedstock particles will also contribute to a size distribution depending on the position of the injection system. This implicates that the route each given particle takes to the substrate surface is size dependent and will have a direct impact on the microstructure of the coating. Figure 3a is an illustration of the size dependence of the particles when using a radial injection. [2], [4]

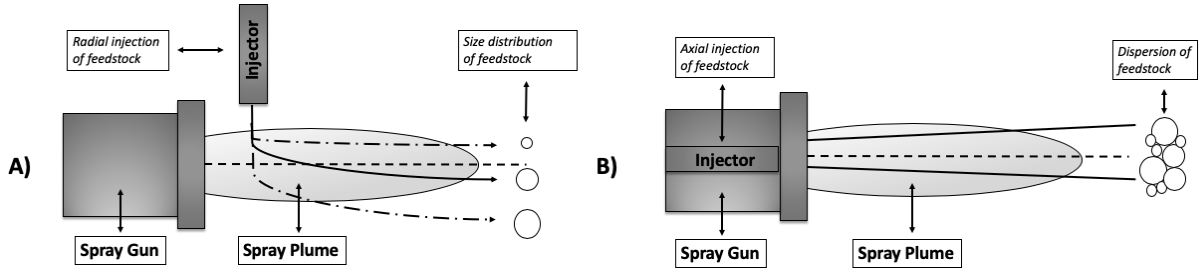

Figure 3. Injections systems and size distributions dependence of the feedstock. Adapted from A. Ganvir [2]

If an axial injection system is used instead, the trajectory of the particles due to the size is minimalized and there is a uniform treatment of the feed during the inflight time in the spray plume, as illustrated in Figure 3b. [2], [4] However, even if the axial injection system has a more uniform heat treatment, the size distribution of the powder particles is still something that should be considered as a to large disparity would still result in different degrees of heating and acceleration during the in-flight stage. [4]

The particle temperature and velocities will also affect the coating structure. In order to create a dense coating, it is generally a necessity to either have an efficiently high temperature or velocity. This would provide particles with an adequate momentum to fill possible defects in underlaying layers below, reduce porosity and improve the bonding between the splats. [4]

Three subvariants of the thermal spraying variants are high velocity air fuel (HVAF), atmospheric plasma spraying (APS) and suspension plasma spraying (SPS). The relative velocities and temperatures of these spraying processes are illustrated in Figure 4 and are discussed in more detail in the next sections. [3]

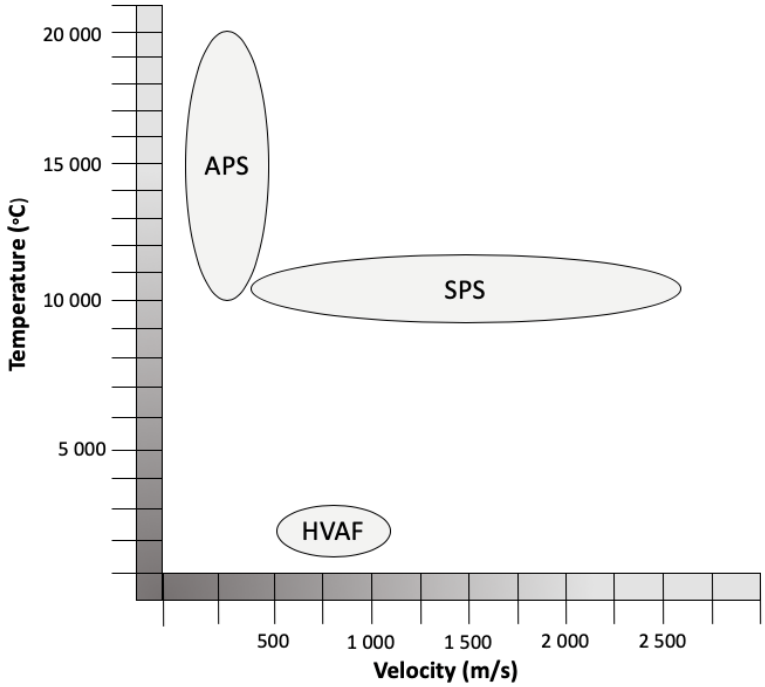

Figure 4. Schematic illustration of the relative velocities and temperatures of the APS and HVAF spraying procedures. Adapted from T. Hussain et al. [19]*, Bexxon* [20] *and* [21].

2.1 High velocity air fuel

High velocity air fuel is a thermal spraying technique that uses a flame as heating source which is produced by a mixture of compressed air and fuel gas. [2], [22] The fuel is typically a combination of hydrogen, propane and propylene and is introduced to the combustion chamber along with a powder feedstock. [2] An advantage with HVAF is the high particle speed which usually ranges between 500 – 1200 m/s. [20], [23] This enable the formation of relatively smooth, dense coatings with good adhesion. As compressed air is used as a combustion agent, higher powder feed rates are enabled together with a lower combustion temperature, often ranging around 1900 °C. [2], [22]–[25] The lower process temperature can reduce the oxidation of the feedstock material during the in-flight time. [2], [22], [24], [25] Lower particle temperatures also allow for a minimized decarburization together with a reduced formation of brittle structures in the coating. [22] Low heat input also has the benefit that potential phase transformations of the feed material are reduced during the in-flight time. [2]

As HVAF primarily produces coatings via high velocity, mechanical bonding is often the main bonding mechanism between particles and splats. This can affect certain properties of the coatings, such as the strength, liquid and gas permeability. [26]

2.2 Atmospheric plasma spraying

Atmospheric plasma spraying is the most commonly used thermal spraying process to apply coatings on substrates. This is due to its low production cost and flexible measures. [19], [27] The feedstock is normally solid coarse powder with a typical size range between 10 – 100 μm. These particles are then melted or semi-melted in the plasma plume, which can reach up to 20000 °C. The high temperature enables most materials as feedstocks. The particles can then accelerated to speeds around 200 – 300 m/s depending on the particle size distribution and then impact and spread onto the substrate in form of splats. [2], [19] Ideally, round disc splats are formed in contrast to star-shaped splats, illustrated in Figure 5. [2]

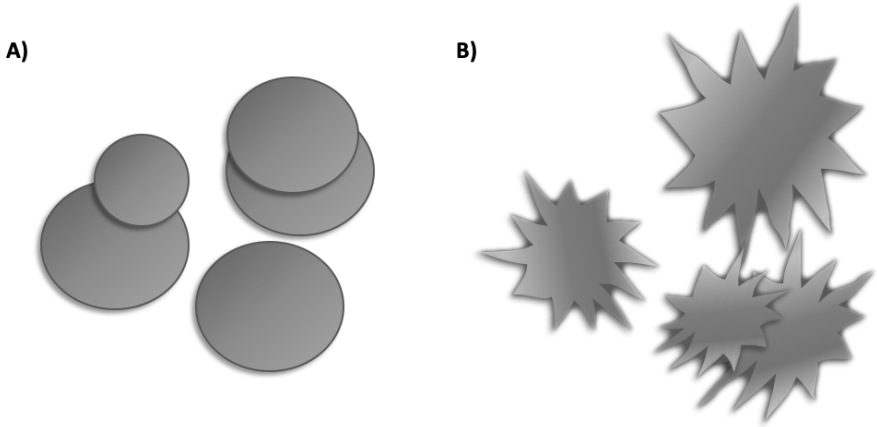

Figure 5. Shapes of splats. The left figure illustrates a disc shaped splat while the right shows starshaped splats.

The shape of the splats will influence the mechanical performance of the coating. Porosity, adhesion strength and roughness are some properties that are affected by the form of the splats and it will determine the bonding between the splats as well as to the substrate. The form in which the splats will take when solidifying depends on several process parameters such as the in-flight particle distribution, process temperature, velocity, degree of solidification and the

substrate material and its temperature. In contrast to disc shaped splats and their formation of dense coatings, starshaped splats may result in weak and porous coatings. This is due to the irregular forms that are created as the next splat hits the fingerlike structure that already lays underneath as the coating is built up. Applying coatings on cold surfaces often results in irregular splats while using a heated substrate instead will give more circular disc shaped splats. The critical temperature of the surface in which the splat shape is altered, however, depends on the substrate material. [5]

When the molten feed hits the surface, it solidifies and shrink. When APS coatings are generated, lamellar microstructures are often formed. [2], [27] These coatings are heterogeneous with numerous microstructural features such as fine pores, globular pores, delaminations and cracks. The microstructure of the coating will influence properties like the lifetime of the coating, thermal insulation, porosity, stiffness, thermal cyclic fatigue, thermal shock lifetime. [2]

A limitation with standard APS is the particle size of the powder feed. Fine powder feedstock, between 20 nm – 5 μm, does not have an adequate flowability or a significant enough momentum to enter higher velocity plasma streams. [2], [28] Fine powders can also have negative effects on both environmental and health aspects. [2] Some problems associated with fine powder feedstocks may be reduced by introducing them into a liquid feed instead, such as in SPS. This would also enhance the momentum and assist the particles with the insertion into the thermal jet core. [2], [19] The agglomeration may also be reduced both during storage and loading into APS equipment if a suspension is used. [2]

2.3 Suspension plasma spraying

An interesting feature with suspension plasma spraying is the possibility of generating columnar microstructures. This type of configuration can provide coatings with better cyclic lifetime, sintering resistance, low thermal conductivity and strain tolerance behavior compared to APS coatings. [29]–[31] This technique is based on the APS system where a liquid feed is used instead and injected into the plasma plume to generate a coating. [27] Via a liquid injection, the momentum of the particles is increased and thus aiding fine particles to enter the plasma plume. [2], [19]

The columnar arrangement that can be seen when employing SPS, is thought to arise from the generation of very fine droplets from the suspension. During the in-flight time, the suspension droplets are subjected to strong shear forces, thus causing fragmentation of the liquid feed that provides micron sized particles once the solvent has evaporated. [2], [4], [21], [29], [31] The microstructures are, however, strongly linked to the suspension properties such as the density, surface tension and viscosity. [31] The suspension itself is often created via mixing a solvent, often water or alcohol, together with nano- or micron-sized powder to provide a liquid feed. As there is a risk of agglomeration of the components when using a suspension, dispersants and mixing of the liquid feed can be utilized to prevent any clustering. [2], [27]

In SPS, the size of the particles plays a big role in governing the microstructure. As particles smaller than 5 μm have a relatively low momentum [2], [4], they are influenced by the drag of the plasma stream. Due to this, the particles will follow a curved path (with a trajectory parallel to the substrate) when getting close to the substrate, leading to shadowing effects. The shadowing effect is larger the smaller the particles. This is due to that the particles approach the substrate surface at a relatively shallow angle (trajectory parallel to the substrate) and, as a

consequence, different microstructures are generated. Figure 6 illustrates the shadowing effects and particle size dependence. [2], [4], [29]

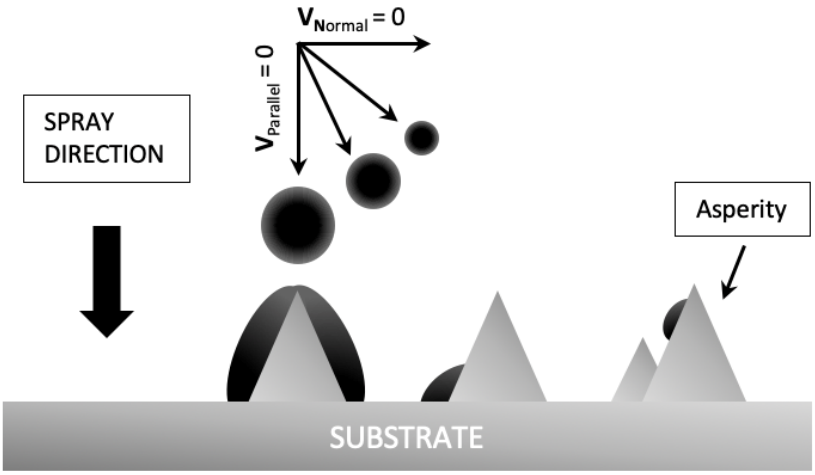

Figure 6. Shadowing effects of smaller particles during SPS. Adapted from A. Ganvir. [2]

Varying the size of the suspension droplet after the fragmentation is one factor that can affect the microstructure of a coating. In general, three distinctive appearances are often seen. With droplet sizes less than 1 μm, there is a large shadowing effect which can lead to columnar structures. However, if the droplet size is larger, between 1 – 5 μm, porosity bands perpendicular to the substrate can be also be incorporated within the columnar configurations and thus provide columnar structures with vertical cracks. As seen in Figure 6, the trajectory can be changed depending on the particle size. As a result, the particles are affected by the plasma drag at different levels leading to various microstructures. However, with a particle size above 5 μm, there is a direct impact instead as there is no, or minimal, effect of the plasma flow that alters the path onto the substrate surface. This would then in most cases result in a laminar or vertically cracked structure, similar to the coatings obtained by APS technique. [2], [4]

2.4 Hybrid powder-suspension

HVAF, APS and SPS create various fine microstructure coatings. However, using a hybrid powder-suspension feed during a spray process might induce new types of novel composite coatings with unique properties and characteristics. Therefore, the idea is to simultaneously spray with two axial injection feeds, both a suspension and a powder feedstock. By controlling and varying the feed compositions, new and unique microstructures may be attainable. [28]

In this thesis, axial hybrid powder-suspension thermal spraying was examined in a HVAF setup. The powder feedstock consisted of hard, wear resistant material while the suspension feedstock contained soft, lubricating constituents. The influence of spraying one premixed suspension feedstock containing both a hard, wear resistant component and soft, lubricating phase in a plasma spraying setting was also studied. The impact of spray distance and hBN content in the suspension feed will also be reviewed. The microstructure and element constituents will be the primarily features that will be examined in this report. In order to enable improved tribological properties, NiCr-Cr_3C_2 and Cr_2O_3 were chosen as hard and wear-resistant materials, while the soft and lubricating component was hBN.

The economic aspects will not be taken into consideration. Only axial HVAF and APS spraying will be examined, with a maximum of two feedstocks for the HVAF process. Thermal spraying

processing will be done as described in Table 1 and 2 in the experimental section below. The influence of the hBN content in the Cr_2O_3 suspension feed will be examined where the hBN content will vary between either 0, 5 or 10 wt%. Also, the effect of the spray distance (between 100 – 130 mm) will be studied for the Cr_2O_3 sprayed coatings. Other spray process parameters will remain constant.

2.5 Objectives

The objective of the master's thesis will be to investigate the microstructure and element composition of axial thermal sprayed coatings. Questions to be answered:

- Can a combination of a "coarse" hard material and a "fine" soft material be successfully co-sprayed to yield dense coatings?
- How does a suspension injection feed affect the microstructure of the coating when it is simultaneously sprayed with a powder feed?
- How are the morphology, microstructure and element distribution of the coatings affected by an additional, simultaneously sprayed feed during the coating process?
- How are the microstructure and topography affected by a varied spray distance?

3. Experimental

Thermal spraying was done at University West in Trollhättan. Table 1 and 2 lists the samples, the corresponding feedstock forms and feed rate used during the thermal spray process.

Table 1. The table lists the samples and their corresponding feedstock forms used during the HVAF and plasma spraying for each sample coating. If two feedstocks were used, ***Feedstock 1*** *is related to the first term in the sample name and* ***Feedstock 2*** *to the second term. The %hBN shows the wt% of hBN in the suspension.*

SAMPLE	FEEDSTOCK 1	FEEDSTOCK 2
NiCr-Cr_3C_2 (350 mm)	Powder	-
NiCr-Cr_3C_2 + water (350 mm)	Powder	Water
NiCr-Cr_3C_2 + 15% hBN (350 mm)	Powder	Suspension
Cr_2O_3 (120 mm)	Suspension	-
Cr_2O_3 + 5% hBN (100 mm)	Suspension	-
Cr_2O_3 + 5% hBN (110 mm)	Suspension	-
Cr_2O_3 + 5% hBN (130 mm)	Suspension	-
Cr_2O_3 + 10% hBN (130 mm)	Suspension	-

Table 2.The table lists the corresponding feed rates of the feedstocks for each sample shown in Table 1.

SAMPLE	FEEDSTOCK 1	FEEDSTOCK 2
NiCr-Cr_3C_2 (350 mm)	75 g/min	-
NiCr-Cr_3C_2 + water (350 mm)	75 g/min	50 ml/min
NiCr-Cr_3C_2 + 15% hBN (350 mm)	75 g/min	50 ml/min
Cr_2O_3 (120 mm)	40 ml/min	-
Cr_2O_3 + 5% hBN (100 mm)	40 ml/min	-
Cr_2O_3 + 5% hBN (110 mm)	40 ml/min	-
Cr_2O_3 + 5% hBN (130 mm)	40 ml/min	-
Cr_2O_3 + 10% hBN (130 mm)	40 ml/min	-

The NiCr-Cr_3C_2 containing coatings were HVAF sprayed while the Cr_2O_3 and Cr_2O_3 + hBN coatings were plasma sprayed. The feedstocks were simultaneously injected into the nozzle when two feeds were used during the spraying process, i.e. for the NiCr-Cr_3C_2 coatings with water and hBN, respectively, as according to Table 1 and 2. The liquid feeds for both NiCr-Cr_3C_2 + water and NiCr-Cr_3C_2 + hBN samples were sprayed at the same velocity.

For the Cr_2O_3 + hBN coatings, a Cr_2O_3 suspension (40 wt%) was mixed with a hBN suspension (5 or 10 wt%) and sprayed as a single feed. The spray distance was changed between 100 – 130 mm for the Cr_2O_3 + 5% hBN coatings in order to examine the influence of the stand-off distance. The wt% of the hBN suspension feed was also changed from 5% to 10% at a 130 mm injector distance from the substrate for the Cr_2O_3 + hBN coatings.

For all suspension solutions, water was used as the solvent.

3.1 Methods

Figure 7 illustrates a schematic workflow of the sample preparation and investigations done on each sample type. There were two different sample types, powder and thermal sprayed coatings.

On the thermal sprayed coatings, both the topography and cross section were investigated according to Figure 7.

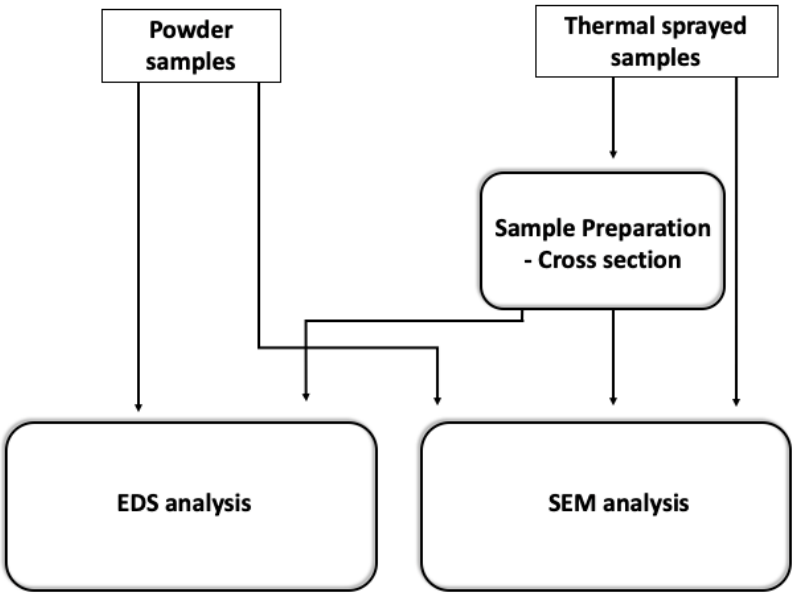

Figure 7. Workflow of the corresponding preparations and analyzes done on each sample type.

3.1.1 Sample preparation for the cross-section analysis using SEM and EDS

The cross sections of the samples were obtained via cutting of the corresponding coupons. They were then subsequently grinded to remove any sharp edges. Afterwards, the samples were molded into separate polyfit frames in a Struers CitoPress-20 mounting machine. The mounting step was initiated with a heating step at 180 °C under 250 bar pressure during 3.5 min followed by a cooling step for 1.5 min. Sharp edges on the polyfit frames were removed through another grinding step. Subsequently, the samples were polished in four steps in a Struers TegraPol-31/Tegraforce-5 polishing machine. In the first step, plane surfaces of the samples were attained via grinding the samples with SiC-paper 220# (60 s, 300 rpm, 30 N per sample). For the second step, DiaPro Allegro/Largo, a 9 µm suspension solution, together with a MD-Largo polishing plate were used (5 min, 150 rpm, 30 N per sample). In the third step, DiaPro Dac, a 3 µm suspension solution, together with a MD-Dac surface plate were used (5 min, 150 rpm, 30 N per sample). Lastly, DiaPro Nap, a 1 µm suspension solution, together with a MD-Nap plate were used as finishing step (60 s, 150 rpm, 20 N per sample). After each polishing step, the samples were cleaned and dried before proceeding to the following stage.

3.1.2 Scanning electron microscopy - Energy dispersive spectroscopy (SEM-EDS analysis)

SEM and EDS are used to evaluate topography, chemical contrasts and chemical composition of a specimen. When an electron beam is interacting with the sample, several types of radiations are generated. The generated radiations come from different depths of the sample. This is illustrated in the interaction volume in Fig. 8. The size of the interaction volume depends on the accelerating voltage of the incident electron beam and the mean atomic number of the sample. The interaction volume will be larger for a larger accelerating voltage, but smaller for

samples with a higher mean atomic number. The generated radiations are used for imaging and analysis. [32]

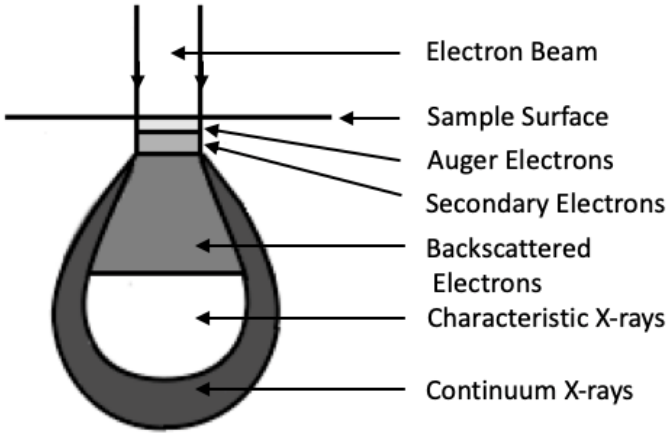

Figure 8. Radiations types and their origin in the interaction volume. Adapted from [32].

Secondary electrons (SE) can provide topographical contrast while backscattered electrons (BSE) allow for imaging the sample with chemical contrasts. A higher atomic number provides more backscattered electron and thus gives a brighter contrast image. [32]

For EDS analysis, compositional mapping and chemical spot analysis can be performed to obtain information of the element distribution and chemical composition in the material. Analyzing the emitted characteristic X-rays provides information about the components in the material and allows to determine the chemical composition in the analyzed spot or area. [32]

In this thesis, SEM was used to study the topographies and cross sections of the thermal sprayed coatings. The cross sections were also analyzed with EDS to provide chemical compositions and element distributions of the coated samples. The samples were cleaned with compressed air before examining them in the SEM. When powder samples were investigated, they were fixed on conductive tape. The instrument used for imaging and analyses was a Philips XL30 ESEM with an Oxford Instruments INCA x-sight.

4. Results and discussion

4.1 NiCr-Cr_3C_2 vs NiCr-Cr_3C_2 + water vs NiCr-Cr_3C_2 + hBN

Figure 9 illustrates SEM images of the surface topography of NiCr-Cr_3C_2, NiCr-Cr_3C_2 + water and NiCr-Cr_3C_2 + 15% hBN. Figure 9A, C and E show the samples at a lower scale using SE and 10b, d and f displays them at a higher magnitude using BSE.

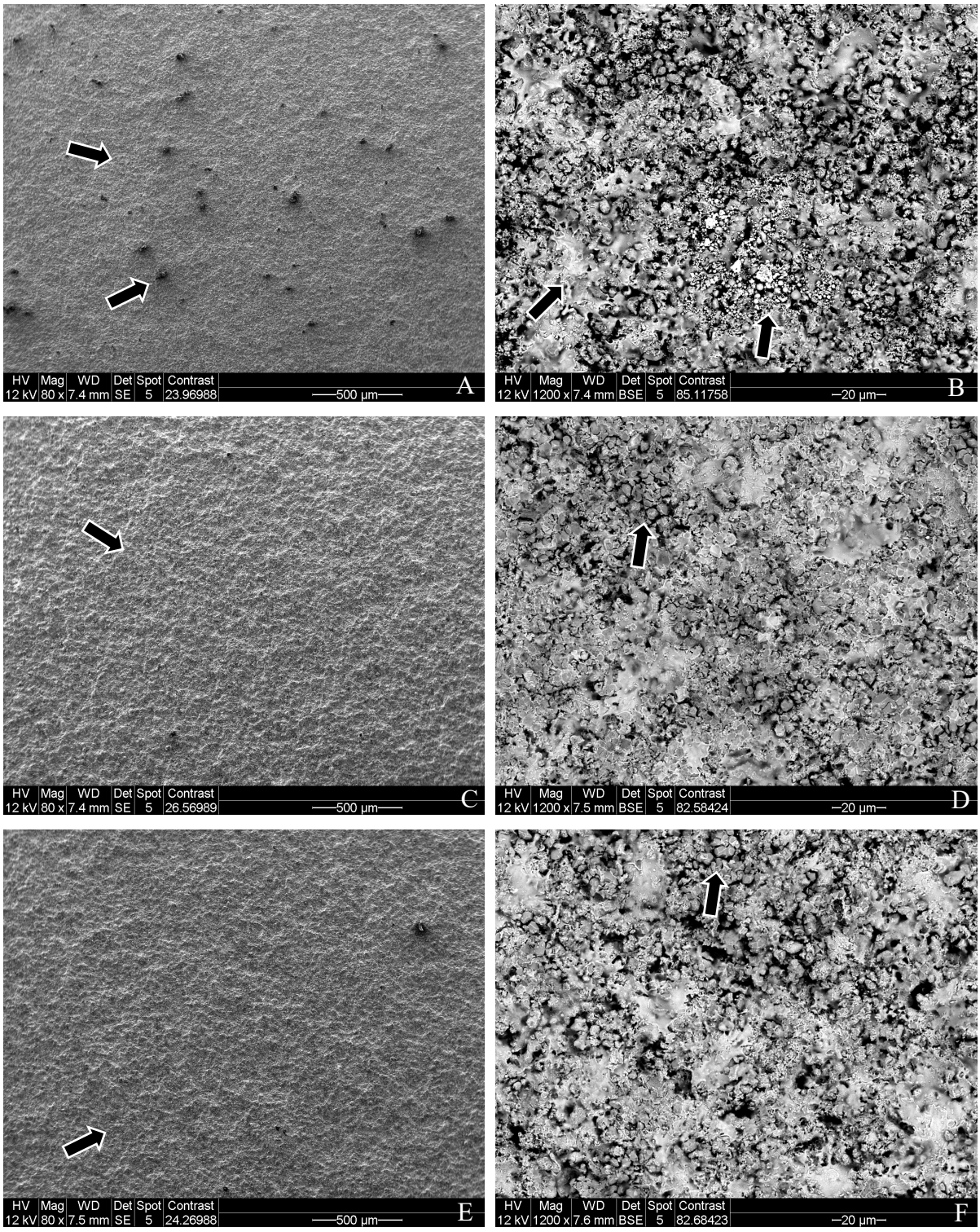

Figure 9. SE and BSE images with a lower and higher magnification displaying A-B) NiCr-Cr_3C_2, *C-D)* NiCr-Cr_3C_2 + water and E-F) NiCr-Cr_3C_2 + 15%hBN.

In general, all NiCr-Cr_3C_2 based coatings appear to have a fairly flat surface. However, the NiCr-Cr_3C_2 sample has numerous larger black spots that distinguish it from the other two coatings, illustrated by arrows in Figure 9A. Otherwise the sample has an overall smoother surface compared to the other NiCr-Cr_3C_2 + water and NiCr-Cr_3C_2 + hBN coatings that appear to be rougher, see arrows in Figure 9C and E.

At higher magnification, more dissimilarities can be seen. The common appearance for all coatings is that they contain splats of various sizes and shapes together with fragments of particle clusters. In the NiCr-Cr_3C_2 coating, there are regions with smaller particles, either more grouped together or spread out over the coating, see arrows in Figure 11B. In the NiCr-Cr_3C_2 + water coating, there seems to be more splats present on the surface as well as more rougher particles as compared to the NiCr-Cr_3C_2 coating. A similar trend can also be observed in the NiCr-Cr_3C_2 + hBN sample. In general, when an additional liquid feed has been used during the spraying process, there seems to be a higher fraction of particles with shaper edges embedded into the coating, which are possibly fragments of unmolten particles, see arrows in Figure 9D and F. This is especially apparent for the NiCr-Cr_3C_2 + water coating and is illustrated in more detail in Figure 10 where the coatings are displayed at higher magnification.

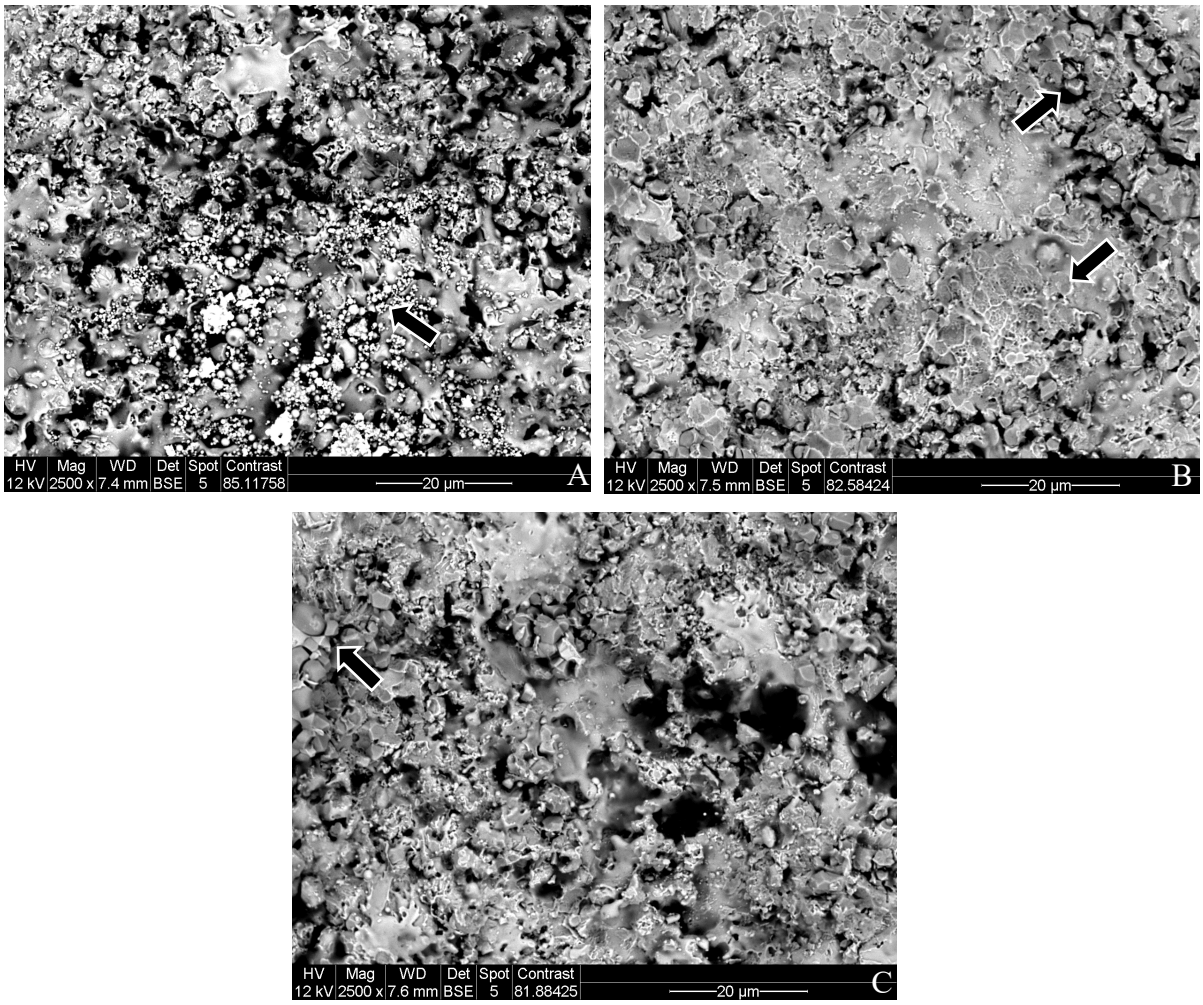

Figure 10. BSE images taken at higher magnification on A) NiCr-Cr_3C_2, B) NiCr-Cr_3C_2 + water and C) NiCr-Cr_3C_2 + 15%hBN.

Figure 11 shows the NiCr-Cr_3C_2 particles in the powder feedstock as well as the NiCr-Cr_3C_2 + water and NiCr-Cr_3C_2 + hBN coatings at higher magnifications. Size measurements of various features on both the powder and coating particles are illustrated in Figure 11.

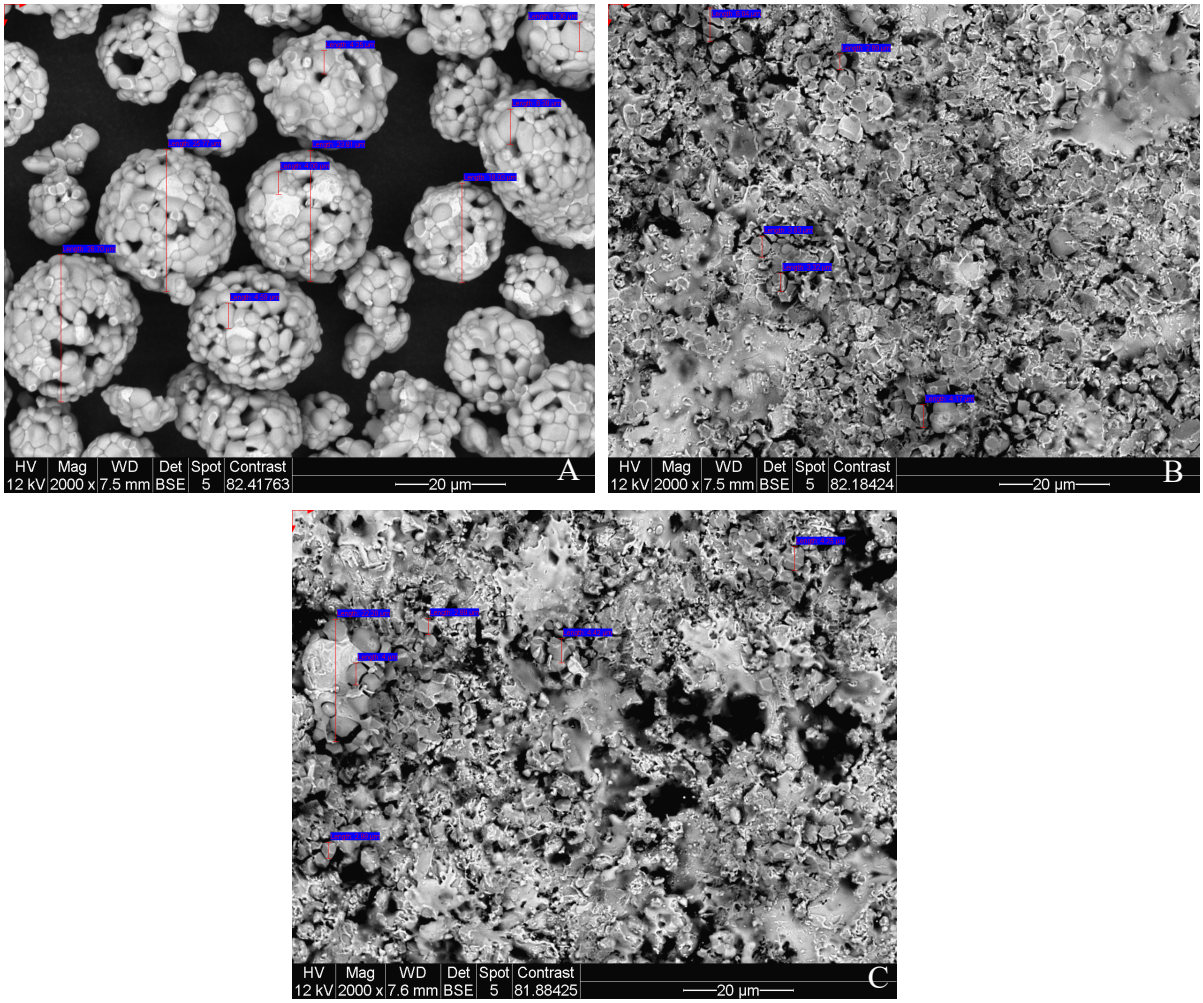

Figure 11. BSE images with size measurements of A) NiCr-Cr_3C_2 powder and B) NiCr-Cr_3C_2 + water and C) NiCr-Cr_3C_2 + 15%hBN.

The rougher particles seen in Figure 10B and C, illustrated by arrows, and Figure 11B and C have a similar appearance as the initial NiCr-Cr_3C_2 powder seen in Figure 11A. These types of particles with sharp edges are not as apparent in the NiCr-Cr_3C_2 coating and thus indicate that the additional liquid feed influences the state of particles. A possible reason for the unmolten particles and rougher appearance might be due to that an additional liquid feed during the spraying processes affects the in-flight conditions. More energy is required to remove the excess liquid and can thus influence the NiCr-Cr_3C_2 powder feed and, consequently, generate more unmolten or semi-molten particles embedded into the coating. Size measurements done on the powder particles and different components on it also show comparable size ranges to that of the rougher particles seen in the hybrid sprayed coatings. These measurements support the idea of semi- or unmolten particles embedded into the coating.

An additional finding in the NiCr-Cr_3C_2 + water coating is the presence of areas of "grouped cavities" on top of some splats as seen in Figure 10B, illustrated by arrows. This aspect has not been as apparent in the other coatings. More illustrative images of the surface topography for all NiCr-Cr_3C_2 containing coatings can be found in Appendix 1.1, 2.1 and 3.1.

Figure 12 displays the cross sections of the NiCr-Cr_3C_2, NiCr-Cr_3C_2 + water and NiCr-Cr_3C_2 + hBN coatings where Figure 12A, C and E show that cross section at a lower magnification, and Figure 13B, D and F illustrate the cross sections at higher magnification.

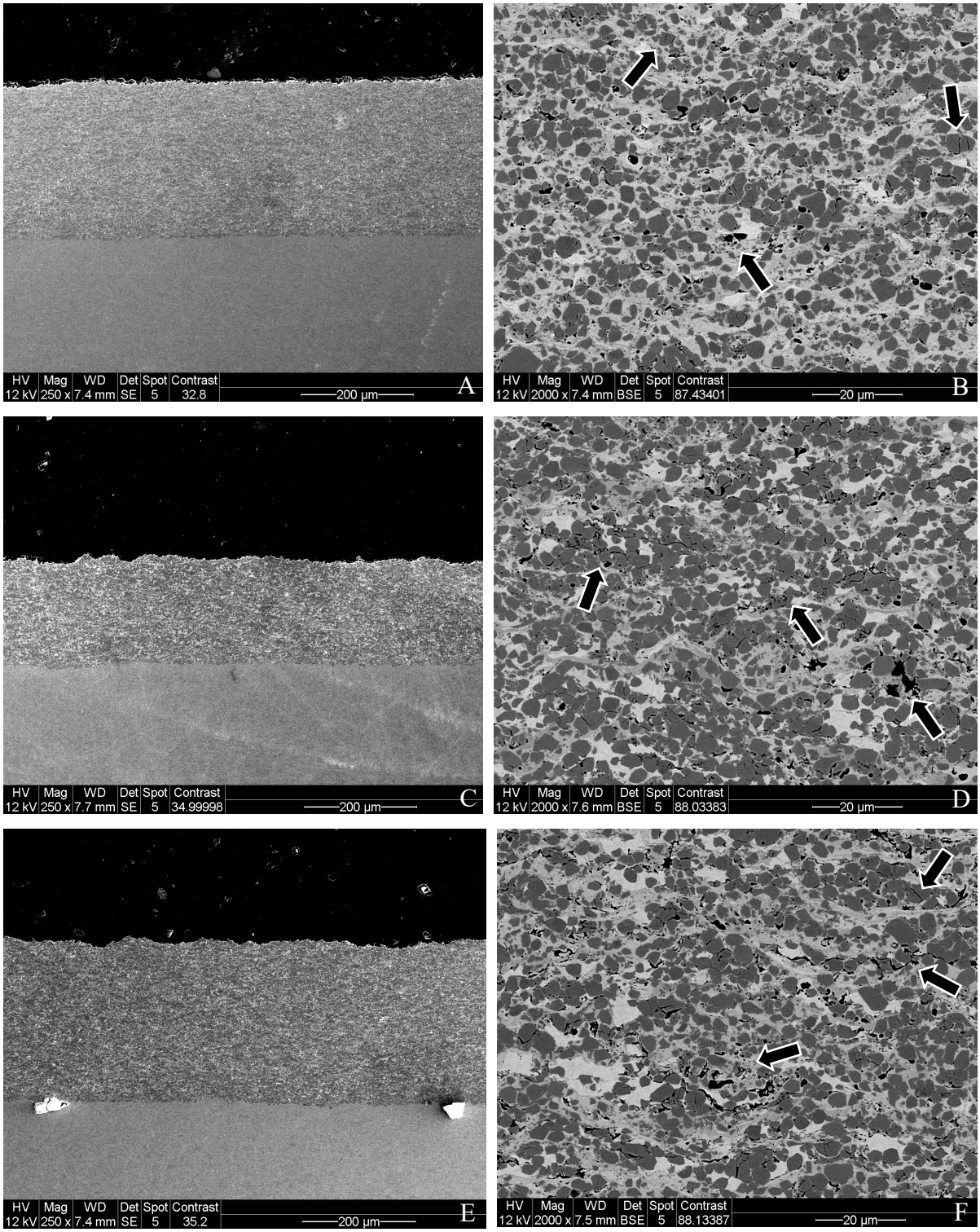

Figure 12. SEM (SE and BSE) of the cross sections at lower and higher magnification on A-B) NiCr-Cr_3C_2, C-D) NiCr-Cr_3C_2 + water and E-F) NiCr-Cr_3C_2 + hBN. Porosity, cracks and delaminations are seen in the coatings, illustated from arrows.

The SEM images at lower magnification show that all coatings appear to be uniform and dense. No cracks are observed throughout the coatings. The thickness of the NiCr-Cr_3C_2 + water coating is, however, thinner in comparison to the other two coatings.

From the images taken at a higher magnification, at least two distinct phases can be observed by compositional contrast. The microstructures of the coatings appear to be very similar. They all display tendencies for having both fine and globular pores as well as smaller cracks in the different phases, especially the lighter phase, as illustrated by the arrows in Figure 12. There is, however, a clear tendency for increased delaminations when an additional liquid feed has been used during the spraying process (i.e. NiCr-Cr_3C_2 + water and NiCr-Cr_3C_2 + hBN), illustrated by arrows in Figure 12 D and F. However, they still form relative dense coatings.

The cross section at the surface of the corresponding coatings are displayed in Figure 13.

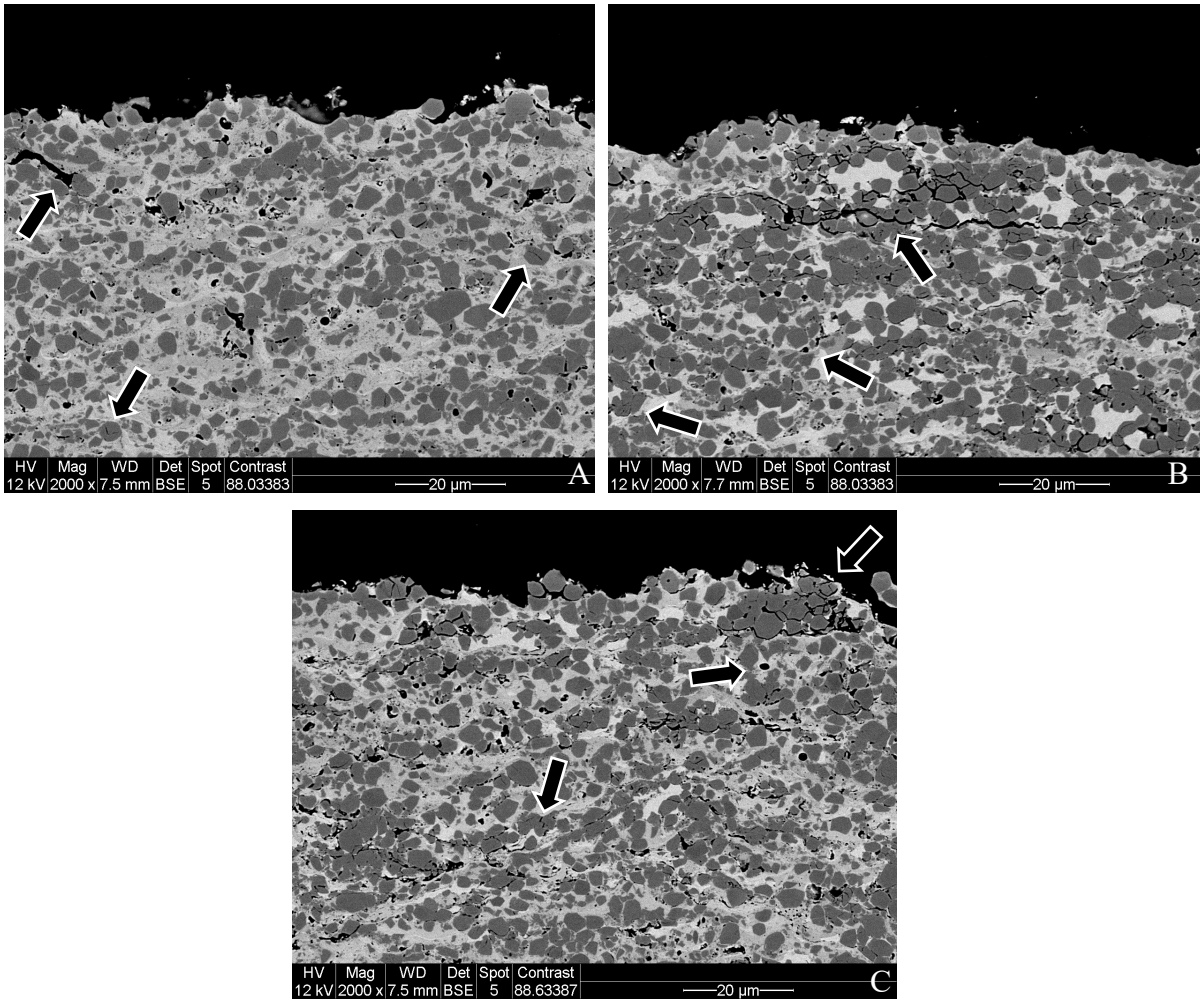

Figure 13. SEM images (BSE) of the cross sections close to the surface and at a higher magnification on A) NiCr-Cr_3C_2, B) NiCr-Cr_3C_2 + water and C) NiCr-Cr_3C_2 + hBN.

The same observation of fine and globular pores as well as minor cracks in some of the phases are also seen close to the surface of the coatings. Both NiCr-Cr_3C_2 + water and NiCr-Cr_3C_2 + hBN also show delaminations close to the surface, see arrows. Overall, the microstructures in the middle of the coatings are similar to the microstructure close to the surface. More images of the cross sections can be found in Appendix 1.2, 2.2 and 3.2.

Figure 14, 15 and 16 show EDS mapping done on the cross sections of NiCr-Cr_3C_2, NiCr-Cr_3C_2 + water and NiCr-Cr_3C_2 + hBN coatings. The figures display SE images of the analyzed areas and the Cr and Ni distributions in the corresponding areas. More images of the EDS mapping can be found in Appendix 1.3, 2.3 and 3.3.

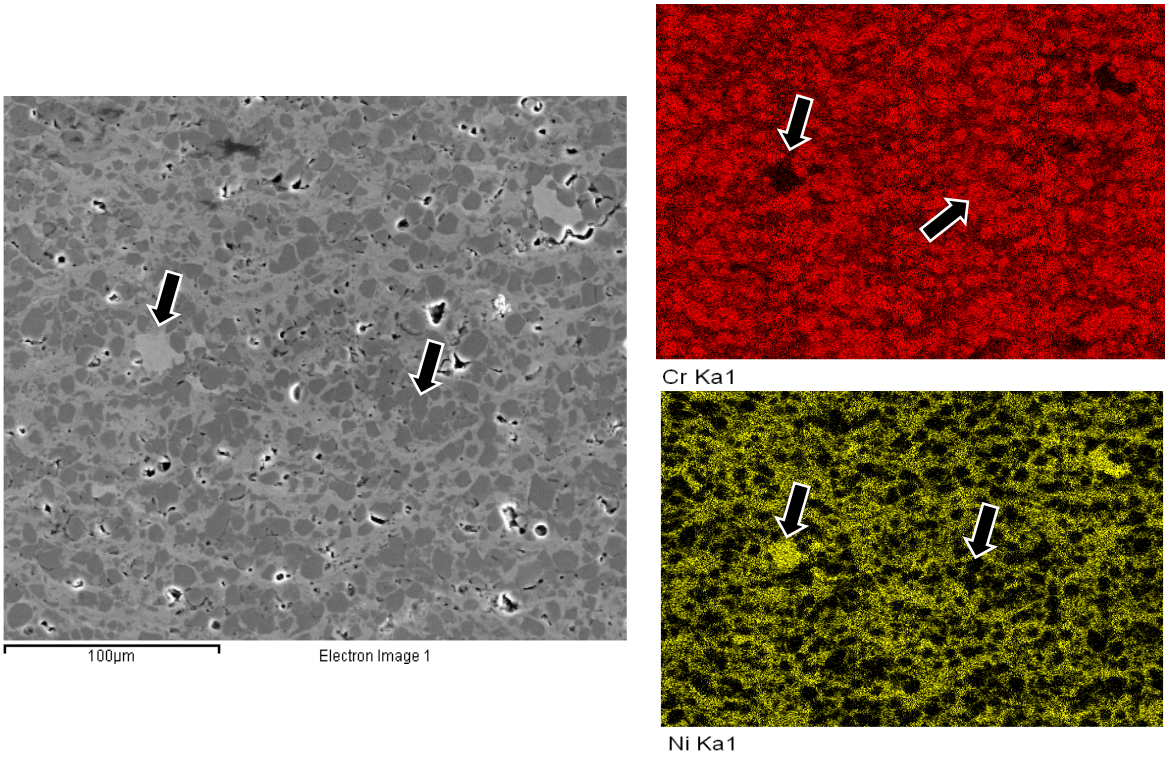

Figure 14. SE images and EDS mapping on the cross section of NiCr-Cr_3C_2 showing the Cr and Ni element distribution across the analyzed area.

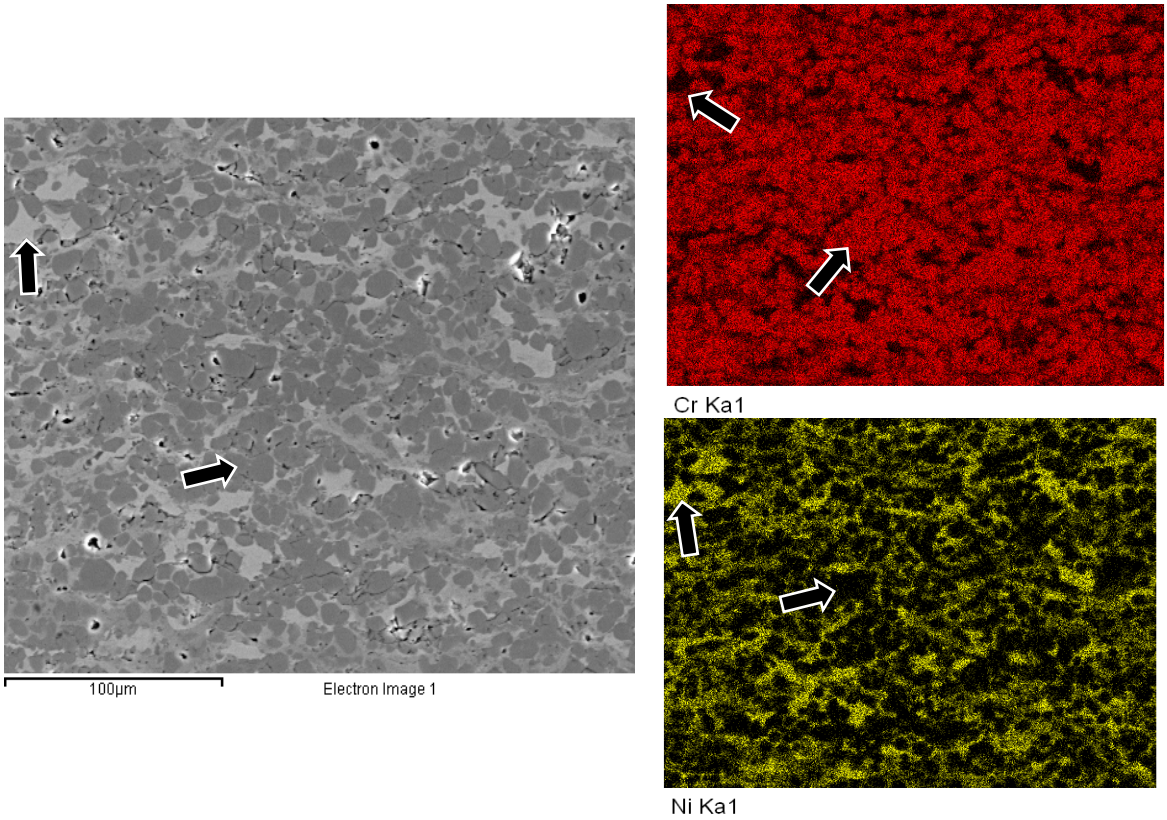

Figure 15. SE images and EDS mapping on the cross section of NiCr-Cr_3C_2 + water showing the Cr and Ni element distribution across the analyzed area.

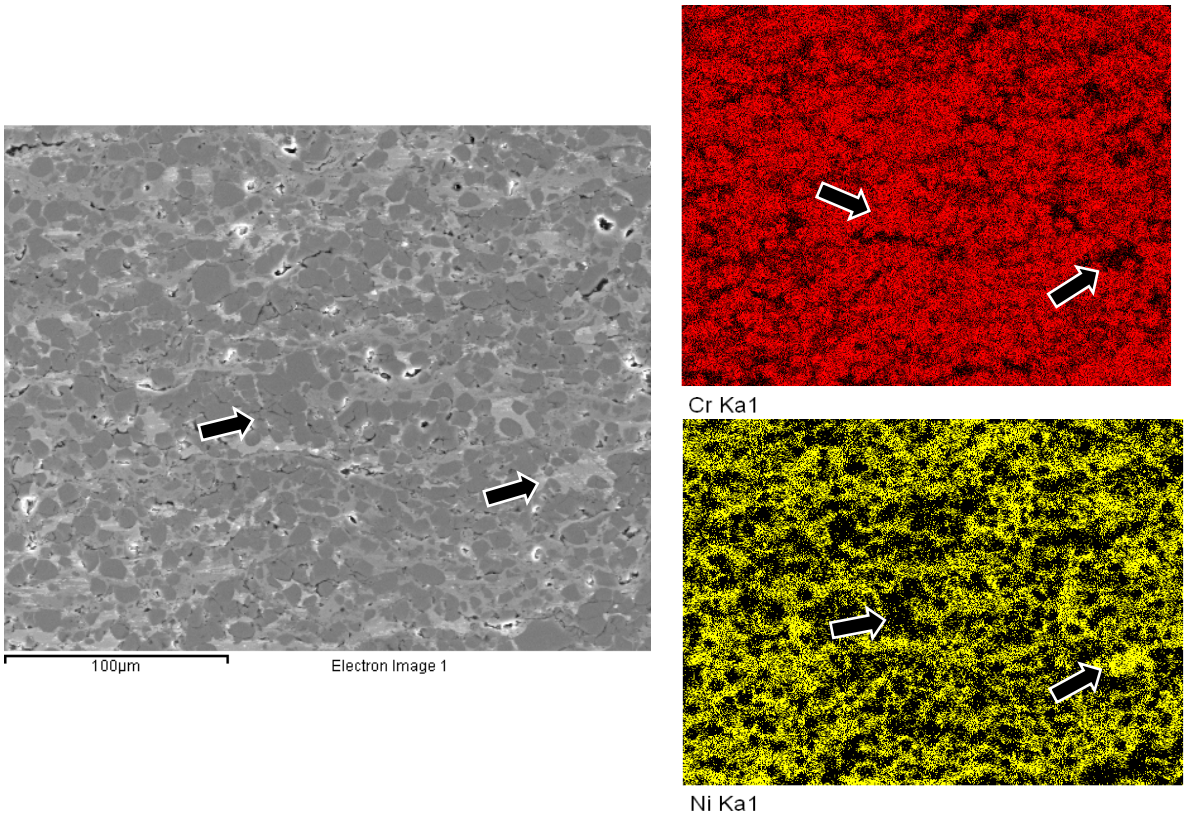

Figure 16. SE images and EDS mapping on the cross section of NiCr-Cr_3C_2 + 15%hBN showing the Cr and Ni element distribution across the analyzed area.

From the EDS mappings, distinct Ni rich and Ni deficient areas are seen, illustrated by arrows. Comparing the Ni mappings to the Cr and SE images indicates the presence of Ni and Cr rich phases. Contrast differences, illustrated by arrows, also suggests the existence of two different Ni phases with different Ni content.

EDS spot analysis on the measured areas indicates the presence of Cr-C and Ni-Cr phases in the coatings. Table 3 illustrates the approximate ranges of the Ni, Cr, C and O elements found in the different Ni-Cr and Cr-C phases during EDS spot analysis.

Table 3. Element compositions and approximate ranges of the different NiCr and CrC phases found in the NiCr-Cr_3C_2, NiCr-Cr_3C_2 + water and NiCr-Cr_3C_2 + hBN coatings. Possible outliers from the norm ranges have not been included.

	NiCr-Cr_3C_2			**NiCr-Cr_3C_2 + water**		**NiCr-Cr_3C_2 + hBN**		
ELEMENT	*Ni-Cr Phase 1*	*Ni-Cr Phase 2*	*Cr-C*	*Ni-Cr*	*Cr-C*	*Ni-Cr Phase 1*	*Ni-Cr Phase 2*	*Cr-C*
Ni (wt%)	49 - 60	83 – 84		82 – 86		47 – 65	74 – 81	
Cr (wt%)	32 - 41	13 - 14	81 – 84	13 – 17	83 - 84	22 – 36	12 - 13	70 – 74
C (wt%)	5 – 7	3	13 – 14	0	14	11 – 13	5 – 7	24 – 26
O (wt%)	2 – 4	1	2 – 3	1	2 – 3	2 – 6	1 – 2	0 – 5

Cross reference to binary Ni-Cr diagrams suggest two different Ni-Cr phases are likely to be present in the coatings. According to the phase diagram, between approximately 0 - 70 wt% Ni, a $CrNi_2$ + BCC (Cr) phase is expected to be present and for Ni contents of 70 – 90 wt%, the $CrNi_2$ + FCC (Ni) phase should exist. This indicates that both NiCr-Cr_3C_2 and NiCr-Cr_3C_2 + hBN contain two different NiCr phases in the coatings as they both have a Ni content which ranges between 50 – 85 wt% together with 10 – 40 wt% Cr. These phases can also be observed in the SEM and EDS images in Figure 14, 15 and 16, where a contrast difference between the two Ni-Cr phases can be observed, one brighter than the other. For the NiCr-Cr_3C_2 + water sample, most EDS spectra indicate a higher Ni content and thus making the $CrNi_2$ + FCC (Ni) phase more probable. A few spectra show a lower Ni content, around 39 and 54 Ni wt%, that might indicate that there are two different NiCr phases present in this coating as well, but more analyzes have to be performed to confirm this.

For the Cr-C phase, cross reference with corresponding phase diagram indicates that up to approximately 85 wt% Cr, there is only Cr_3C_2 present. This thus suggests that Cr_3C_2 is the primary Cr-C phase in the NiCr-Cr_3C_2 coatings.

There are a few EDS spectra that have deviating compositions for Ni and Cr. This, however, might be due to the interaction volume and that information from another phase was included, thus providing mixed results of the phases. EDS spot analysis results can be found in Appendix 1.4, 2.4 and 3.4.

To examine the presence of hBN in NiCr-Cr_3C_2 + hBN coating, EDS analyses were also performed with 10 keV and lower spot size (in this case spot size 4). However, despite using these settings, it was still difficult to detect hBN in the cross section sample. Results can be found in Appendix 3.5

4.2 Cr_2O_3 + 5% hBN (100 – 130 mm) vs Cr_2O_3 (120 mm)

Figure 17 displays the SEM images of the surface topographies of Cr_2O_3 + 5% hBN samples sprayed at a 100 – 130 mm spray distance together with Cr_2O_3 suspension sample sprayed at 120 mm. Figures 15A, C, E and G show the surface of the samples at lower magnification in topographical contrast (SE images), while 15B, D, F and H show the coatings at a higher magnification and in compositional contrast (BSE images).

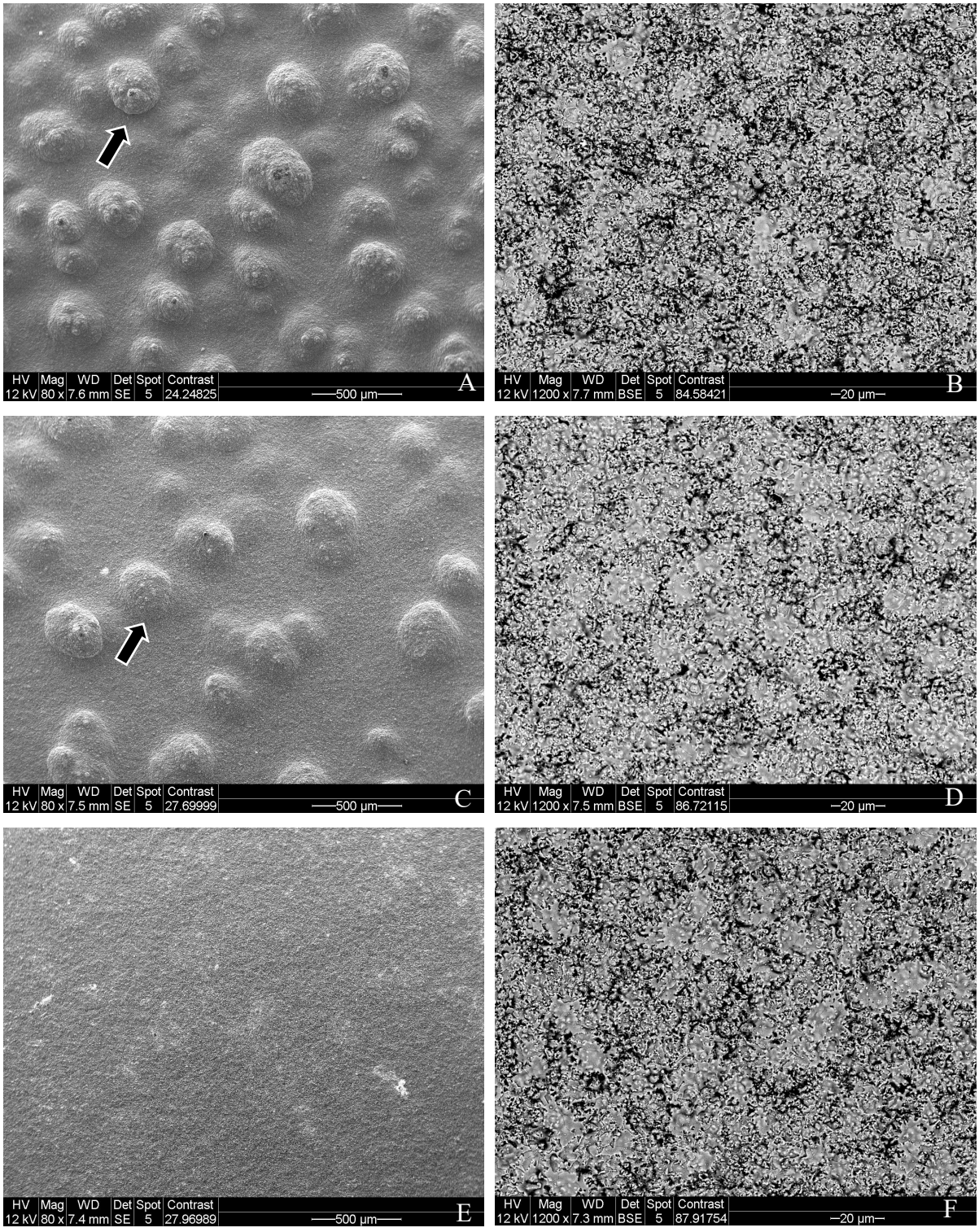

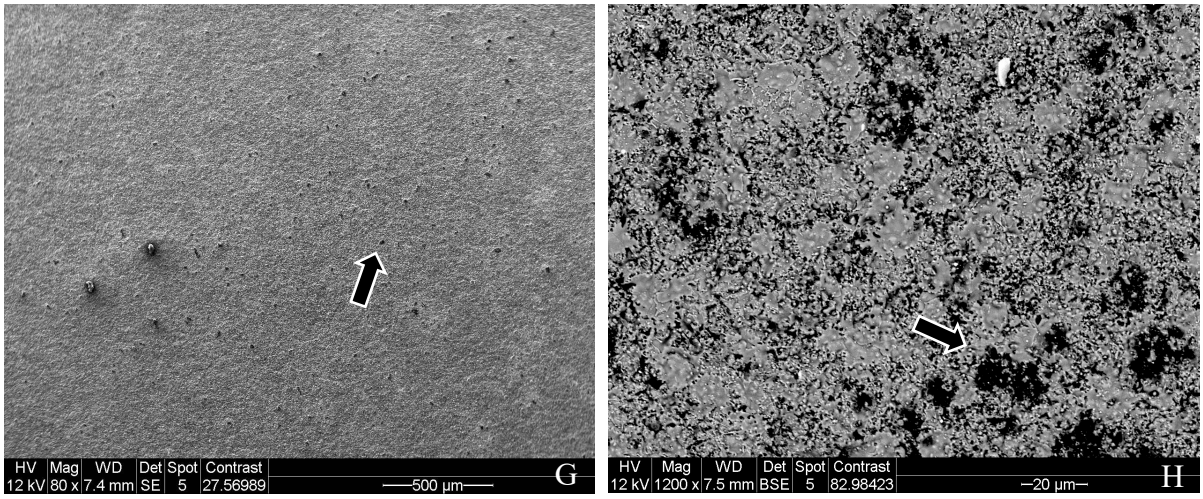

Figure 17. SEM images of the surface morphology at a lower and higher magnification on Cr_2O_3 + 5% hBN at A-B) 100 mm C-D) 110 mm E-F) 130 mm stand of distance and G-F) Cr_2O_3 (120 mm).

From comparing the surface structures at lower magnification, one can see that the Cr_2O_3 + 5% hBN samples sprayed at a 100 – 110 mm injection distance exhibit larger bulges on the surface, illustrated by arrows in Figure 17A and C, while at a 130 mm injection distance, the bulges have vanished. The same flat appearance is also seen for the Cr_2O_3 coating sprayed at a 120 mm spray distance. A higher number of bulges is also observed on the 100 mm sample compared to that of the 110 mm coating. Thus, the spray distance has an impact on the surface morphology where a shorter spray distance tends to produce a surface topography consisting of more bulges.

Looking at the images taken at higher magnification, the surface appearance for the Cr_2O_3 + 5% hBN samples look very similar no matter the spray distance. A mixture of splats of various sizes are seen in all of the samples as seen in Figure 17. Comparison between these coatings to the Cr_2O_3 sample show that the Cr_2O_3 coating has more and smaller darker spots on the surface. They can be observed at both lower and higher magnification, illustrated by arrows in Figure 17G and H. More images can be seen in Appendix 4.1, 5.1, 6.1 and 7.1.

Figure 18 displays the surfaces of the samples at a higher magnification.

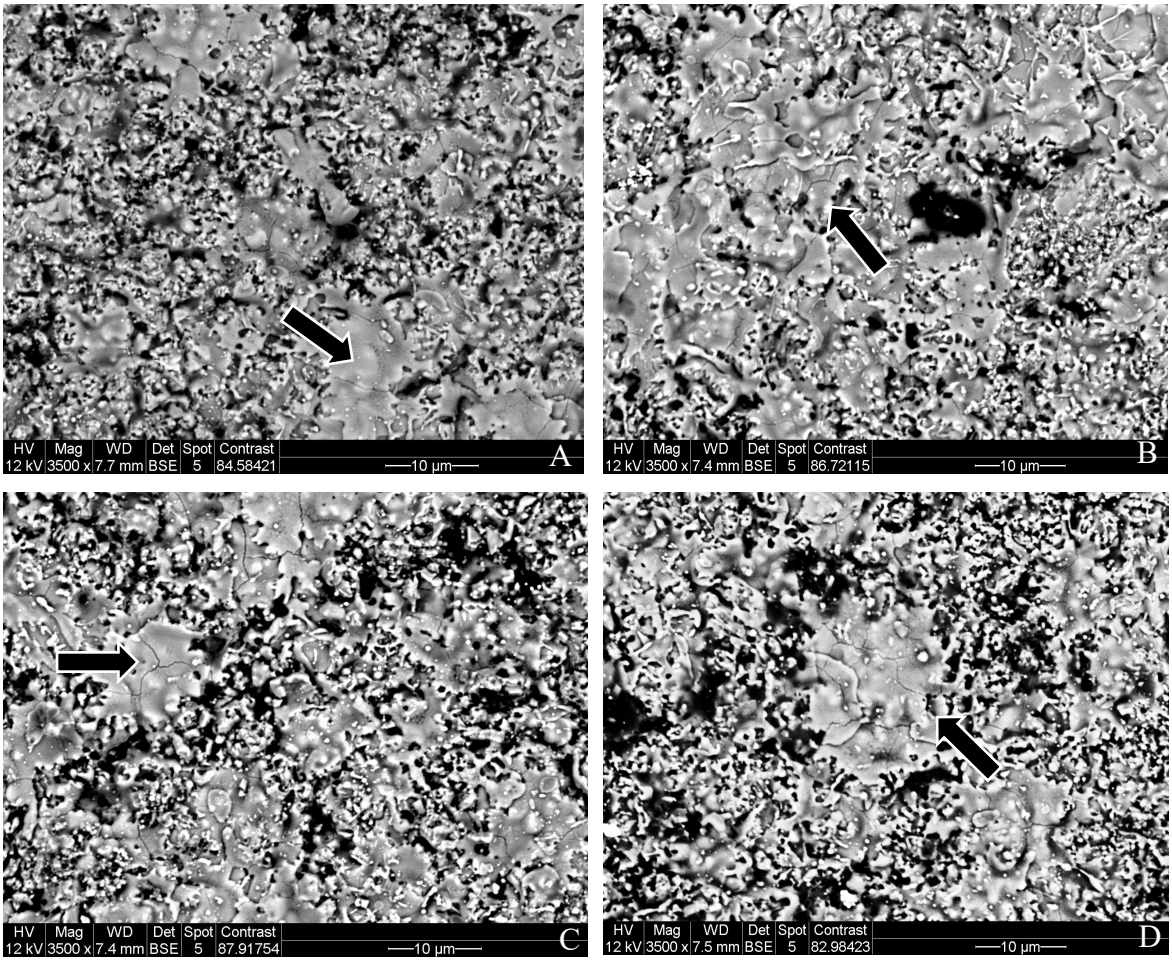

Figure 18. SEM images of the surface of Cr_2O_3 + 5% hBN sprayed with A) 100 mm B) 110 mm and C) 130 mm spray distance, and D) Cr_2O_3 (120 mm).

Overall, the appearance of all coatings at higher magnification is very similar. They consist of splats in various sizes, some with irregular shapes, together with small particle clusters. All coatings exhibit cracks in the splats, illustrated by arrows.

Figure 19 shows the cross sections of the Cr_2O_3 and Cr_2O_3 + 5% hBN coatings. The images on the left side (A, C, E, and G) show the cross sections at a lower magnification while on the right side (B, D, F, H), higher magnification images of the coatings are provided.

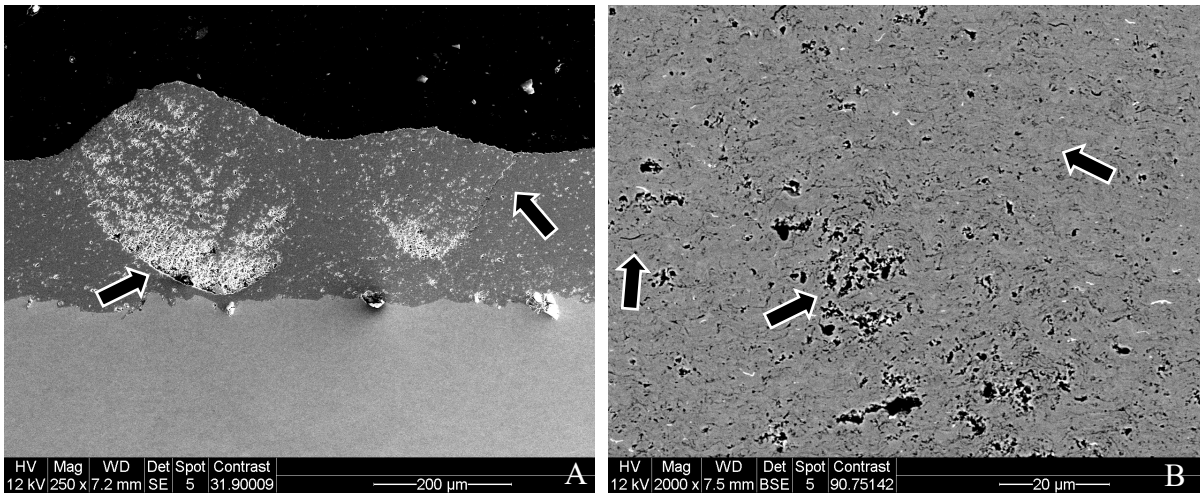

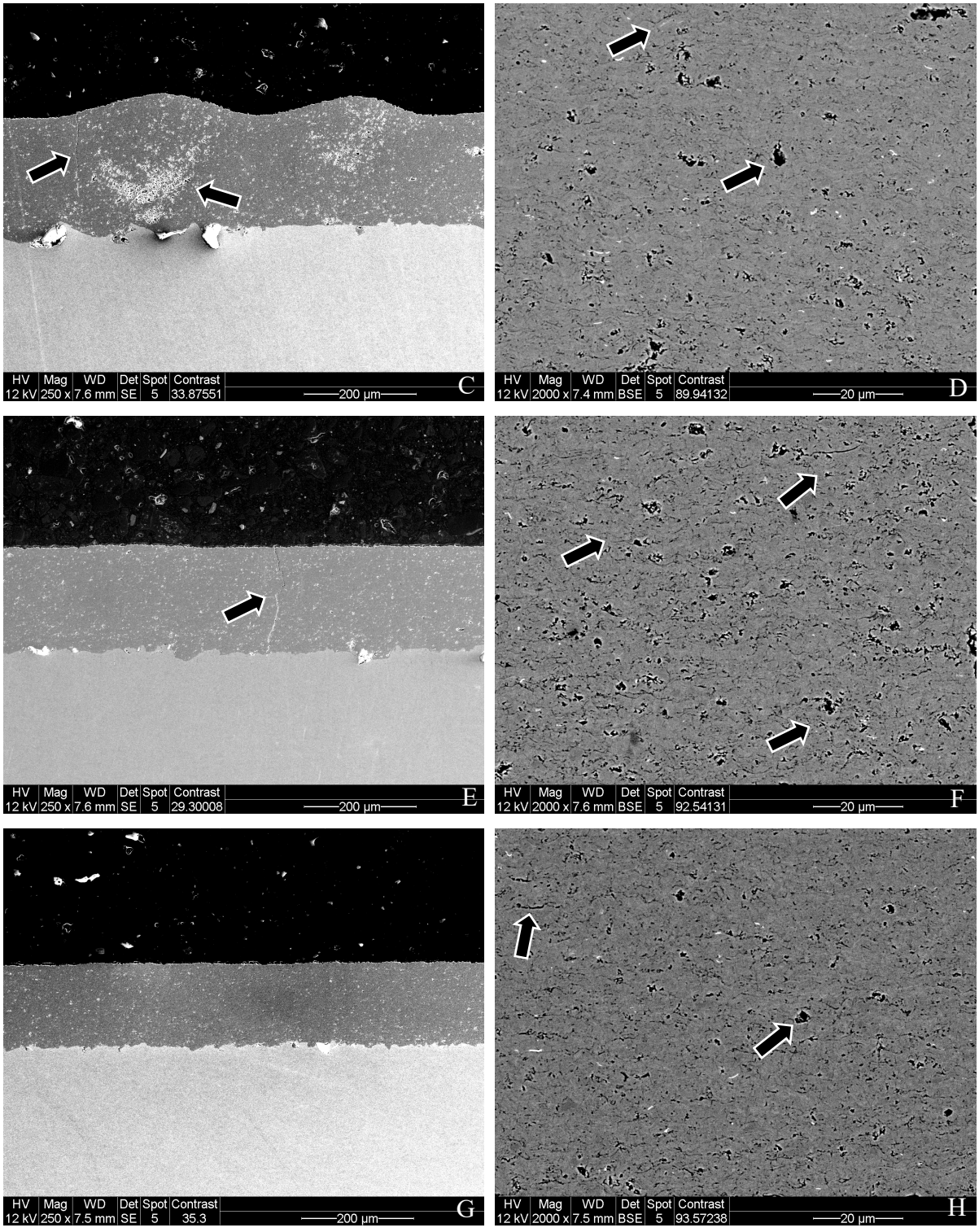

Figure 19. SEM images of the cross sections at lower and higher magnification of Cr_2O_3 + 5% hBN at A-B) 100 mm C-D) 110 mm, E-F) 130mm spray distance and G-H) Cr_2O_3 (120 mm).

Dense coatings are achieved for the Cr_2O_3 samples. However, the coatings contain fine and globular pores as well as some minor delaminations, illustrated by arrows in Figure 19B, D, F and H. No apparent second phase can be seen in the cross-section images in either of the coatings. The cross sections of the samples also reveal that Cr_2O_3 and Cr_2O_3 + 5% hBN sprayed at longer stand of distances, 120 and 130 mm, look relatively flat while this is not the case for a shorter spray distance.

When a bulge is present in the Cr_2O_3 + 5% hBN coatings, it often has porosity underneath, illustrated by arrows in Figure 19A and C. The bulges and the porosity form feathery or cone-like structures. This indicates the beginning of the formation of a feathery or columnar structure where inter-columnar porosity is present. Cracks are also a frequent observation in connection with the bulges, especially in the case of the larger.

Large vertical or diagonal cracks going through the coatings are observed in all Cr_2O_3 + 5% hBN samples. This behavior is not observed in the Cr_2O_3 coating. More SEM images of the coatings in cross section can be found in Appendix 4.2, 5.2, 6.2 and 7.2.

Figure 20 shows images takes on cross sections and close to the surface of the corresponding samples.

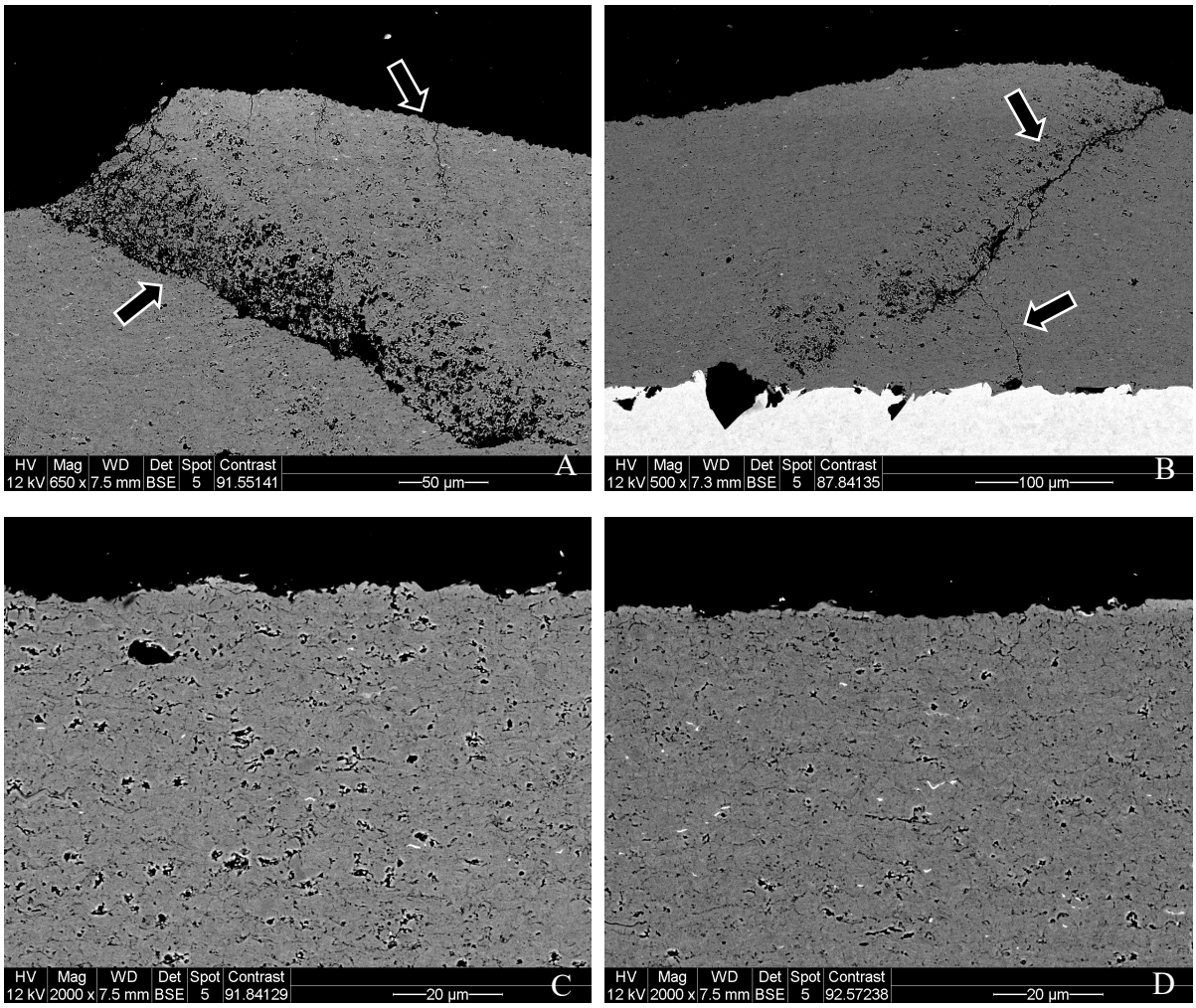

Figure 20. SEM images of cross sections close to the surface of Cr_2O_3 + 5% hBN at A) 100 mm B) 110 mm and C) 130mm stand of distance and D) Cr_2O_3 (120 mm). The arrows in (A) are a guide for the eye to the porosity and the crack at the surface.

As for the microstructures seen in Figure 19, the cross section images of the coatings all display the same dense microstructures with globular and fine pores. In Figure 20A and B, porosity agglomerates extending from the surface down towards the substrate are seen. Fractures of various sizes, either on top of the bulges or within the porosities, are also observed. These features are illustrated by arrows in Figure 20. In oppose to the Cr_2O_3 coatings sprayed at a 100-

and 110-mm spray distance, the samples sprayed at 120- and 130-mm display relatively dense and flat coatings close to the surface, as seen in Figure 20C and D.

Figure 21 illustrates the SE cross section and EDS mapping on Cr_2O_3 (120 mm). The Cr and O element distributions on analyzed area are displayed. The EDS mappings of all of the Cr_2O_3 + hBN sprayed coatings shows similar distributions of Cr and O elements to that of the Cr_2O_3 coating. See Appendix 4.3, 5.3, 6.3, 7.3 and 8.3 for more EDS mapping results.

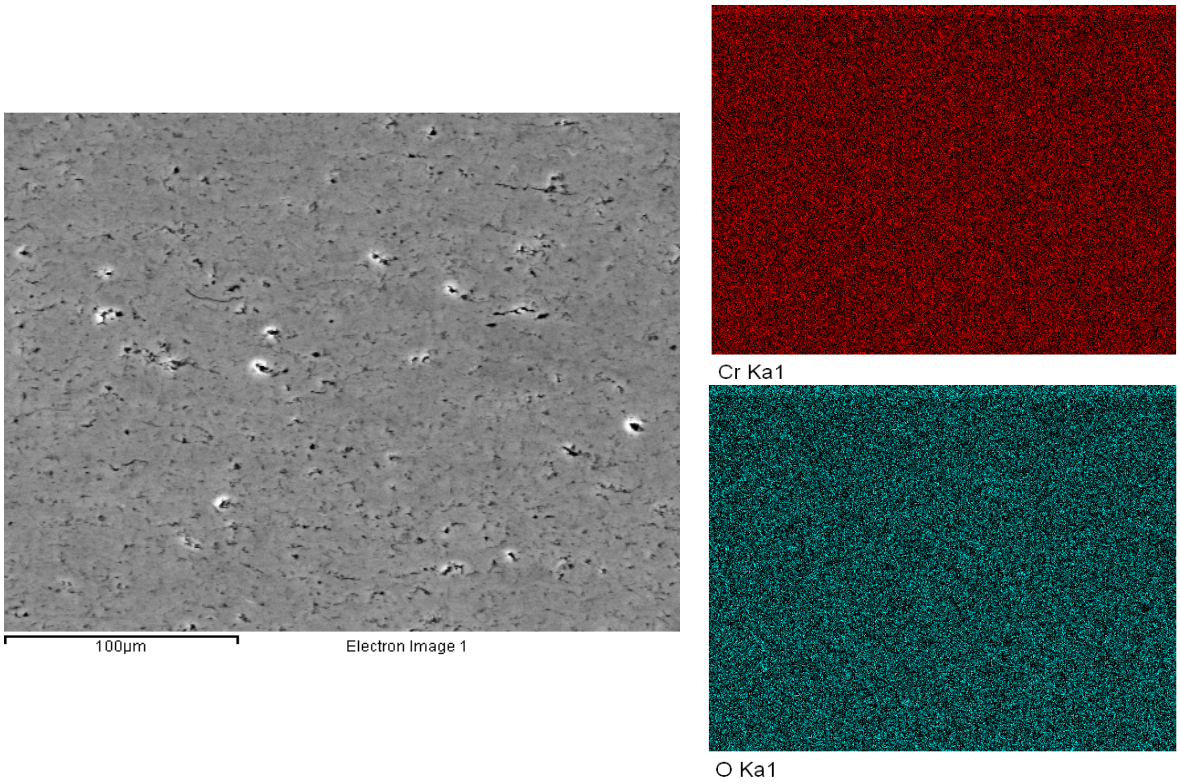

Figure 21. EDS mapping on the cross section of Cr_2O_3 showing the Cr and O element distributions over the analyzed area.

The EDS mappings of the analyzed areas show relatively even distributions of Cr and O. EDS spot analysis results also indicates that Cr and O are the most occurring elements in all of the Cr_2O_3 and Cr_2O_3 + hBN sprayed coatings. Cross reference EDS results with Cr – O phase diagrams suggest that Cr_2O_3 is the primary phase in the coatings. Trace elements, such as Ca or Fe, were also found in some of the coatings.

To study the incorporation of hBN in the coatings, investigations were performed using 10 keV accelerating voltage and spot size 4. Figure 22 illustrates one case of hBN found the Cr_2O_3 + 5% hBN (100 mm).

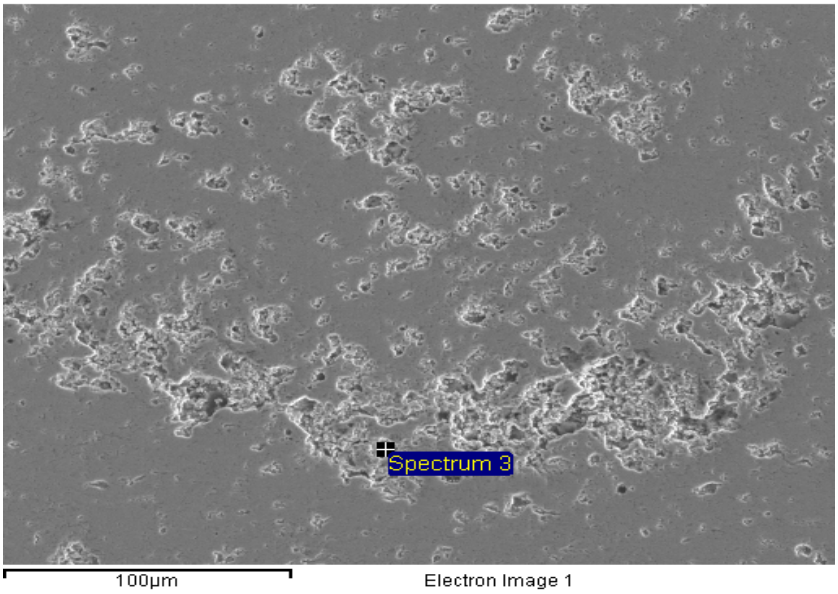

Figure 22. SE cross section image of Cr_2O_3 + 5%hBN (100 mm) highlighting hBN found in the coating during an EDS spot analysis performed with 10 keV accelerating voltage and spot size 4.

The hBN was, however, rather difficult to detect and analyze in most of the coatings. There are hints suggesting that more hBN is embedded into the coating when a shorter injection distance was used since there were more cases of detected B and N in those coatings. This, however, needs more investigations. More EDS spot analysis results on the different Cr_2O_3 and Cr_2O_3 + hBN coatings can be found in Appendix 4.4, 5.4, 5.5, 6.4, 6.5, 7.4 and 7.5.

4.3 Cr_2O_3 + 5% hBN vs Cr_2O_3 + 10% hBN (130 mm) vs Cr_2O_3 (120 mm)

In Figure 23, the surface morphologies of Cr_2O_3, Cr_2O_3 + 5% hBN (130 mm) and Cr_2O_3 + 10% hBN (130 mm) are displayed. The figures on the left-hand side (A, C and E) are taken at lower

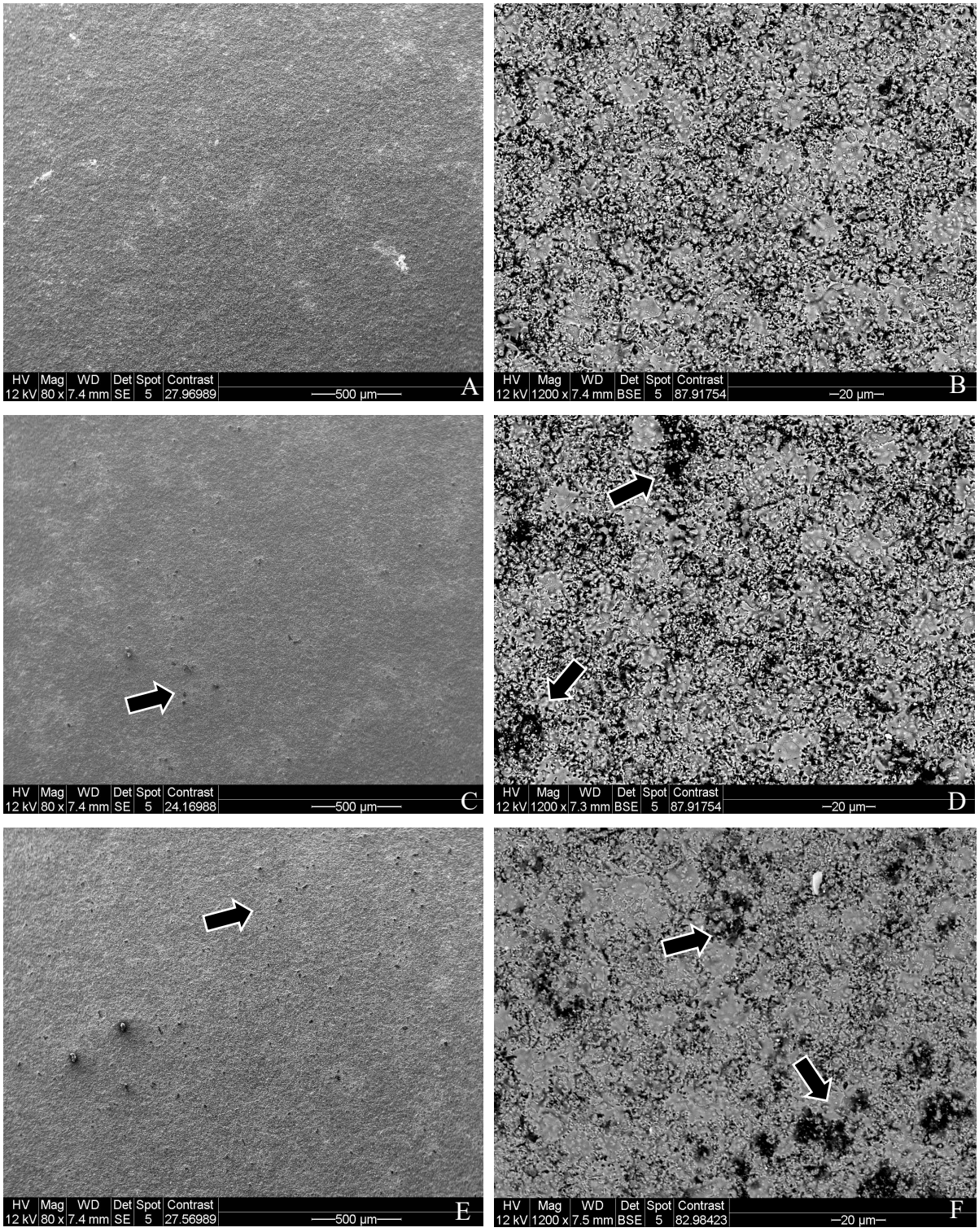

Figure 23. SEM images on the surface morphology at a lower and higher magnification on A-B) Cr_2O_3 + 5% hBN, C-D) Cr_2O_3 + 10% hBN with a 130 mm spray distance, and E-F) Cr_2O_3 sprayed at a 120 mm injector distance.

magnification, and on the right-hand side (B, D, and F), the coating surfaces are shown at a higher magnification.

From the lower magnification images, it is seen that all three samples have relative flat and smooth surfaces. Cr_2O_3 and Cr_2O_3 + 10% hBN have small dark spots on the surface which are not present on the surface of the Cr_2O_3 + 5% hBN coating, illustrated by arrows.

At higher magnification, splats of various sizes and forms can be seen that are evenly spread out over the coating surfaces. Both Cr_2O_3 and Cr_2O_3 + 10% hBN display dark sections in the BSE images that are not as apparent in the Cr_2O_3 + 5% hBN coating, see arrows. Figure 24 illustrates the coatings at a higher magnification.

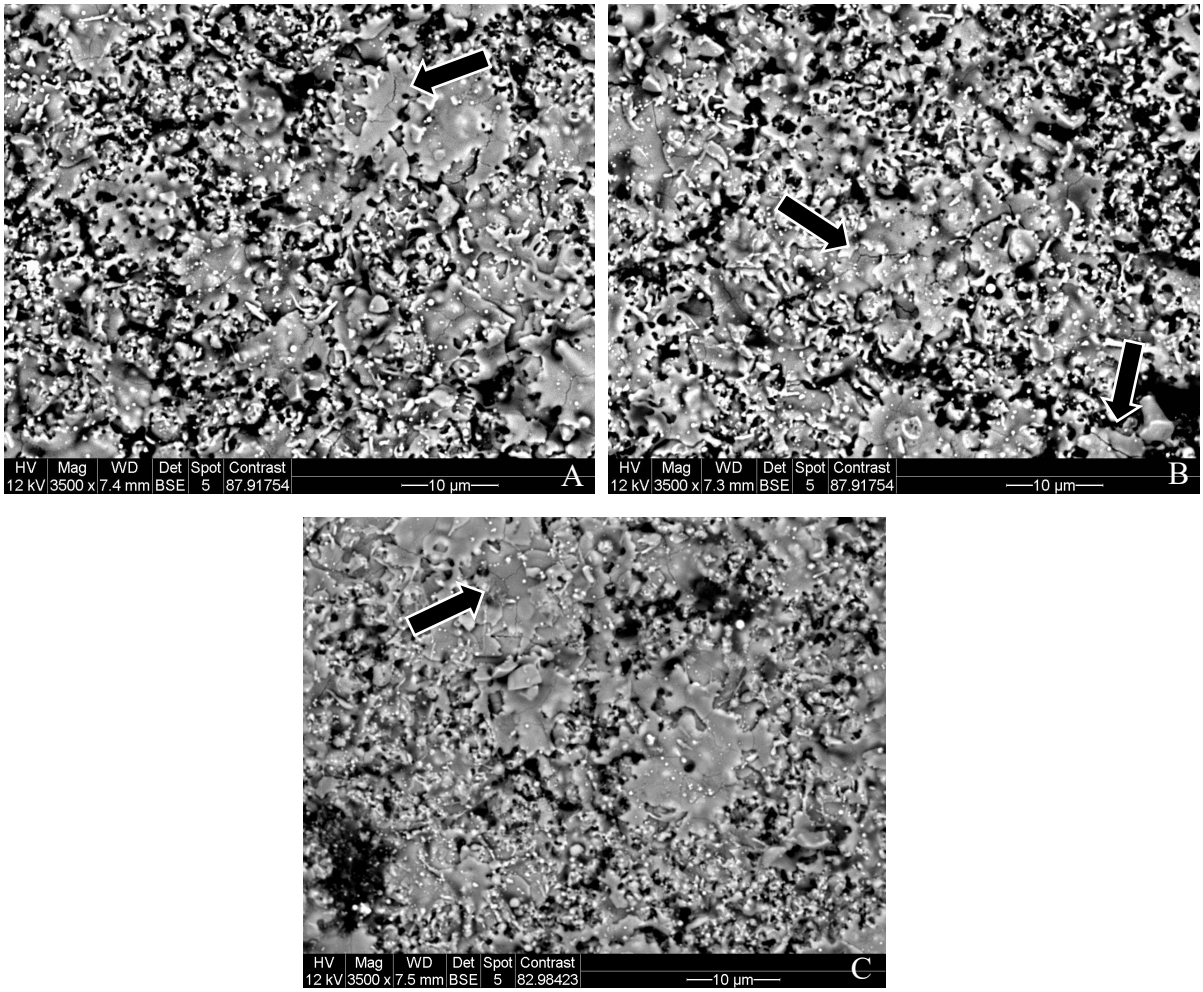

Figure 24. SEM images of the surface morphology at a higher magnification of A) Cr_2O_3 + 5% hBN, B) Cr_2O_3 + 10% hBN at a 130 mm spray distance, and C) Cr_2O_3 sprayed at a 120 mm injector distance.

From the SEM images, cracks were observed in splats of all coatings, illustrated by arrows. Some irregular splats are also seen together with some particle clusters. It is rather difficult to determine if and how hBN affects the topography. More illustrative images can be found in Appendix 4.1, 7.1 and 8.1.

The cross sections of the coatings are shown in Figure 25. The images to the left (A, C, and E) give an overview of the general appearance of the coatings in cross section at a lower magnification. The images to the right (B, D, and F) show the corresponding microstructures at a higher magnification.

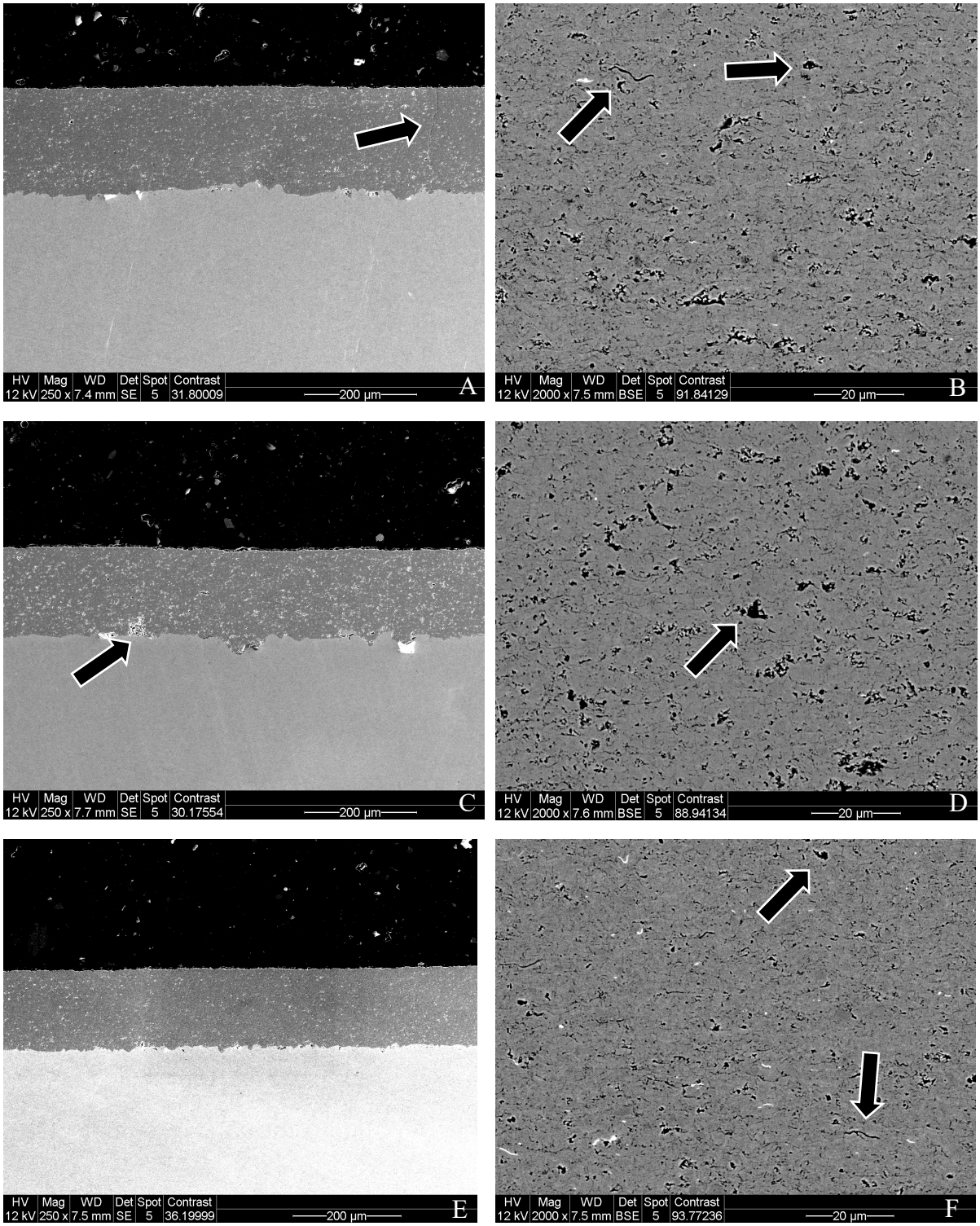

Figure 25. SEM pictures on the cross section at a lower and higher magnitude on A-B) Cr_2O_3 + 5% hBN, C-D) Cr_2O_3 + 10% hBN at a 130 mm spray distance and E-F) Cr_2O_3 sprayed at a 120 mm injector distance.

The coatings appear to have a flat and smooth surface. They all have dense laminar microstructures with both fine and globular pores distributed across the coatings. Smaller delaminations can be observed spread throughout the cross sections in all samples. The arrows in Figure 25B, D and F illustrates delaminations, fine and globular pores. Arrows in Figure 25A and C point at a crack and at agglomerated pores at the substrate interface, respectively. The pores do not affect the microstructure. As seen in Figure 25, Cr_2O_3 + 5% hBN seems to be more

prone to larger vertical cracks compared to both Cr_2O_3 and Cr_2O_3 + 10% hBN. Images of the microstructures close to the surface of the coatings are shown in Figure 26.

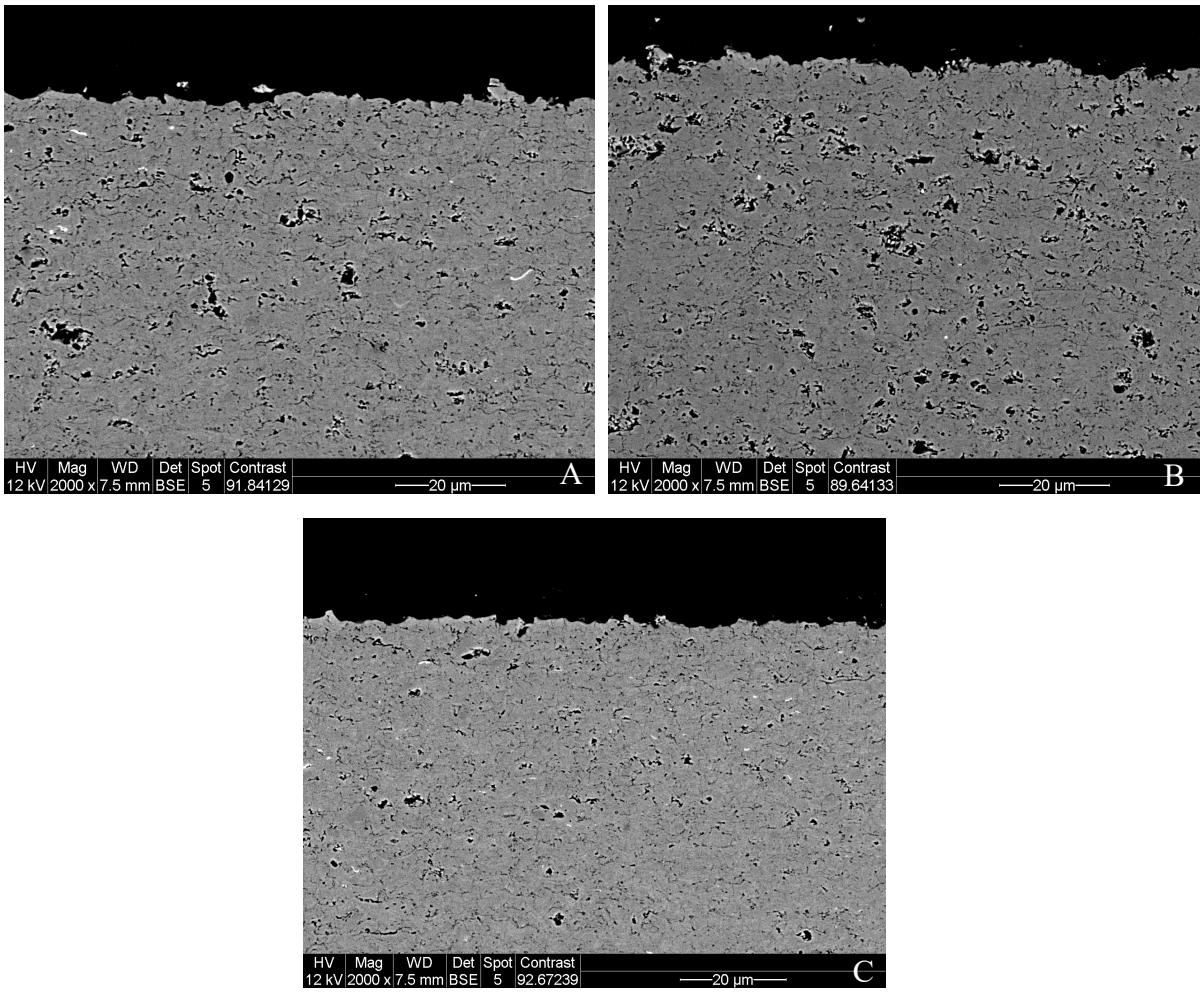

Figure 26. SEM images of the cross section close to the surface at a higher magnification of A) Cr_2O_3 + 5% hBN and B) Cr_2O_3 + 10% hBN at a 130 mm spray distance, and C) Cr_2O_3 sprayed at a 120 mm injector distance.

There is no obvious difference in the microstructures when investigated in cross section and close to the surface compared to that of their corresponding midsections for each of the given coatings.

As stated previously, EDS mapping performed on the cross sections of the Cr_2O_3 and Cr_2O_3 + hBN coatings shows relatively even distribution of both Cr and O in the analyzed areas, seen in Appendix 4.3, 7.3 and 8.3. The results from EDS spot analyze show that Cr and O are the primary elements in the coatings. C, Ca and Fe could also be found in some coatings. Cross reference EDS results with Cr-O phase diagrams suggest that Cr_2O_3 is the primary phase in the coatings. However, further XRD measurements should be performed to confirm this.

To analyze the hBN content in the Cr_2O_3 + hBN sprayed samples, 10 keV accelerating voltage and spot size of 4 were used during the EDS spot analyses. It was difficult to detect hBN, hence, the results are rather inconclusive. Only in a few cases hBN could be found in the Cr_2O_3 + 5%hBN (130 mm) and Cr_2O_3 + 10%hBN (130 mm). Further measurements should be done to analyze the hBN content in the coatings. EDS spot analysis results on the different Cr_2O_3 and Cr_2O_3 + hBN coatings can be found in Appendix 4.4, 7.4, 7.5, 8.4 and 8.5.

5. Conclusion

The surface topographies of the NiCr-Cr_3C_2 and hybrid sprayed NiCr-Cr_3C_2 + water and NiCr-Cr_3C_2 + 15%hBN coatings are relatively smooth. But NiCr-Cr_3C_2 + water and NiCr-Cr_3C_2 + 15%hBN have a slightly rougher surface compared to that of NiCr-Cr_3C_2. The NiCr-Cr_3C_2 coating has also numerous "dark spots" on the surface that are not observed on the other two coatings. At higher magnification and when investigating the surfaces, it is seen that using a hybrid powder-suspension feed affects the surface structure the coating. Using an additional liquid feed during the spraying process creates a surface that contains a higher amount of rougher semi- or unmolten particles with sharper edges together with more spread-out splats on the surface. The occurrence of rougher particles might be due to that a liquid feed affects the in-flight conditions and more energy is required to remove the excess liquid. This can lower the overall temperature of the spray plume and thus influences the NiCr-Cr_3C_2 powder feed. Additionally, when only water was used as the additional suspension feed, smaller, grouped cavities were observed on the top of the coating.

Cross section imaging reveals relatively dense and flat coatings that have both fine and globular pores distributed throughout the coatings. In the HVAF hybrid powder-suspension sprayed coatings, delaminations are a common feature that is not seen to the same extent in the HVAF powder sprayed NiCr-Cr_3C_2 coating. An additional liquid feed seems to introduce a less compact microstructure as compared to when NiCr-Cr_3C_2 powder is sprayed alone. This implies that more delaminations occur when sprayed in a hybrid powder-suspension setting. Imaging also reveals at least two different homogeneously spread phases, with some minor cracks, seen in all of the coatings. EDS measurements indicate the presence of both Cr-C and Ni-Cr phases in all the NiCr-Cr_3C_2 containing coatings. According to the phase diagrams, the probable Ni-Cr phases seen in the samples are Ni_2Cr + BCC (Cr) and Ni_2Cr + FCC (Ni). For the Cr-C phase, Cr_3C_2 is the probable phase.

The surface structures seen for all Cr_2O_3 and Cr_2O_3 + hBN coatings are similar in appearance except for the increased number of dark spots on the Cr_2O_3 and Cr2O3 + 10%hBN samples. Cracks in the splats are a common feature and exist in all Cr_2O_3-containing coatings. The cross sections reveal laminar structures with both fine and globular pores as well as minor delaminations distributed throughout the coatings.

A correlation between the surface structure and stand of distance was seen when changing injector distance between 100 and 130 mm for the Cr_2O_3 and Cr_2O_3 + hBN coatings. A shorter spray distance induces bulges on the surface which disappear when the distance is increased. At 120 mm, a flat surface is seen while at 100 mm, numerous bulges are observed. Cr_2O_3 + 5%hBN sprayed samples with a stand of distance between 100 – 110 mm often have porosity assemblies in a vertical or cone-shaped form directly underneath the bulges. This might be the onset of the formation of a columnar or feathery structure. Surface cracks, and larger diagonal or vertical cracks in close vicinity to the bulges are also frequently seen. Cracks are also observed in the flat parts of the coatings in the Cr_2O_3 + 5%hBN sprayed samples. Cr_2O_3 and Cr_2O_3 + 10%hBN does not show the same tendency for the occurrence of cracking.

EDS analyzes on the Cr_2O_3 and Cr_2O_3 + hBN sprayed samples show Cr and O evenly distributed throughout on the analyzed areas. The presence of C and other trace elements such as Fe and Ca can also be found in some of the coatings. According to the Cr-O phase diagrams, Cr_2O_3 should be the phase present in the coatings. B and N have been difficult to detect. Most hBN was detected in the Cr_2O_3 + 5%hBN sample sprayed at 100 mm distance, followed by the

sample sprayed at 110 mm spray distance. This might suggest a higher hBN content/better incorporation when using a shorter distance. This should, however, be confirmed with additional tests.

5.1 Future work

As there were some difficulties to find and examine hBN in most coatings, there might be a possibility that the hBN compound is removed during the sample preparation of the cross sections. Thus, investigations on fracture surfaces should be done to obtain more information regarding hBN incorporation. Moreover, EDS measurements may not be the best method for the detection of hBN. Other techniques such as AES and TEM may be a more sustainable. To identify phases and compositions, XRD measurements should be performed on coatings and powders. This would also help with determining if hBN is present in the coatings. The XRD equipment in the department of Industrial and Materials Science at Chalmers had a Cr source, which gave inconclusive results regarding the sprayed samples. Other equipment could not be used because of restriction with Covid19. Hardness and scratch tests would also be helpful to assess the durability and performance of the coatings, but measurements had to be postponed because of lab restrictions.

References

[1] G. Di Girolamo and E. Serra, *Thermally sprayed nanostructured coatings for anti-wear and TBC applications: State-of-the-art and future perspectives. State-of-the-art and future perspectives.* Elsevier Ltd, 2015.

[2] A. Ganvir, *Design of Suspension Plasma Sprayed Thermal Barrier Coatings*, no. 20. University West, 2018.

[3] Progressive Surface, "What is thermal spraying?" [Online]. Available: https://www.progressivesurface.com/thermalspraying/process.htm. [Accessed: 27-Jan-2020].

[4] M. Gupta, *Design of Thermal Barrier Coatings. A Modelling Approach*, no. 3. 2010.

[5] M. Pasandideh-Fard, V. Pershin, S. Chandra, and J. Mostaghimi, "Splat shapes in a thermal spray coating process: Simulations and experiments," *J. Therm. Spray Technol.*, vol. 11, pp. 206–217, 2002, doi: 10.1361/105996302770348862.

[6] S. Mohan and A. Mohan, *Anti-Abrasive Nanocoatings: Current and Future Applications*. Elsevier B.V., 2015.

[7] J. M. Guilemany, N. Espallargas, P. H. Suegama, and A. V. Benedetti, "Comparative study of Cr3C2-NiCr coatings obtained by HVOF and hard chromium coatings," *Corros. Sci.*, vol. 48, no. 10, pp. 2998–3013, 2006, doi: 10.1016/j.corsci.2005.10.016.

[8] L. Du, C. Huang, W. Zhang, T. Li, and W. Liu, "Preparation and wear performance of NiCr/Cr3C2-NiCr/hBN plasma sprayed composite coating," *Surf. Coatings Technol.*, vol. 205, no. 12, pp. 3722–3728, 2011, doi: 10.1016/j.surfcoat.2011.01.031.

[9] H. Cetinel, E. Celik, and M. I. Kusoglu, "Tribological behavior of Cr2O3 coatings as bearing materials," *J. Mater. Process. Technol.*, vol. 196, no. 1–3, pp. 259–265, 2008, doi: 10.1016/j.jmatprotec.2007.05.048.

[10] Y. Cao, "Effects of hBN Content on the Microstructure and Properties of Atmospheric Plasma-Sprayed NiCr/Cr3C2-hBN Composite Coatings," *J. Therm. Spray Technol.*, vol. 25, no. 4, pp. 650–659, Apr. 2016, doi: 10.1007/s11666-016-0385-9.

[11] Chemistry LibreTexts, "Phase Diagrams." [Online]. Available: https://chem.libretexts.org/Bookshelves/Physical_and_Theoretical_Chemistry_Textbook_Maps/Supplemental_Modules_(Physical_and_Theoretical_Chemistry)/Physical_Properties_of_Matter/States_of_Matter/Phase_Transitions/Phase_Diagrams. [Accessed: 23-May-2020].

[12] CatCalcPhase, "Phase Diagram Cr-C." [Online]. Available: https://sites.google.com/site/catcalcphase/metal/cr/cr-c. [Accessed: 23-May-2020].

[13] Steel ndsl, "The Cr-C System." [Online]. Available: http://steel.ndsl.kr/htm/Cr-C.htm. [Accessed: 23-May-2020].

[14] Calphad, "Phase diagrams Ni-Cr." [Online]. Available: http://www.calphad.com/nickel-chromium.html. [Accessed: 23-May-2020].

[15] CatCalcPhase, "Phase diagram Ni-Cr." [Online]. Available: https://sites.google.com/site/catcalcphase/metal/ni/ni-cr. [Accessed: 23-May-2020].

[16] CRCT, "Phase diagram Ni-Cr." [Online]. Available: http://www.crct.polymtl.ca/fact/phase_diagram.php?file=Cr-Ni.jpg&dir=FSstel. [Accessed: 23-May-2020].

[17] MTD, "Cr-O." [Online]. Available: http://www.materials-design.co.jp/catcalcSE/XOSE/CrO.htm. [Accessed: 23-May-2020].

[18] Metal lab, "Phase diagram Cr-O." [Online]. Available: https://www.metallab.net/chemsoc/alloys.php?elementno=24&index=4.

[19] D. Tejero-Martin, M. Rezvani Rad, A. McDonald, and T. Hussain, "Beyond Traditional Coatings: A Review on Thermal Sprayed Functional and Smart Coatings," *J. Therm. Spray Technol.*, vol. 28, no. 1, pp. 598–644, 2019, doi:

https://doi.org/10.1007/s11666-019-00857-1.
[20] Bexxon, “What is Thermal Spray?” [Online]. Available: http://www.bexxonglobal.com/what-is-thermal-spray-.html. [Accessed: 28-Apr-2020].
[21] F. A. Kulacki *et al.*, *Handbook of thermal science and engineering*. Springer, 2018.
[22] V. Matikainen, H. Koivuluoto, and P. Vuoristo, “A study of Cr3C2-based HVOF- and HVAF-sprayed coatings: Abrasion, dry particle erosion and cavitation erosion resistance,” *Wear*, vol. 446–447, p. 203188, 2020, doi: 10.1016/j.wear.2020.203188.
[23] HVAF, “HVAF,” 2014. [Online]. Available: http://www.hvaf.com/. [Accessed: 14-Apr-2020].
[24] L. L. Silveira, A. G. M. Pukasiewicz, D. J. M. de Aguiar, A. J. Zara, and S. Björklund, “Study of the corrosion and cavitation resistance of HVOF and HVAF FeCrMnSiNi and FeCrMnSiB coatings,” *Surf. Coatings Technol.*, vol. 374, pp. 910–922, 2019, doi: 10.1016/j.surfcoat.2019.06.076.
[25] D. Liang *et al.*, “Characterization and elevated-temperature tribological performance of AC–HVAF-sprayed Fe-based amorphous coating,” *Surf. Coatings Technol.*, vol. 387, pp. 1–10, 2020, doi: 10.1016/j.surfcoat.2020.125535.
[26] V. Verlotski and T. Gmbh, “Coatings of carbide-metal systems (Cr3C2-NiCr and WC-Co-Cr) deposited by high-velocity atmospheric plasma spraying from specially modified fine-grained powders Coatings of Carbide-Metal Systems (Cr 3 C 2 -NiCr and WC-Co-Cr) Deposited by High-Velocity,” vol. 1, no. 1, pp. 18–23, 2018, doi: 10.jtse/xxxx-xxxx/1-1.4.
[27] R. S. Lima, B. M. H. Guerreiro, and M. Aghasibeig, “Microstructural Characterization and Room-Temperature Erosion Behavior of As-Deposited SPS, EB-PVD and APS YSZ-Based TBCs,” *J. Therm. Spray Technol.*, vol. 28, no. 1–2, pp. 223–232, 2019, doi: 10.1007/s11666-018-0763-6.
[28] S. Björklund, S. Goel, and S. Joshi, “Function-dependent coating architectures by hybrid powder-suspension plasma spraying: Injector design, processing and concept validation,” *Mater. Des.*, vol. 142, pp. 56–65, 2018, doi: 10.1016/j.matdes.2018.01.002.
[29] N. Curry, K. VanEvery, T. Snyder, J. Susnjar, and S. Bjorklund, “Performance testing of suspension plasma sprayed thermal barrier coatings produced with varied suspension parameters,” *Coatings*, vol. 5, no. 3, pp. 338–356, 2015, doi: 10.3390/coatings5030338.
[30] K. P. Jonnalagadda *et al.*, “Failure of Multilayer Suspension Plasma Sprayed Thermal Barrier Coatings in the Presence of Na2SO4 and NaCl at 900 °C,” *J. Therm. Spray Technol.*, vol. 28, pp. 212–222, 2019, doi: 10.1007/s11666-018-0780-5.
[31] S. Joshi and P. Nylen, “Advanced Coatings by Thermal Spray Processes,” *Technologies*, vol. 7, no. 4, pp. 1–14, 2019, doi: 10.3390/technologies7040079.
[32] J. I. Goldstein, D. E. Newbury, J. R. Michael, N. W. M. Ritchie, J. H. J. Scott, and D. C. Joy, *Microscopy and X-Ray Microanalysis*, Fourth Edi. Springer.

Appendix

Appendix 1.1

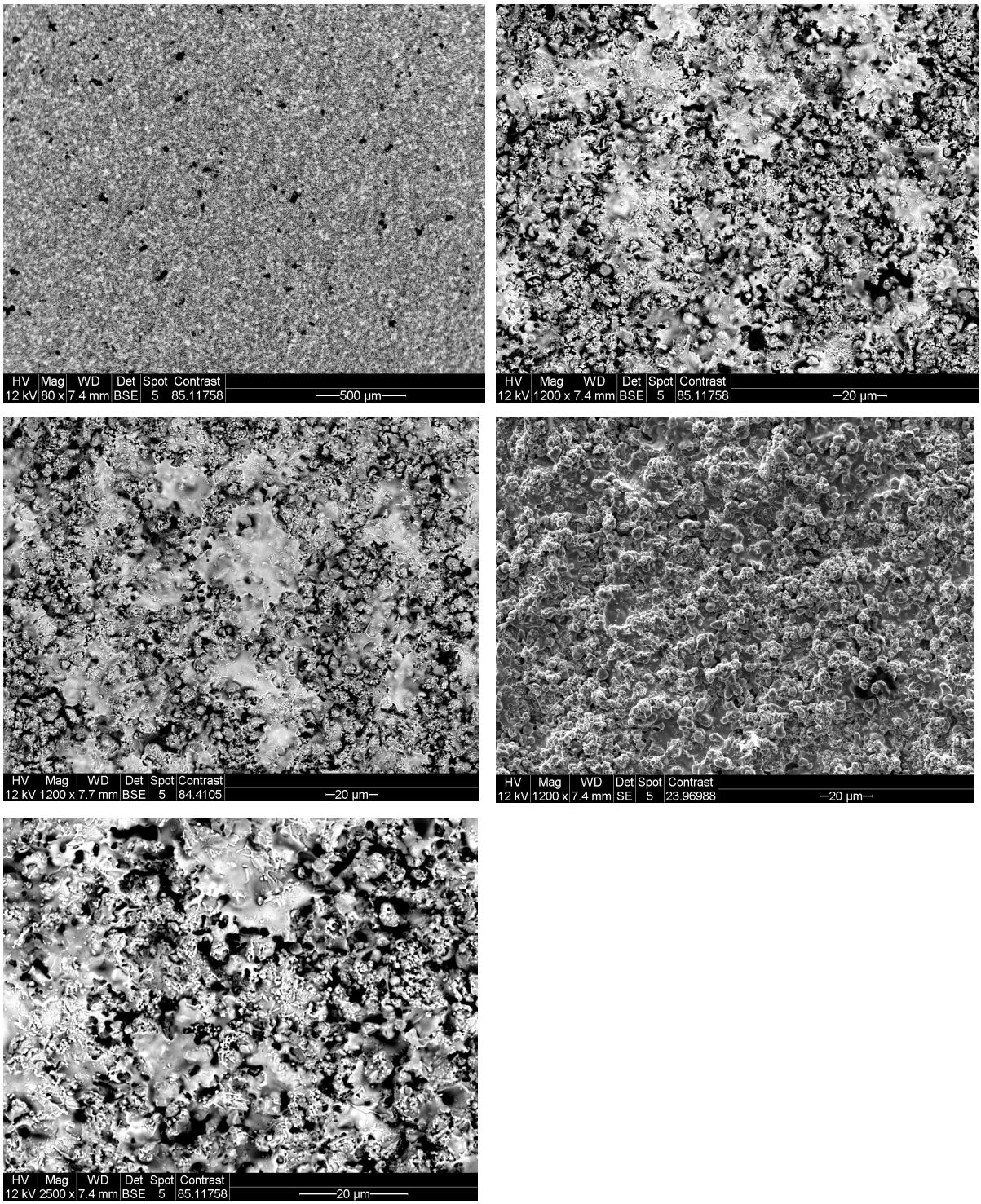

Figure 1. SEM images on the topography on the NiCr – Cr_3C_2 coating at different magnification and positions.

Appendix 1.2

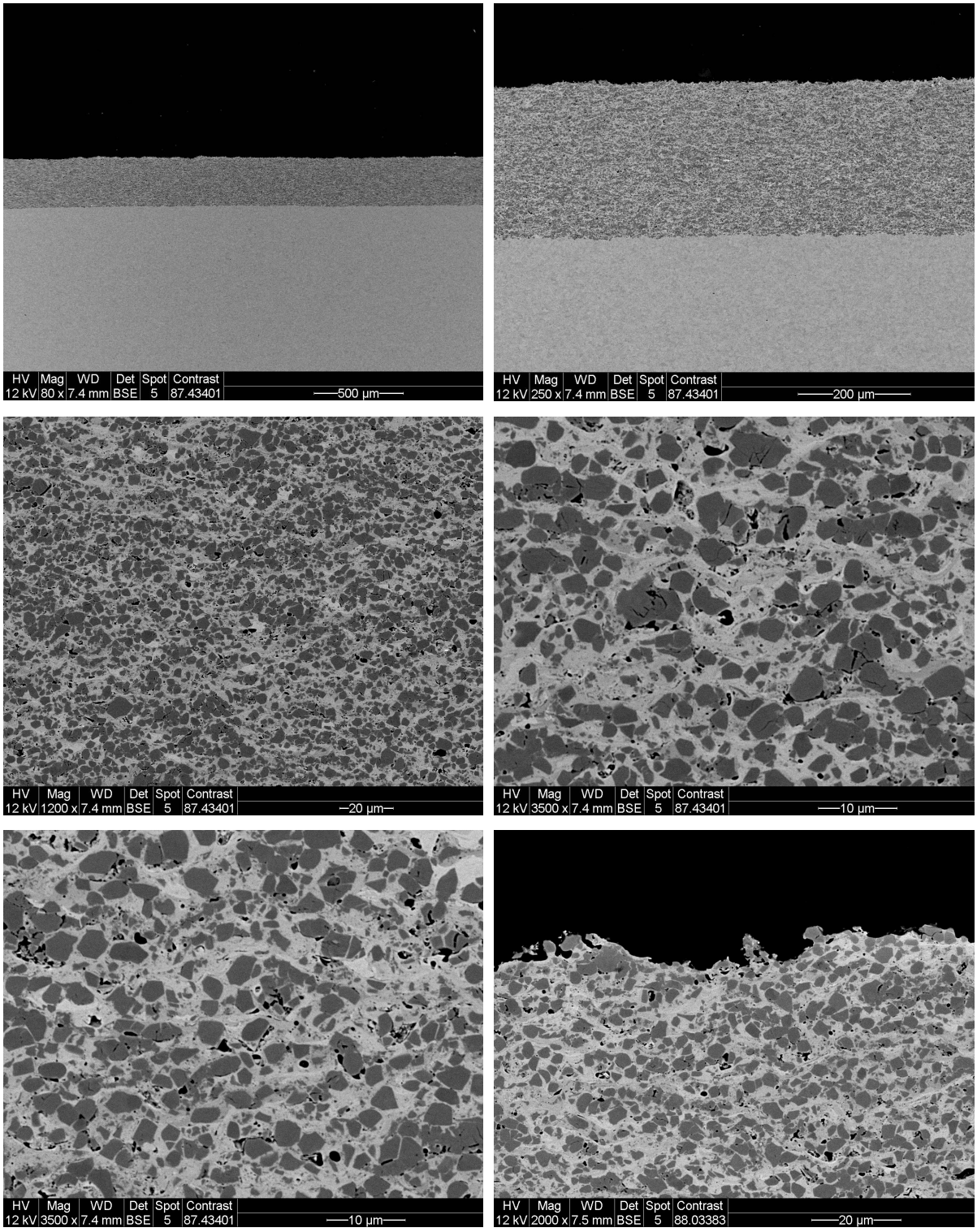

Figure 2. Cross section SEM images on the NiCr – Cr_3C_2 coating at different magnification and positions.

Appendix 1.3

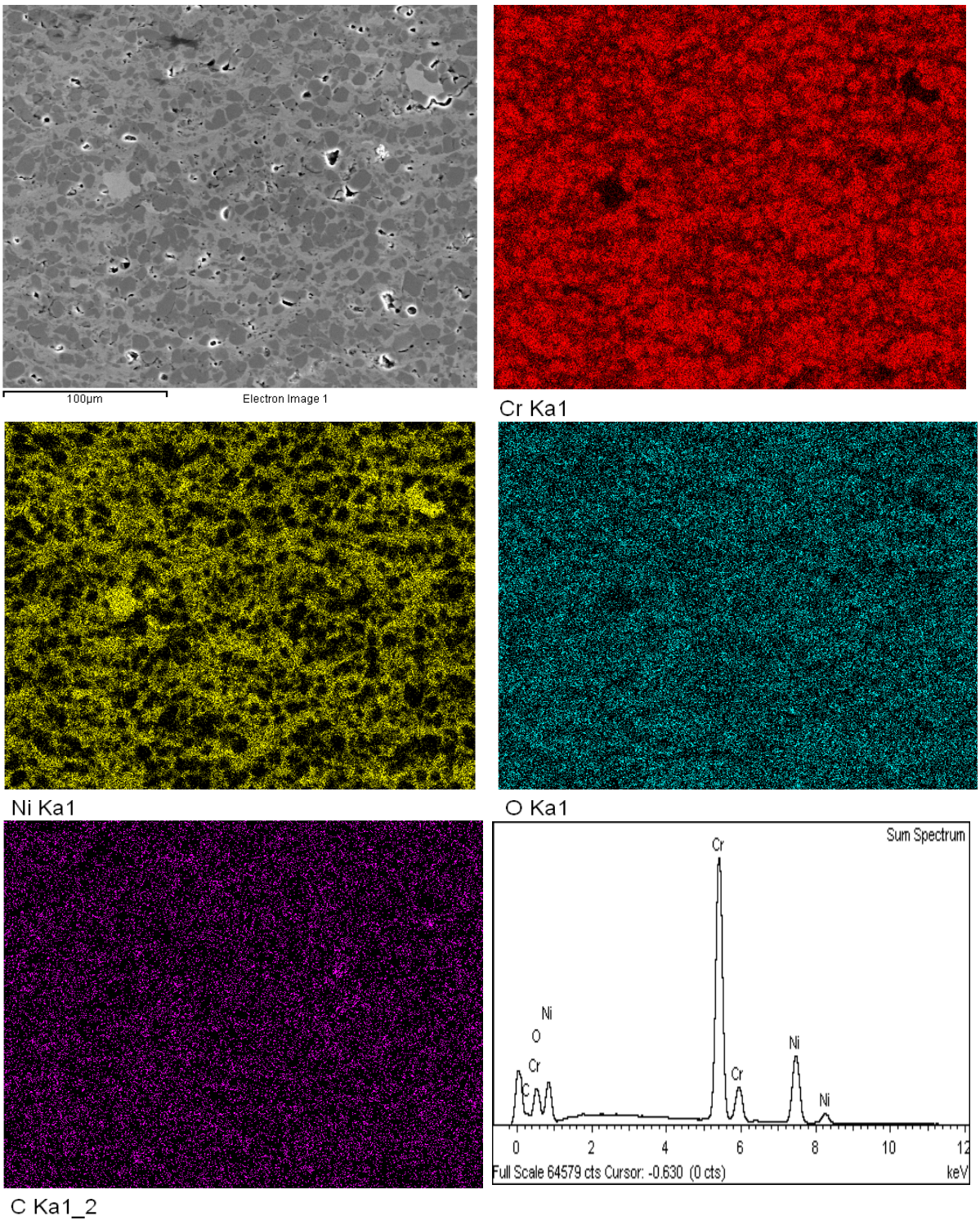

Figure 3. SE and EDS mapping images on the cross section of the NiCr-Cr_3C_2 coating and the sum spectra on the analyzed area.

Appendix 1.4

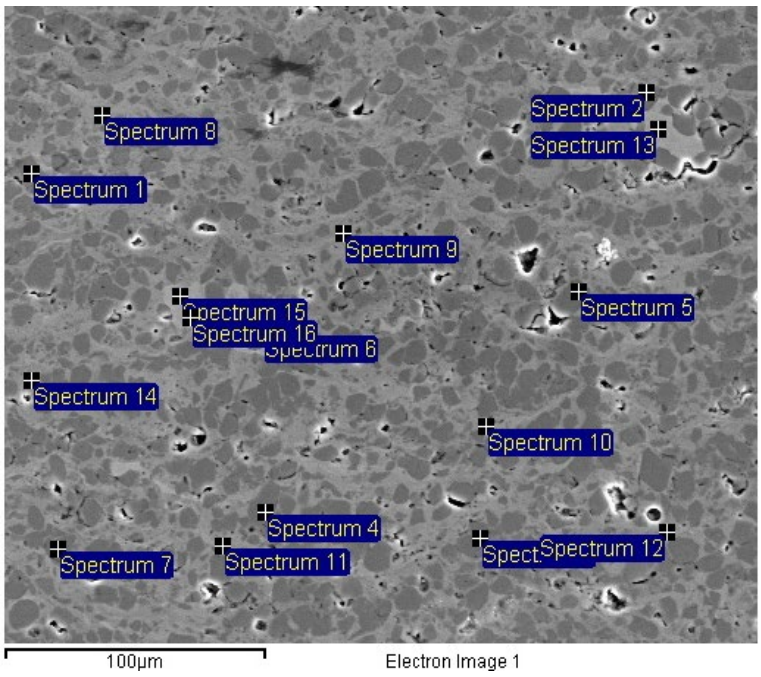
Spectrum 8
Spectrum 2
Spectrum 13
Spectrum 1
Spectrum 9
Spectrum 15
Spectrum 16
Spectrum 5
Spectrum 14
Spectrum 10
Spectrum 4
Spectrum 7
Spectrum 11
Spectrum 12
100µm
Electron Image 1

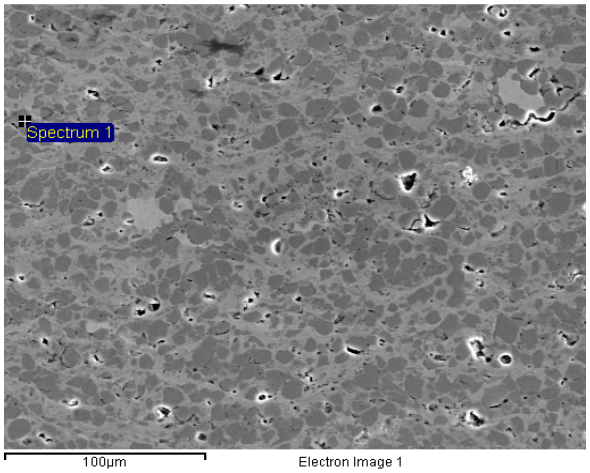
Spectrum 1
100µm
Electron Image 1

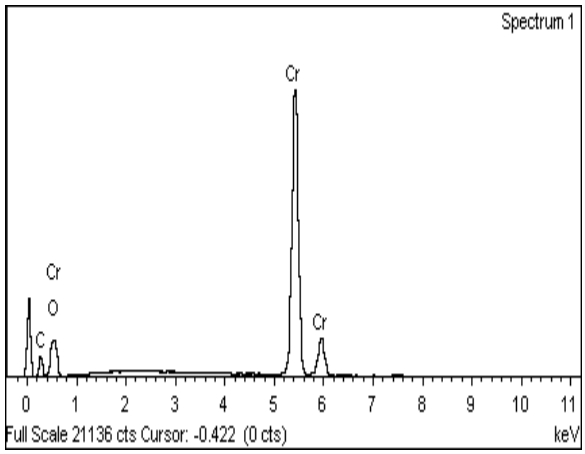
Spectrum 1
Cr
O
C
Cr
Cr
0 1 2 3 4 5 6 7 8 9 10 11
Full Scale 21136 cts Cursor: -0.422 (0 cts)
keV

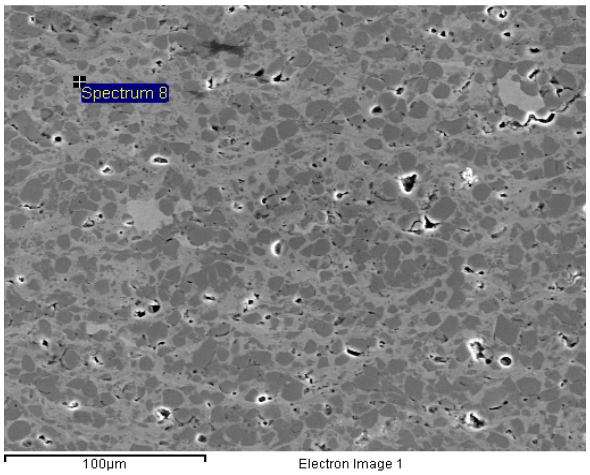
Spectrum 8
100µm
Electron Image 1

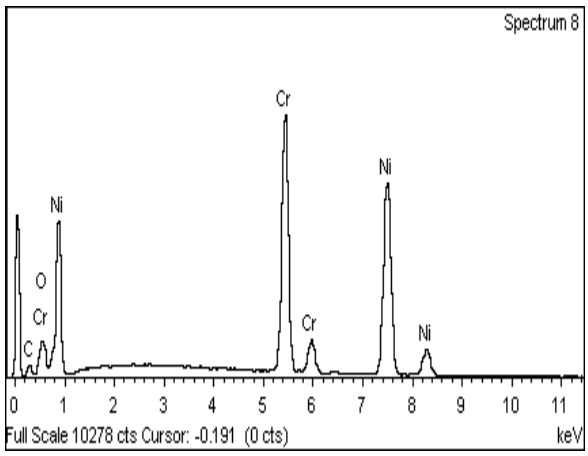
Spectrum 8
Cr
Ni
Ni
O
Cr
C
Cr
Ni
0 1 2 3 4 5 6 7 8 9 10 11
Full Scale 10278 cts Cursor: -0.191 (0 cts)
keV

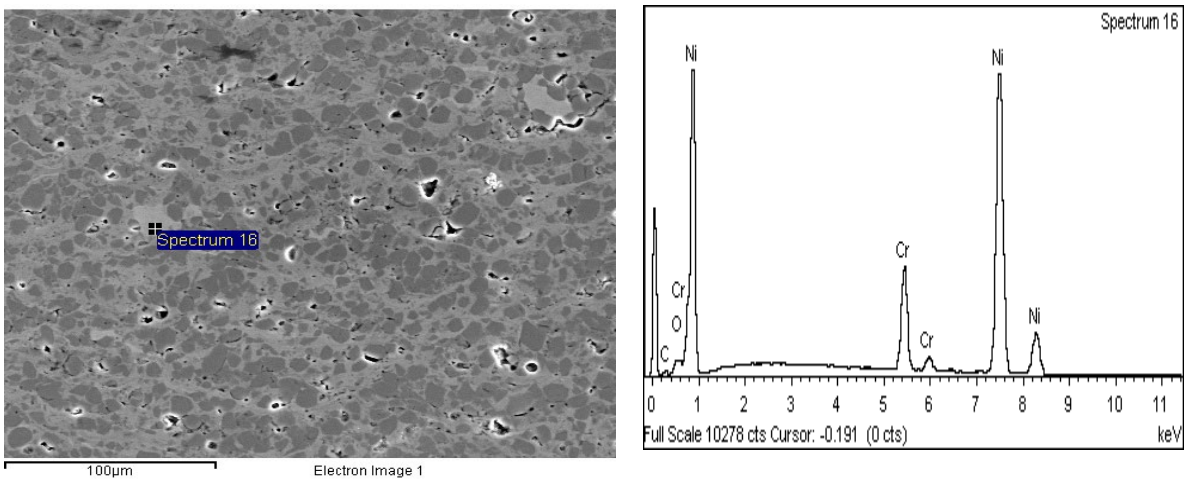

Figure 4. EDS spot analyses on the NiCr-Cr_3C_2 cross section at different locations. The analysis was done with 20 eV and spot size 5.

Table 1. List of elements and composition identified from the EDS spot analysis done on the NiCr-Cr_3C_2 cross section. All analyzed elements are normalized and are given in weight %. The elemental composition of the corresponding EDS mapping is seen as sum spectrum in Appendix 1.3. The position of all the spot analyzes can be seen in the EDS spot analysis image in Figure 4.

Spectrum	**C**	**O**	**Cr**	**Ni**	**Total**
Spectrum 1	14.49	2.56	82.96		100.00
Spectrum 2	13.56	2.39	84.05		100.00
Spectrum 3	13.45	2.73	80.89	2.94	100.00
Spectrum 4	14.14	2.14	83.72		100.00
Spectrum 5	14.17	2.83	83.00		100.00
Spectrum 6	14.07	2.69	83.24		100.00
Spectrum 7	14.02	2.53	83.45		100.00
Spectrum 8	6.50	2.04	34.74	56.72	100.00
Spectrum 9	6.61	1.64	38.42	53.33	100.00
Spectrum 10	6.75	2.26	38.16	52.84	100.00
Spectrum 11	5.28	2.71	31.68	60.34	100.00
Spectrum 12	5.28	2.14	34.32	58.26	100.00
Spectrum 13	2.86	0.81	13.65	82.68	100.00
Spectrum 14	6.58	4.20	40.50	48.71	100.00
Spectrum 15	2.58	0.98	13.65	82.79	100.00
Spectrum 16	2.74	0.59	13.02	83.64	100.00
Sum Spectrum	2.46	1.31	62.55	33.69	100.00
Max.	14.49	4.20	84.05	83.64	
Min.	2.58	0.59	13.02	2.94	

Appendix 2.1

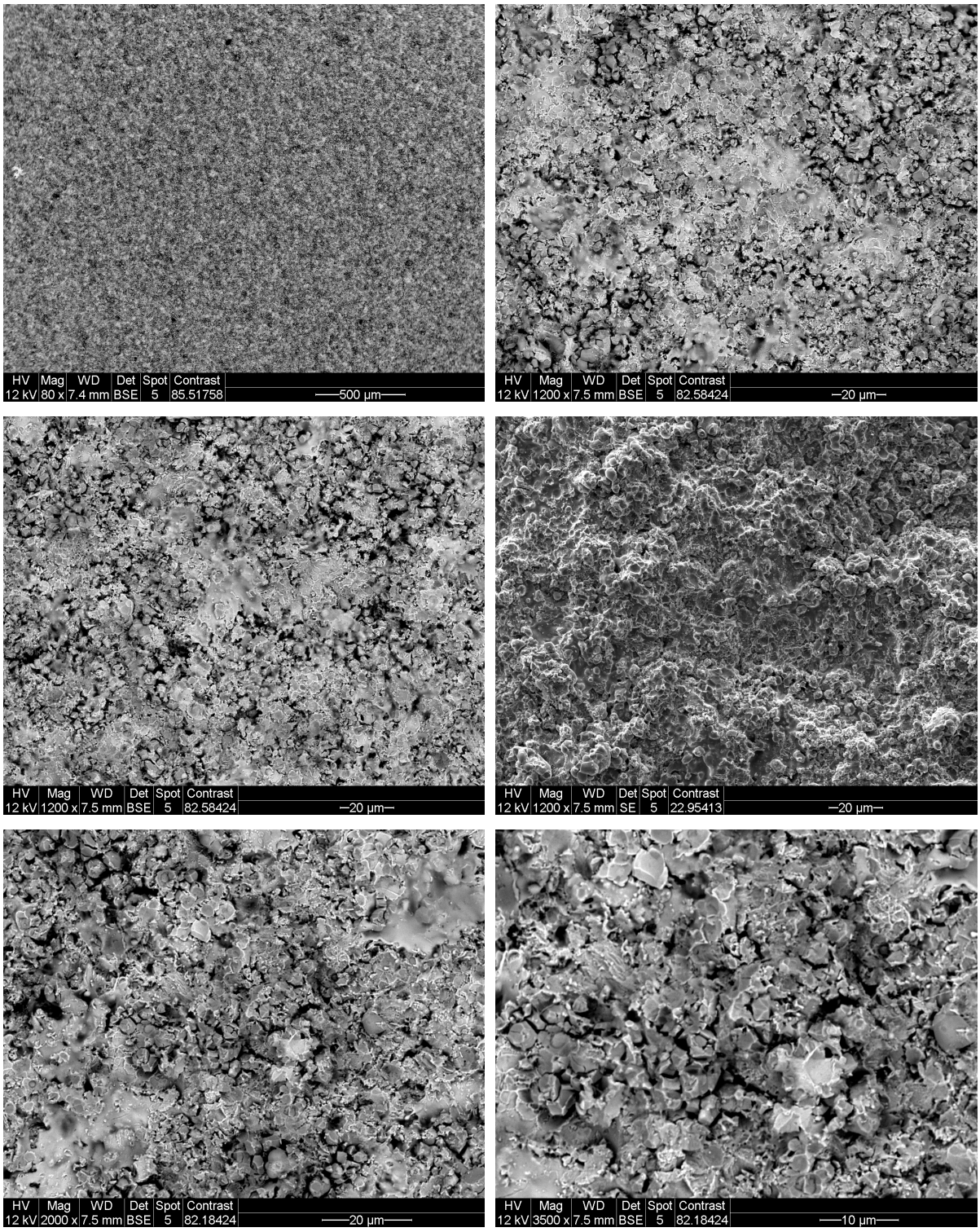

Figure 5. SEM images on the topography on the NiCr – Cr_3C_2 + water coating at different magnification and positions.

Appendix 2.2

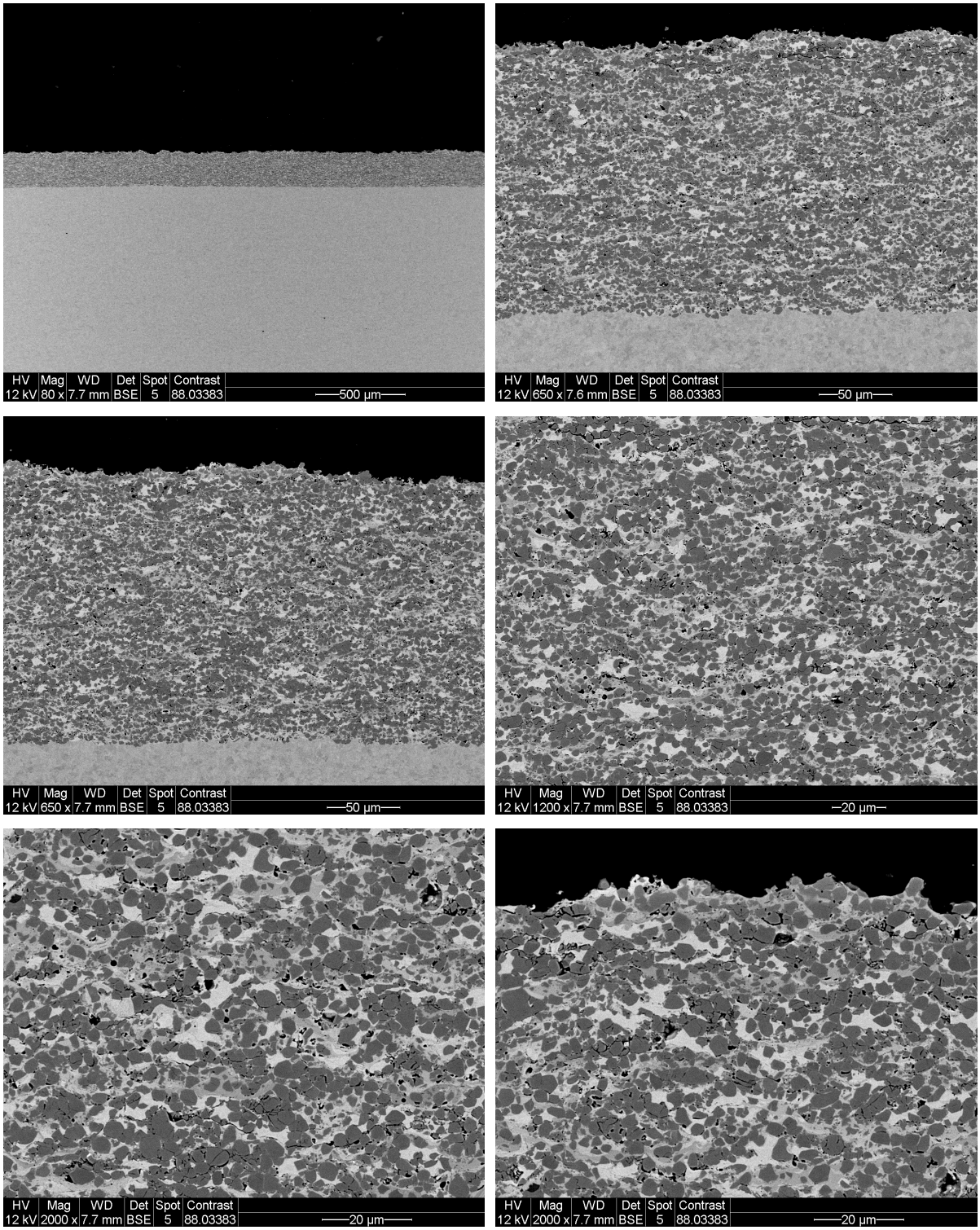

Figure 6. Cross section SEM images on the NiCr – Cr_3C_2 + water coating at different magnification and positions.

Appendix 2.3

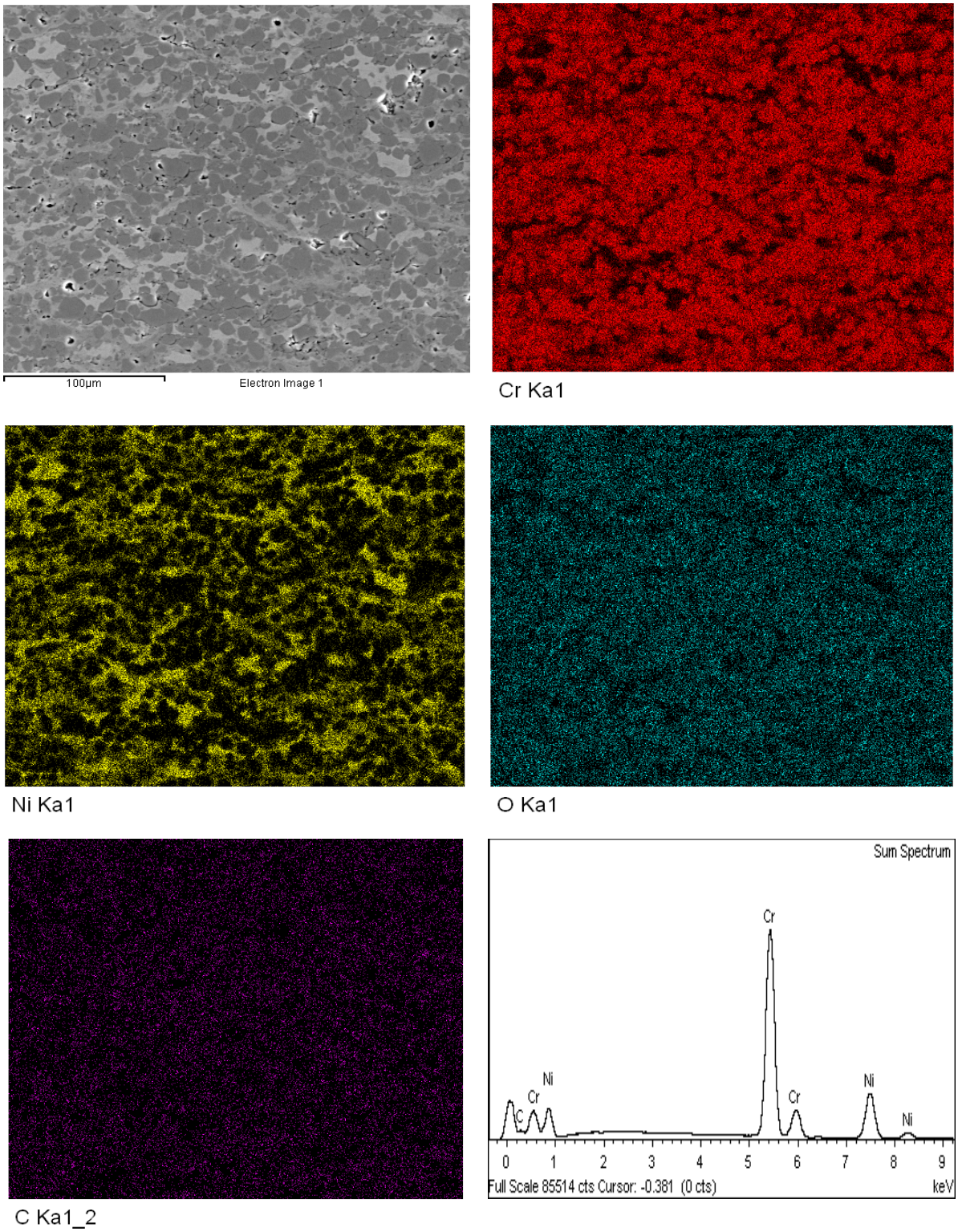

Figure 7. SE and EDS mapping images on the cross section of the NiCr-Cr_3C_2 + water coating and the corresponding sum spectra on the analyzed area.

Appendix 2.4

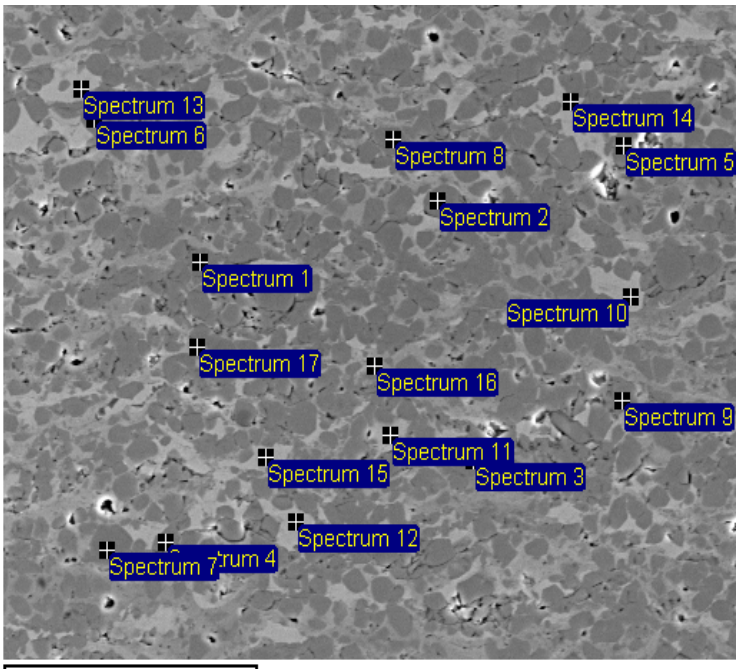
Spectrum 13
Spectrum 6
Spectrum 14
Spectrum 8
Spectrum 5
Spectrum 2
Spectrum 1
Spectrum 10
Spectrum 17
Spectrum 16
Spectrum 9
Spectrum 11
Spectrum 15
Spectrum 3
Spectrum 12
Spectrum 7
rum 4
100µm
Electron Image 1

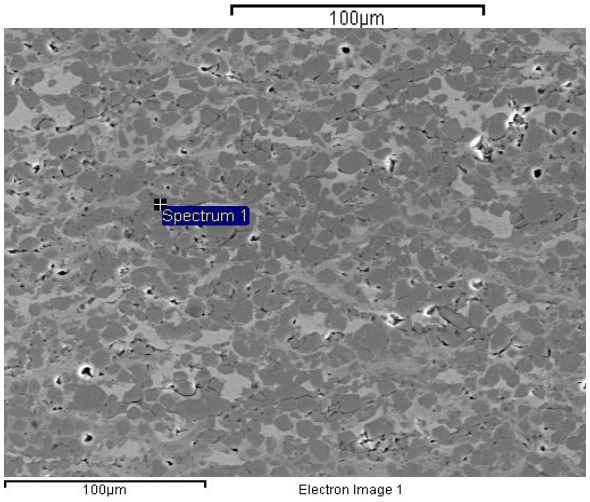
Spectrum 1
100µm
Electron Image 1

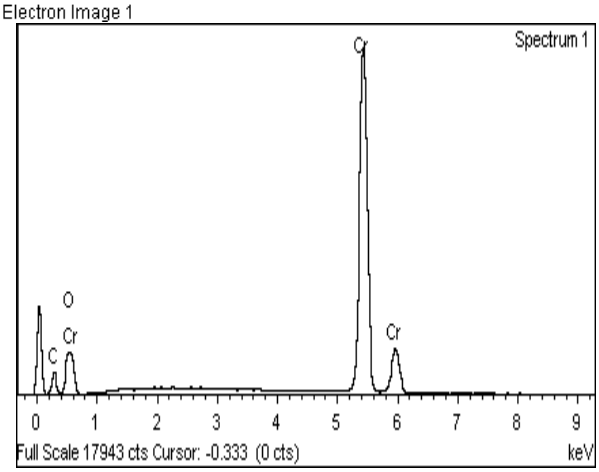
Spectrum 1
Cr
O
Cr
C
Cr
0 1 2 3 4 5 6 7 8 9
Full Scale 17943 cts Cursor: -0.333 (0 cts)
keV

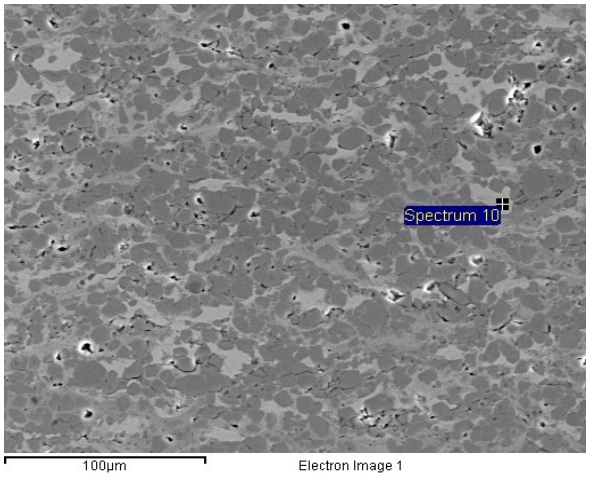
Spectrum 10
100µm
Electron Image 1

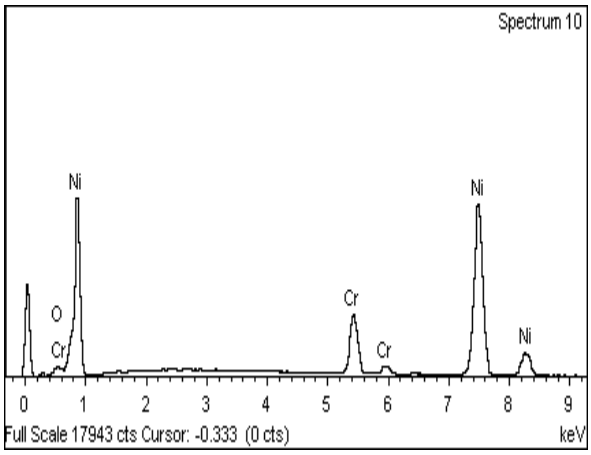
Spectrum 10
Ni
Ni
O
Cr
Cr
Cr
Ni
0 1 2 3 4 5 6 7 8 9
Full Scale 17943 cts Cursor: -0.333 (0 cts)
keV

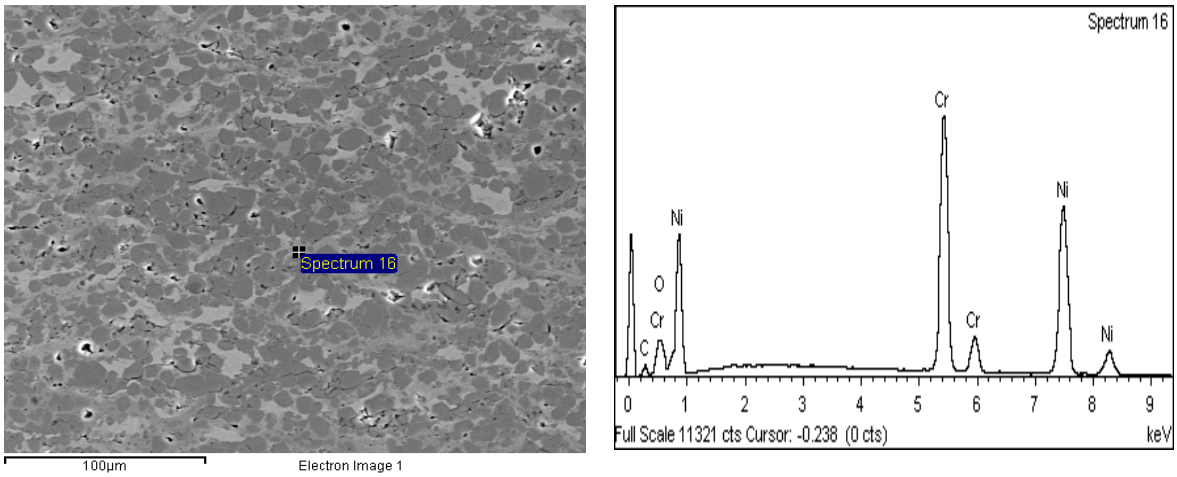

Figure 8. EDS spot analyses on the NiCr-Cr_3C_2 + water cross section at different locations. The analysis was done with 20 eV and spot size 5.

Table 2. List of elements and composition identified from the EDS spot analysis done on the NiCr-Cr_3C_2 + water cross section. All analyzed elements are normalized and are given in weight %. The elemental composition of the corresponding EDS mapping is seen as sum spectrum in Appendix 2.3. The position of all the spot analyzes can be seen in the EDS spot analysis image in Figure 8.

Spectrum	**C**	**O**	**Cr**	**Ni**	**Total**
Spectrum 1	13.95	2.46	83.59		100.00
Spectrum 2	14.57	2.54	82.89		100.00
Spectrum 3	14.33	2.39	83.27		100.00
Spectrum 4	14.26	2.81	82.92		100.00
Spectrum 5	14.42	2.50	83.08		100.00
Spectrum 6	14.27	2.56	83.17		100.00
Spectrum 7	13.77	2.82	82.59	0.81	100.00
Spectrum 8	14.34	2.37	82.67	0.61	100.00
Spectrum 9	14.95	2.58	78.60	3.87	100.00
Spectrum 10		0.72	13.09	86.19	100.00
Spectrum 11		0.88	16.74	82.38	100.00
Spectrum 12		1.03	14.24	84.73	100.00
Spectrum 13		0.66	13.84	85.51	100.00
Spectrum 14		0.74	14.03	85.23	100.00
Spectrum 15		0.67	13.91	85.42	100.00
Spectrum 16	6.31	2.44	37.82	53.42	100.00
Spectrum 17	8.42	3.85	48.48	39.25	100.00
Sum Spectrum	2.92		66.98	30.10	100.00
Max.	14.95	3.85	83.59	86.19	
Min.	2.92	0.66	13.09	0.61	

Appendix 3.1

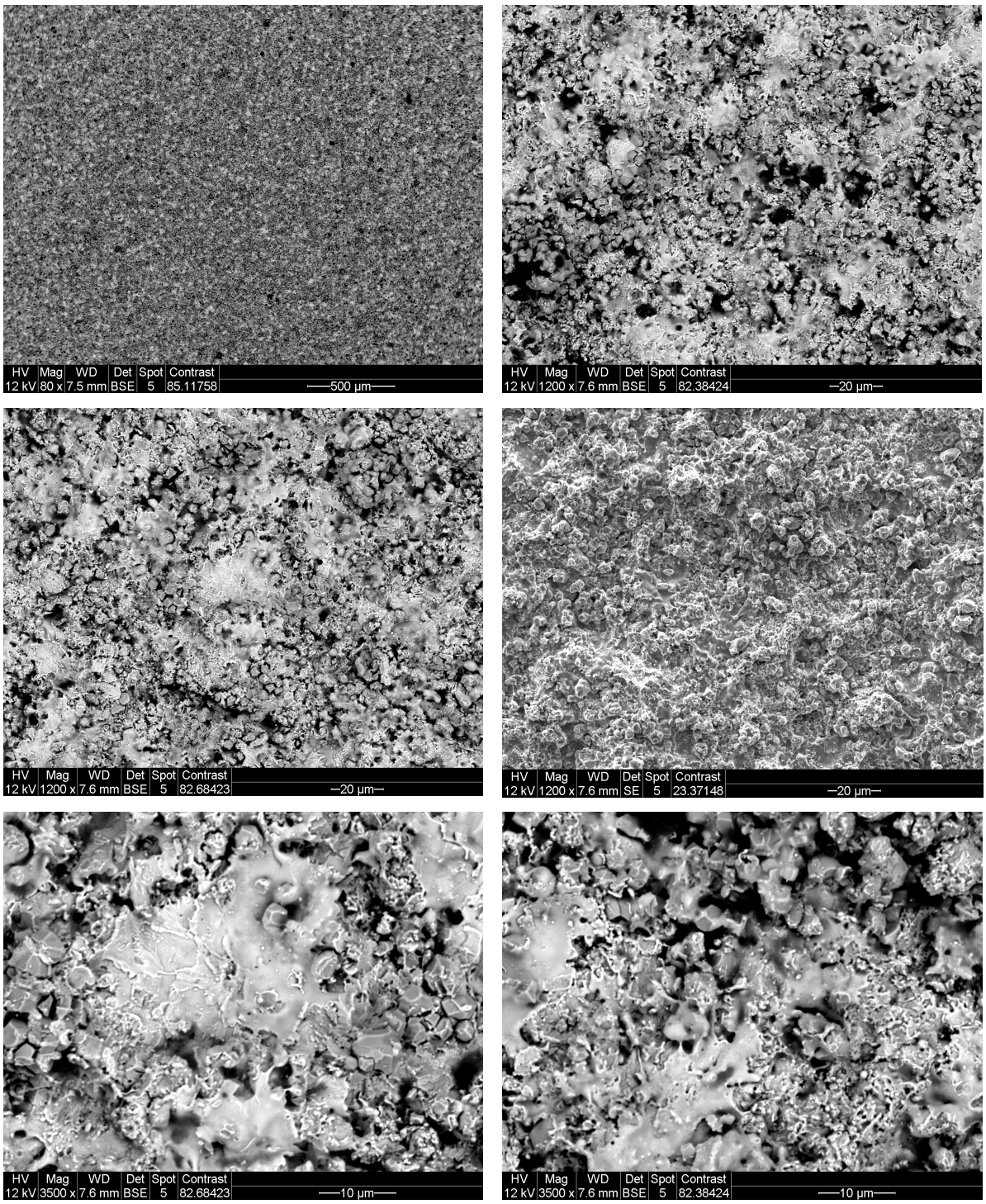

Figure 9. SEM images on the topography on the NiCr-Cr_3C_2 + 15%hBN coating at different magnification and positions.

Appendix 3.2

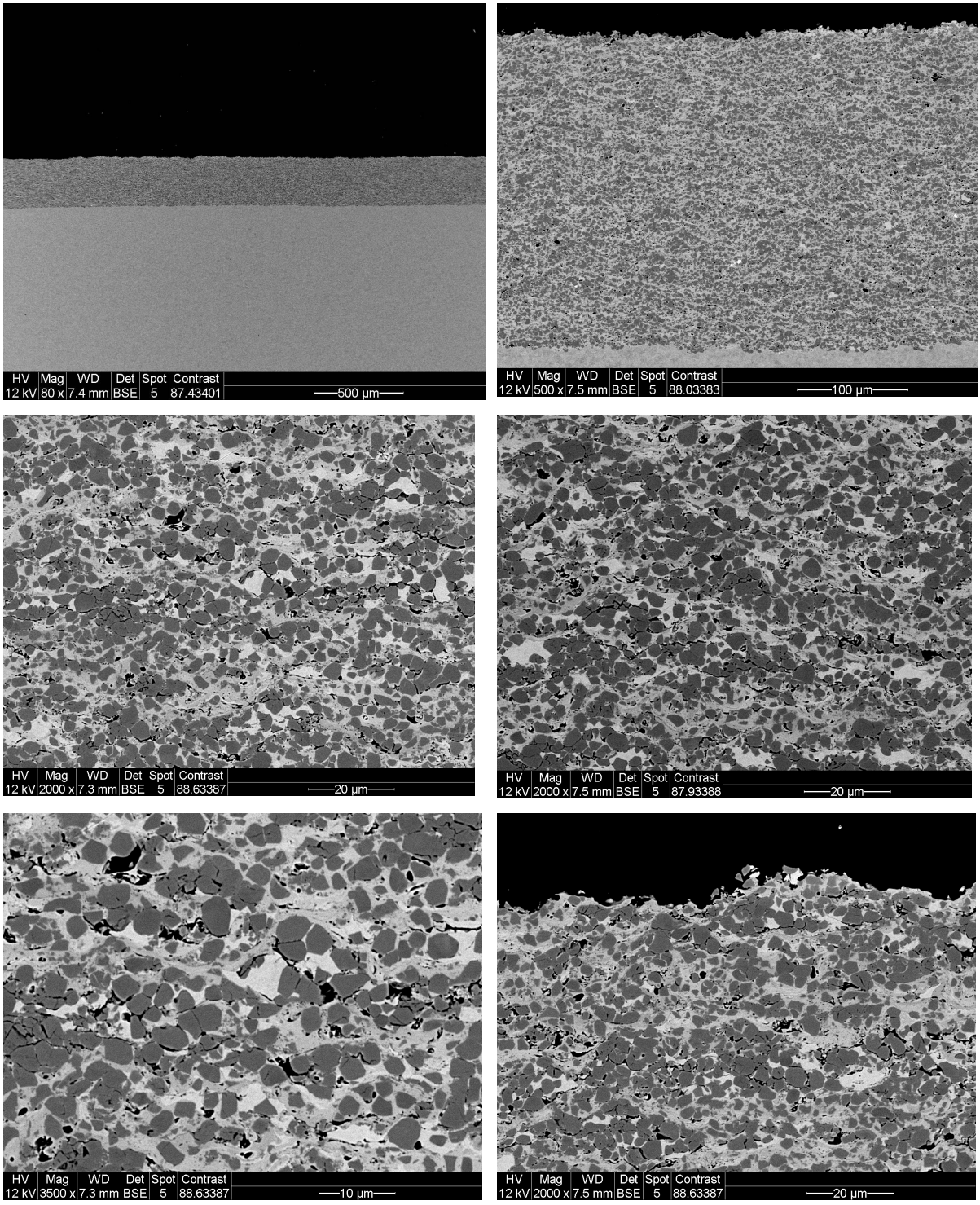

Figure 10. Cross section SEM images on the NiCr-Cr_3C_2 + 15%hBN coating at different magnification and positions.

Appendix 3.3

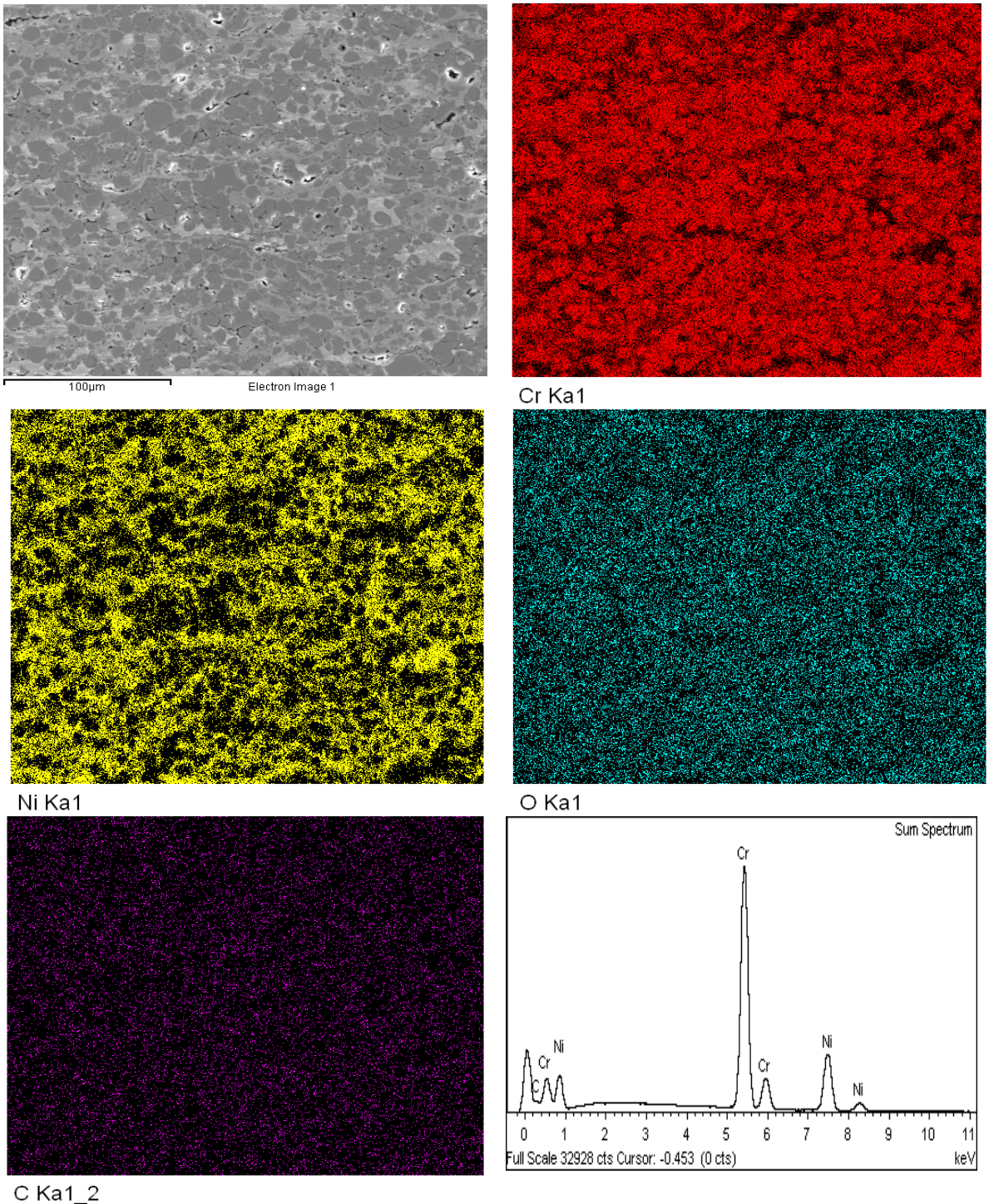

Figure 11. SE and EDS mapping images on the cross section of the NiCr-Cr_3C_2 + 15%hBN sample and the corresponding sum spectra on the analyzed area.

Appendix 3.4

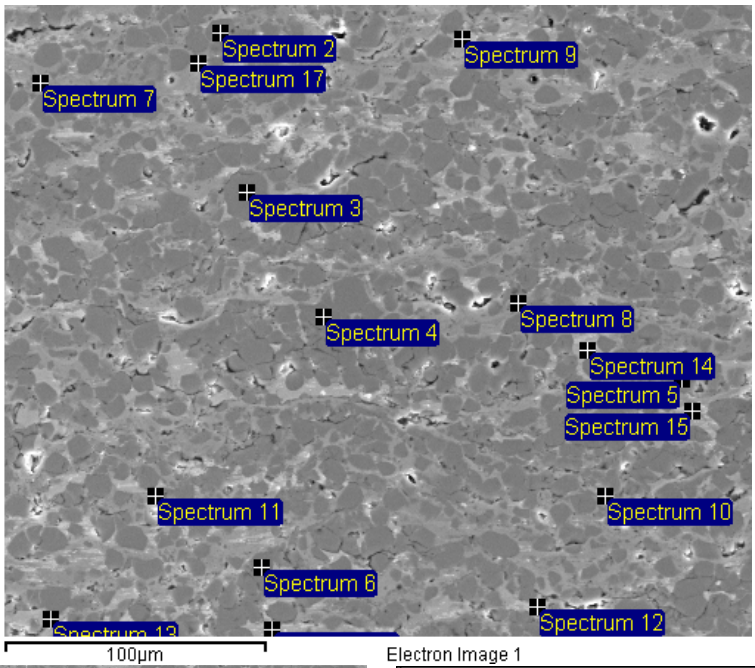
Spectrum 2
Spectrum 9
Spectrum 17
Spectrum 7
Spectrum 3
Spectrum 8
Spectrum 4
Spectrum 14
Spectrum 5
Spectrum 15
Spectrum 11
Spectrum 10
Spectrum 6
Spectrum 12
100µm
Electron Image 1

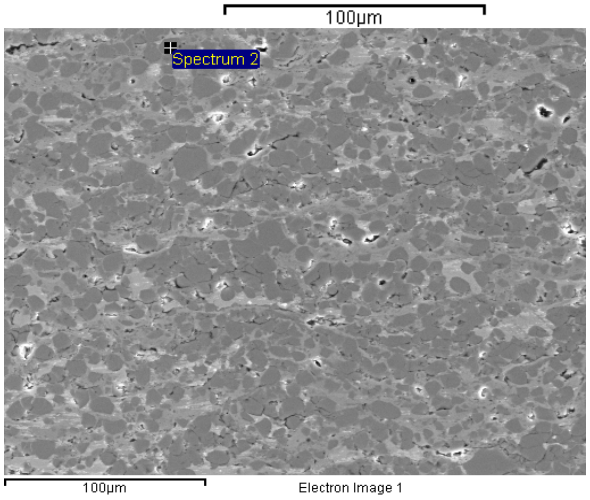
Spectrum 2
100µm
Electron Image 1

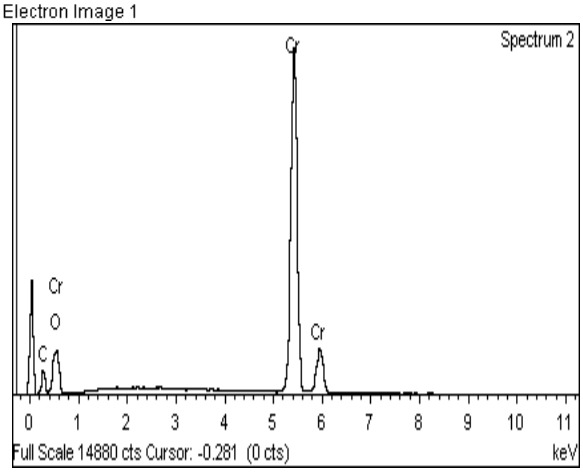
Spectrum 2
Cr
Cr
O
C
Cr
0 1 2 3 4 5 6 7 8 9 10 11
Full Scale 14880 cts Cursor: -0.281 (0 cts)
keV

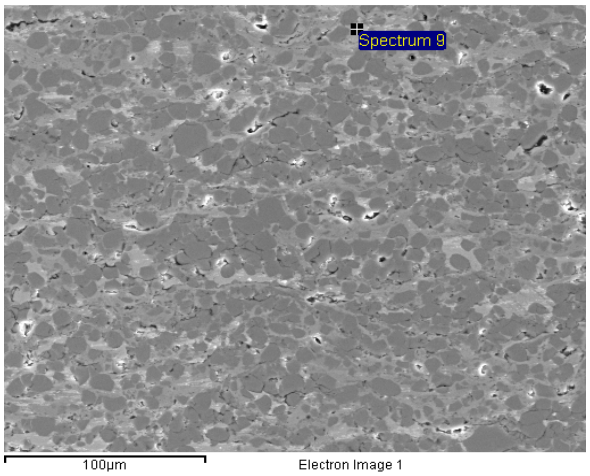
Spectrum 9
100µm
Electron Image 1

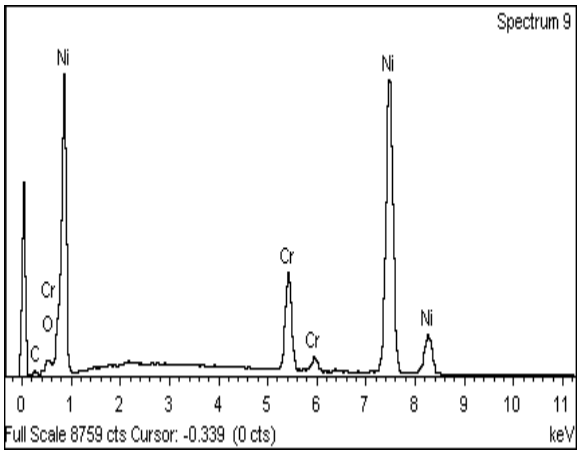
Spectrum 9
Ni
Ni
Cr
Cr
O
C
Cr
Ni
0 1 2 3 4 5 6 7 8 9 10 11
Full Scale 8759 cts Cursor: -0.339 (0 cts)
keV

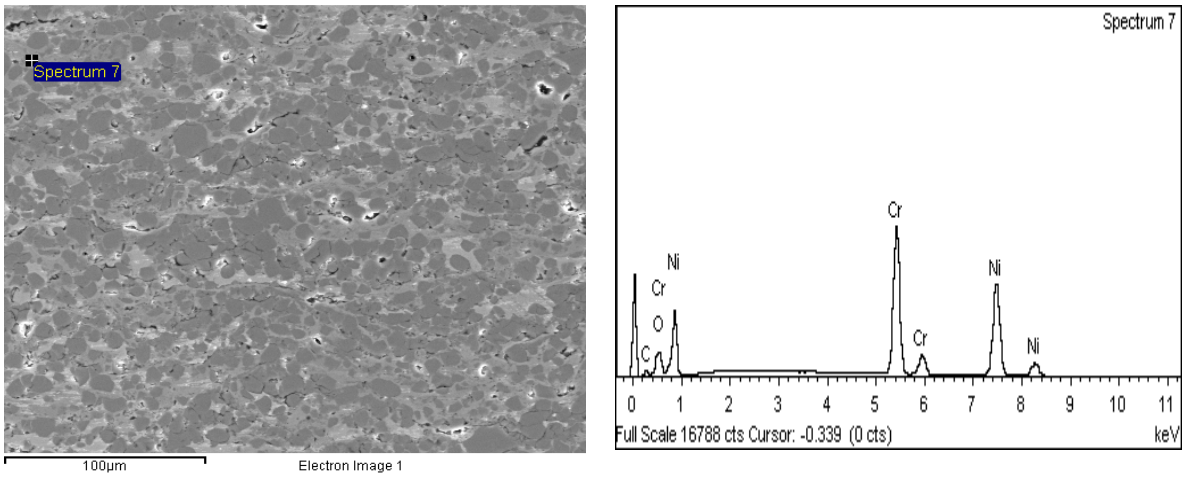

Figure 12. EDS spot analyses on the NiCr-Cr_3C_2 + 15%hBN cross section at different locations. The analysis was done with 20 eV and spot size 5.

Table 3. List of elements and composition identified from the EDS spot analysis done on the NiCr-Cr_3C_2 + 15%hBN cross section. All analyzed elements are normalized and are given in weight %. The elemental composition of the corresponding EDS mapping is seen as sum spectrum in Appendix 3.3. The position of all the spot analyzes can be seen in the EDS spot analysis image in Figure 12.

Spectrum	**C**	**O**	**Cr**	**Ni**	**Total**
Spectrum 2	24.24	5.43	70.34		100.00
Spectrum 3	24.34	4.72	70.94		100.00
Spectrum 4	25.88		74.12		100.00
Spectrum 5	24.10	5.09	70.81		100.00
Spectrum 6	25.79		74.21		100.00
Spectrum 7	11.52	5.86	35.56	47.06	100.00
Spectrum 8	13.64	4.10	33.27	48.99	100.00
Spectrum 9	5.42	1.53	12.22	80.84	100.00
Spectrum 10	10.68	2.71	34.35	52.26	100.00
Spectrum 11	5.64	1.31	12.75	80.30	100.00
Spectrum 12	6.46	1.39	18.14	74.01	100.00
Spectrum 13	6.98	1.41	13.19	78.42	100.00
Spectrum 14	6.34	1.85	12.69	79.12	100.00
Spectrum 15	6.71	1.93	12.83	78.52	100.00
Spectrum 16	11.34	2.00	32.79	53.86	100.00
Spectrum 17	10.72	2.17	22.47	64.64	100.00
Sum Spectrum	4.58		64.21	31.20	100.00
Max.	25.88	5.86	74.21	80.84	
Min.	4.58	1.31	12.22	31.20	

Appendix 3.5

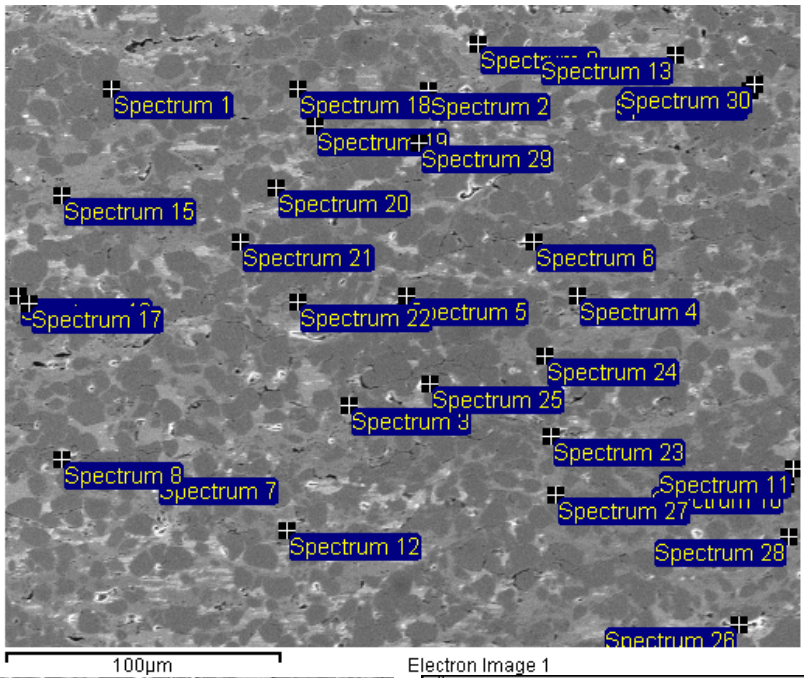
Spectrum 13
Spectrum 1
Spectrum 18
Spectrum 2
Spectrum 30
Spectrum 29
Spectrum 15
Spectrum 20
Spectrum 21
Spectrum 6
Spectrum 17
Spectrum 22
Spectrum 5
Spectrum 4
Spectrum 24
Spectrum 25
Spectrum 23
Spectrum 8
Spectrum 7
Spectrum 11
Spectrum 27
Spectrum 12
Spectrum 28
100µm
Electron Image 1

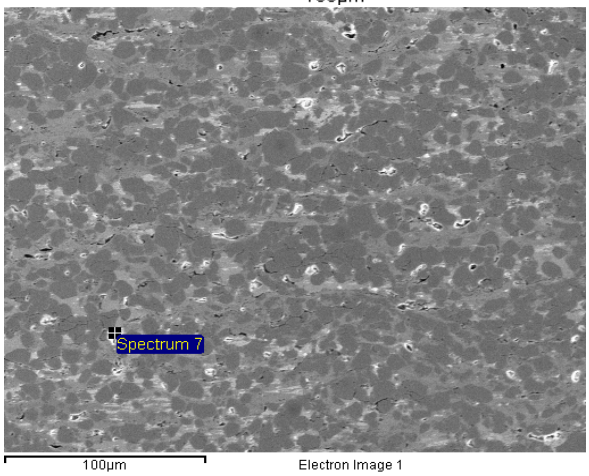
Spectrum 7
100µm
Electron Image 1

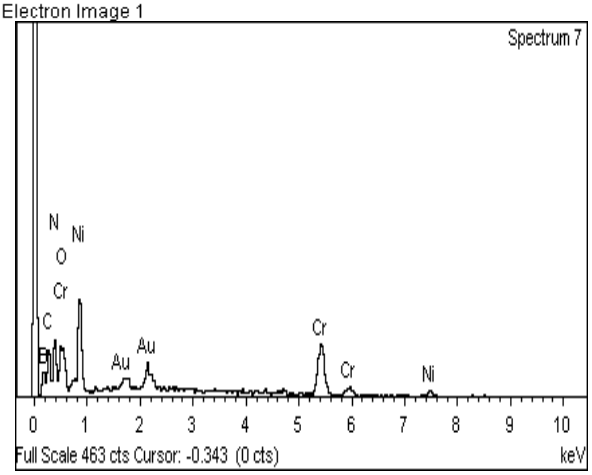
Spectrum 7
N
Ni
O
Cr
C
B
Au
Au
Cr
Cr
Ni
0 1 2 3 4 5 6 7 8 9 10
Full Scale 463 cts Cursor: -0.343 (0 cts)
keV

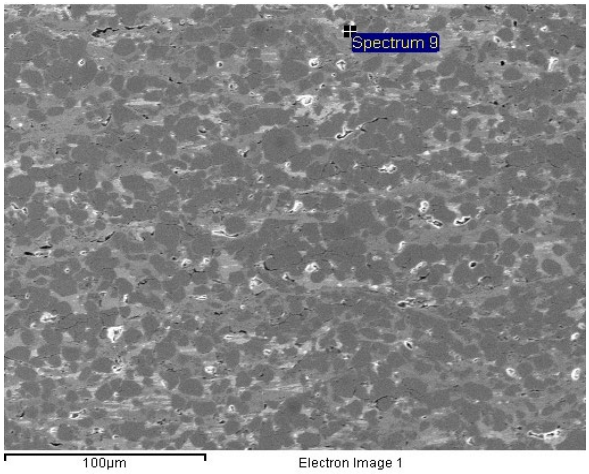
Spectrum 9
100µm
Electron Image 1

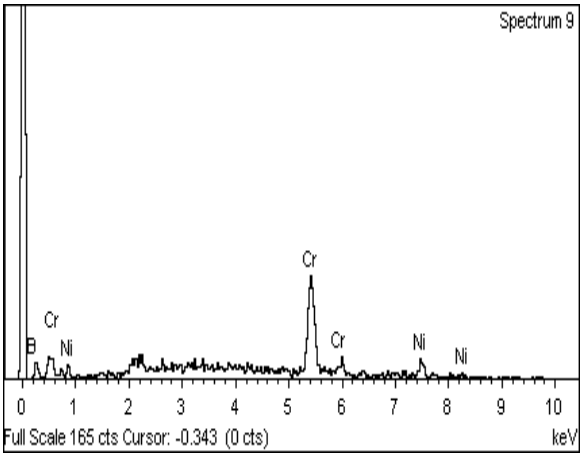
Spectrum 9
Cr
Cr
B
Ni
Cr
Ni
Ni
0 1 2 3 4 5 6 7 8 9 10
Full Scale 165 cts Cursor: -0.343 (0 cts)
keV

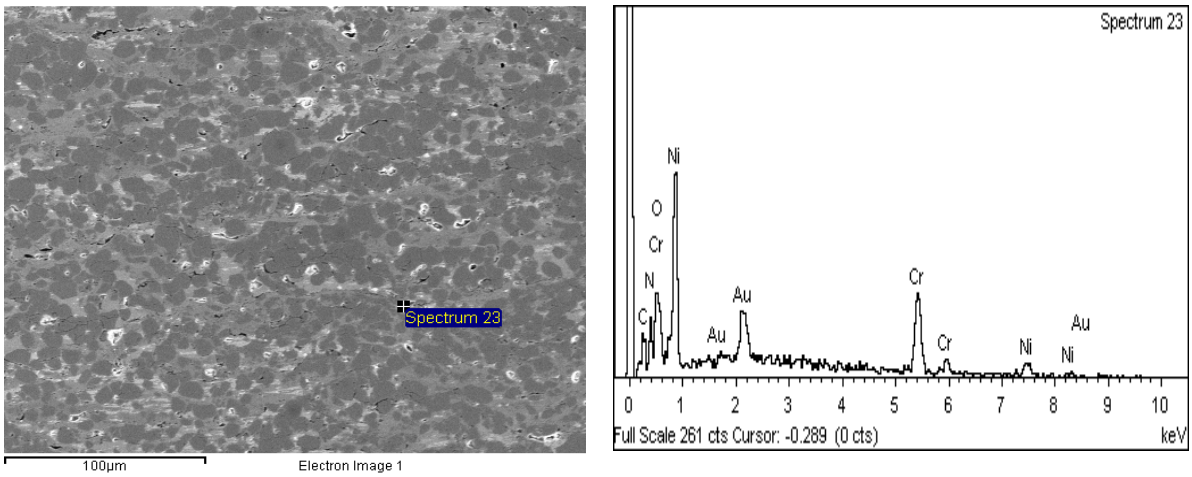

Figure 13. EDS spot analyses on the NiCr-Cr_3C_2 + 15%hBN cross section at different locations. The analysis was done with 10 eV and spot size 4.

Table 4. List of elements and composition identified from the EDS spot analysis done on the NiCr-Cr_3C_2 + 15%hBN cross section. All analyzed elements are normalized and are given in weight %. The position of all the spot analyzes can be seen in the EDS spot analysis image in Figure 13.

Spectrum	B	C	N	O	Cr	Ni	Total
Spectrum 1		48.03		25.52	17.71	8.74	100.00
Spectrum 2		40.30		28.30	21.45	9.95	100.00
Spectrum 3		45.89		34.10	18.96	1.04	100.00
Spectrum 4		57.46		17.13	24.86	0.55	100.00
Spectrum 5		71.39			22.29	6.32	100.00
Spectrum 6		61.55		13.41	25.04		100.00
Spectrum 7	19.72	23.51	40.02	12.07	3.98	0.71	100.00
Spectrum 8		33.32		29.42	34.17	3.09	100.00
Spectrum 9	18.86				58.99	22.15	100.00
Spectrum 10		57.16		17.58	25.25		100.00
Spectrum 11		45.06		22.05	32.89		100.00
Spectrum 12		42.58		30.13	20.13	7.17	100.00
Spectrum 13		37.72		25.86	25.04	11.38	100.00
Spectrum 14		58.29			28.16	13.55	100.00
Spectrum 15		41.88		28.96	19.99	9.17	100.00
Spectrum 16		46.64		25.43	22.48	5.45	100.00
Spectrum 17		43.72		29.22	22.76	4.30	100.00
Spectrum 18		46.30		29.23	17.15	7.33	100.00
Spectrum 19		41.10		32.69	16.82	9.39	100.00
Spectrum 20		61.93			26.22	11.85	100.00
Spectrum 21		51.41			21.22	27.37	100.00
Spectrum 22		47.90		26.97	21.52	3.61	100.00
Spectrum 23		16.69	38.58	27.89	13.12	3.71	100.00
Spectrum 24		67.46			30.13	2.41	100.00
Spectrum 25		49.57		26.17	24.26		100.00
Spectrum 26		41.58			51.71	6.71	100.00
Spectrum 27		59.24			30.36	10.40	100.00
Spectrum 28		64.19			25.28	10.53	100.00
Spectrum 29		40.68		32.41	20.69	6.22	100.00
Spectrum 30		58.56			24.64	16.81	100.00
Max.	19.72	71.39	40.02	34.10	58.99	27.37	
Min.	18.86	16.69	38.58	12.07	3.98	0.55	

Appendix 4.1

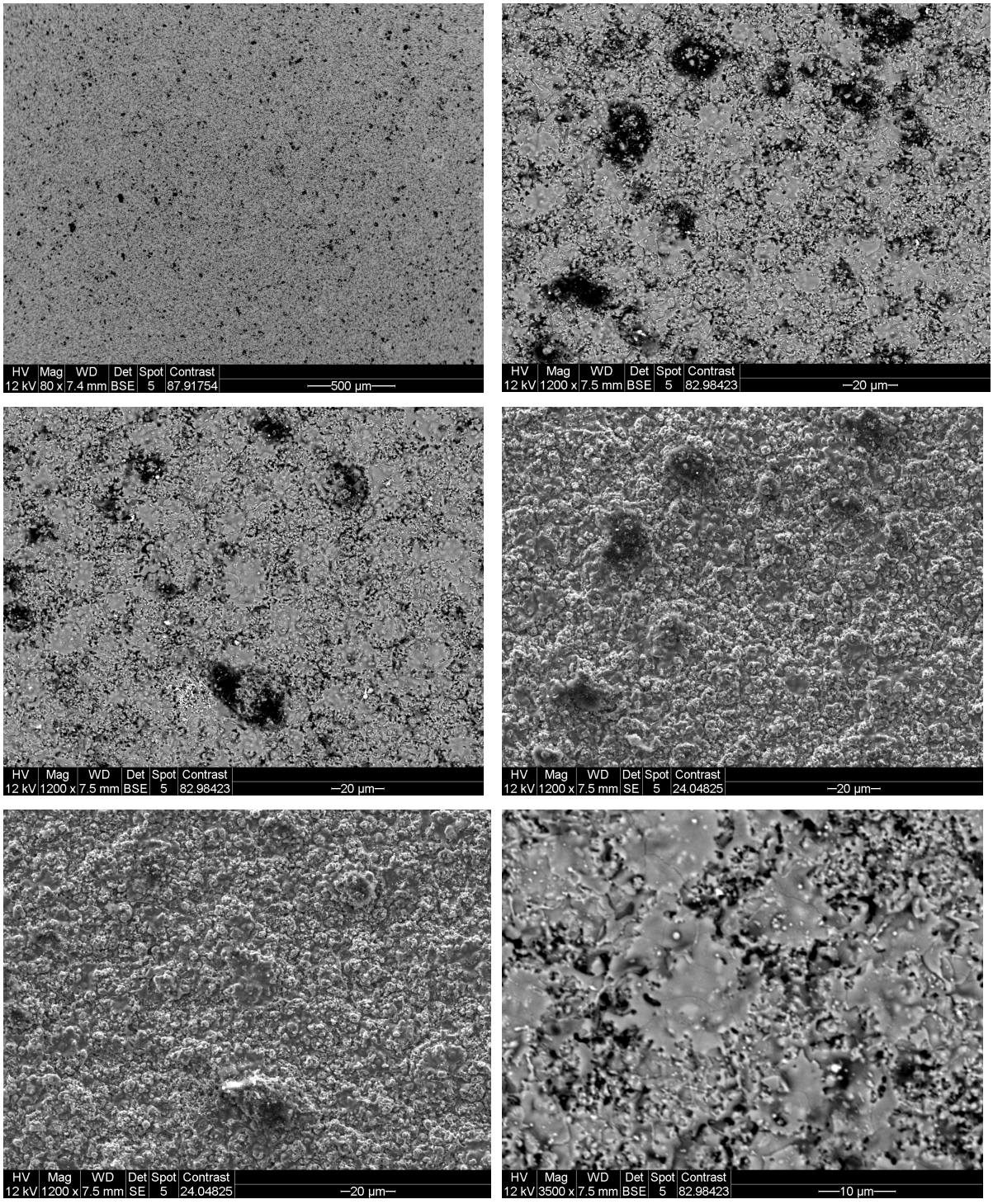

Figure 14. SEM topography images at different magnification and positions on Cr_2O_3 sprayed at a 120 mm spray distance.

Appendix 4.2

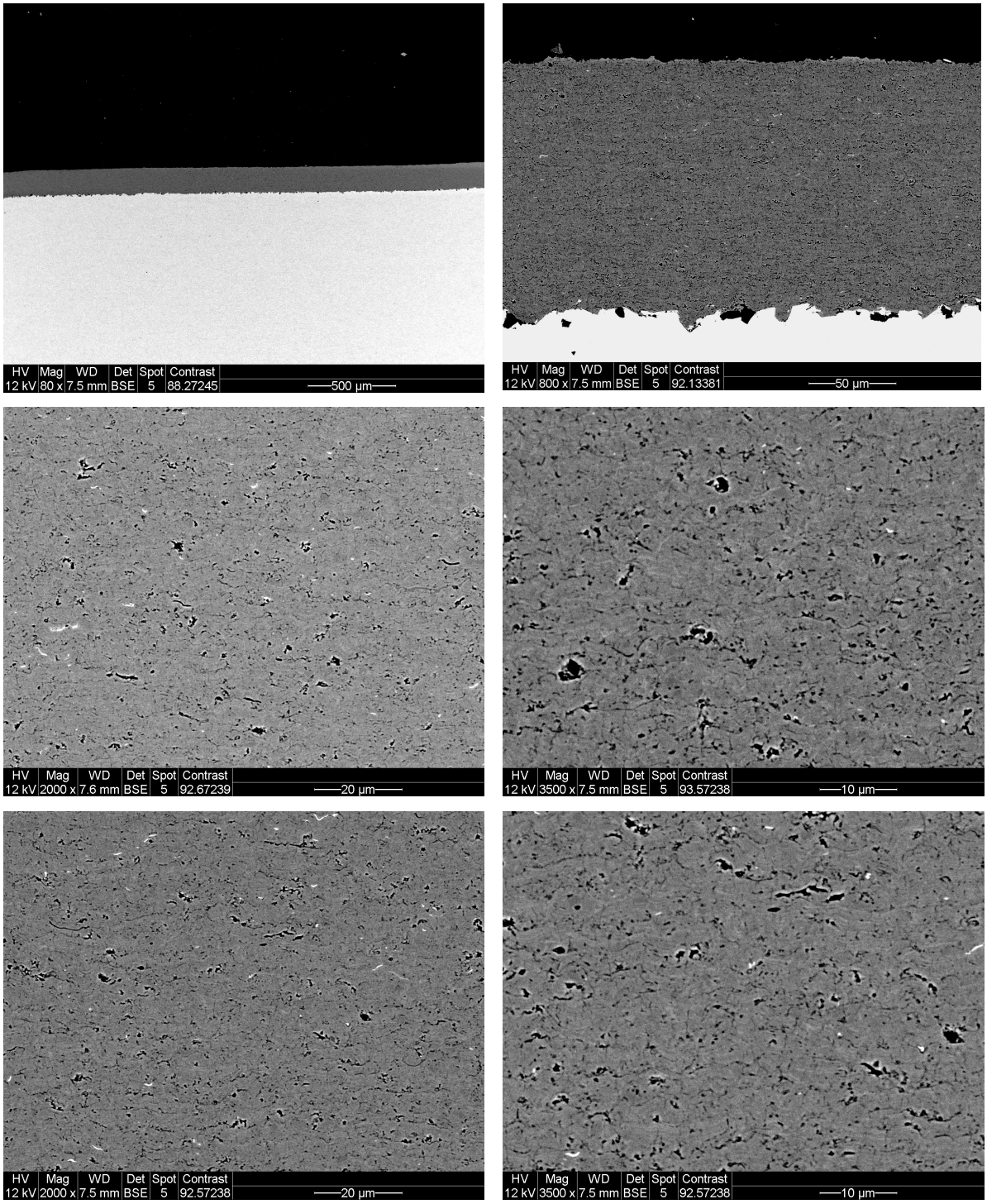

Figure 15. SEM cross section images at different magnification and positions on Cr_2O_3 sprayed at a 120 mm spray distance.

Appendix 4.3

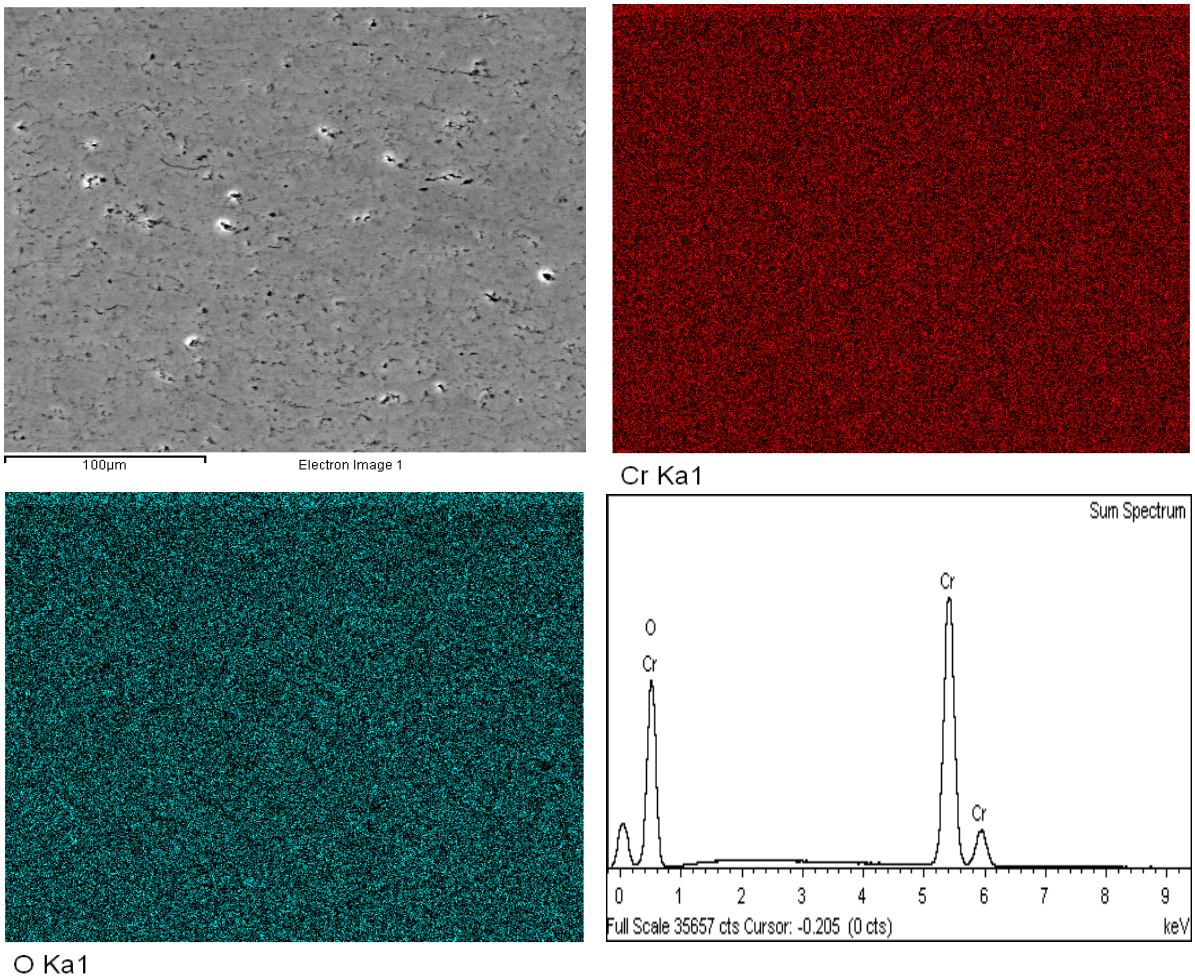

Figure 16. SE and EDS mapping images on the cross section of the Cr_2O_3 coating and the corresponding sum spectra on the analyzed area.

Appendix 4.4

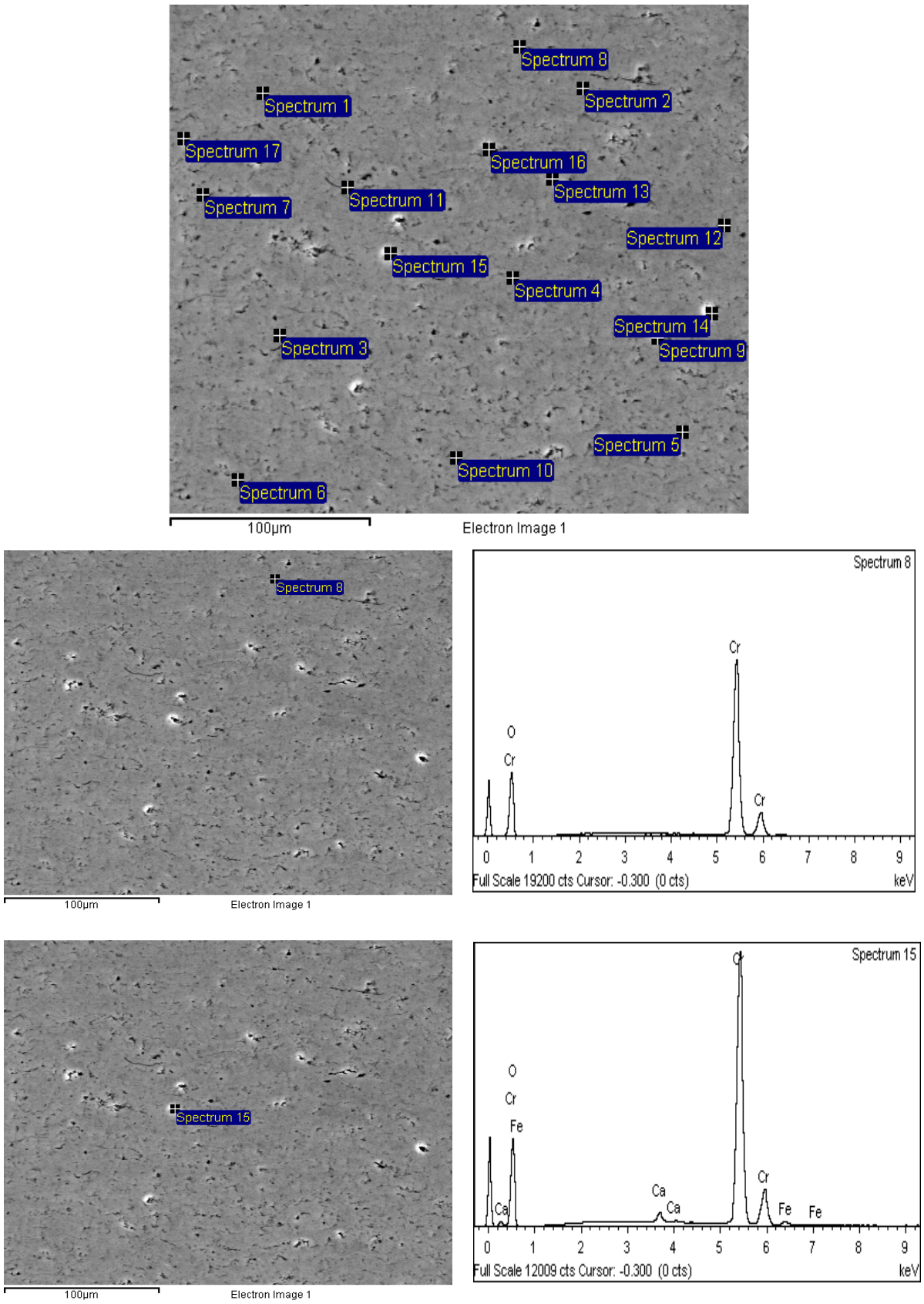

Figure 17. EDS spot analyses on the Cr_2O_3 cross section at different locations. The analysis was done with 20 eV and spot size 5.

Table 5. List of elements and composition identified from the EDS spot analysis done on the Cr_2O_3 cross section. All analyzed elements are normalized and are given in weight %. The position of all the spot analyzes can be seen in the EDS spot analysis image in Figure 17.

Spectrum	**C**	**O**	**Ca**	**Cr**	**Fe**	**Total**
Spectrum 1	1.83	33.90		64.28		100.00
Spectrum 2		34.18		65.82		100.00
Spectrum 3		34.23		65.77		100.00
Spectrum 4		34.72		65.28		100.00
Spectrum 5		34.62		65.38		100.00
Spectrum 6		34.19		65.81		100.00
Spectrum 7		34.78		65.22		100.00
Spectrum 8		19.26		80.74		100.00
Spectrum 9		23.64	1.25	75.11		100.00
Spectrum 10	1.55	35.14		63.32		100.00
Spectrum 11		34.87	2.58	62.55		100.00
Spectrum 12		28.58		71.42		100.00
Spectrum 13		26.58		73.42		100.00
Spectrum 14		18.06		81.94		100.00
Spectrum 15		17.95	1.26	79.20	1.60	100.00
Spectrum 16	1.66	34.40		63.94		100.00
Spectrum 17	1.83	37.09		61.08		100.00
Sum Spectrum		34.04		65.96		100.00
Max.	1.83	37.09	2.58	81.94	1.60	
Min.	1.55	17.95	1.25	61.08	1.60	

Appendix 5.1

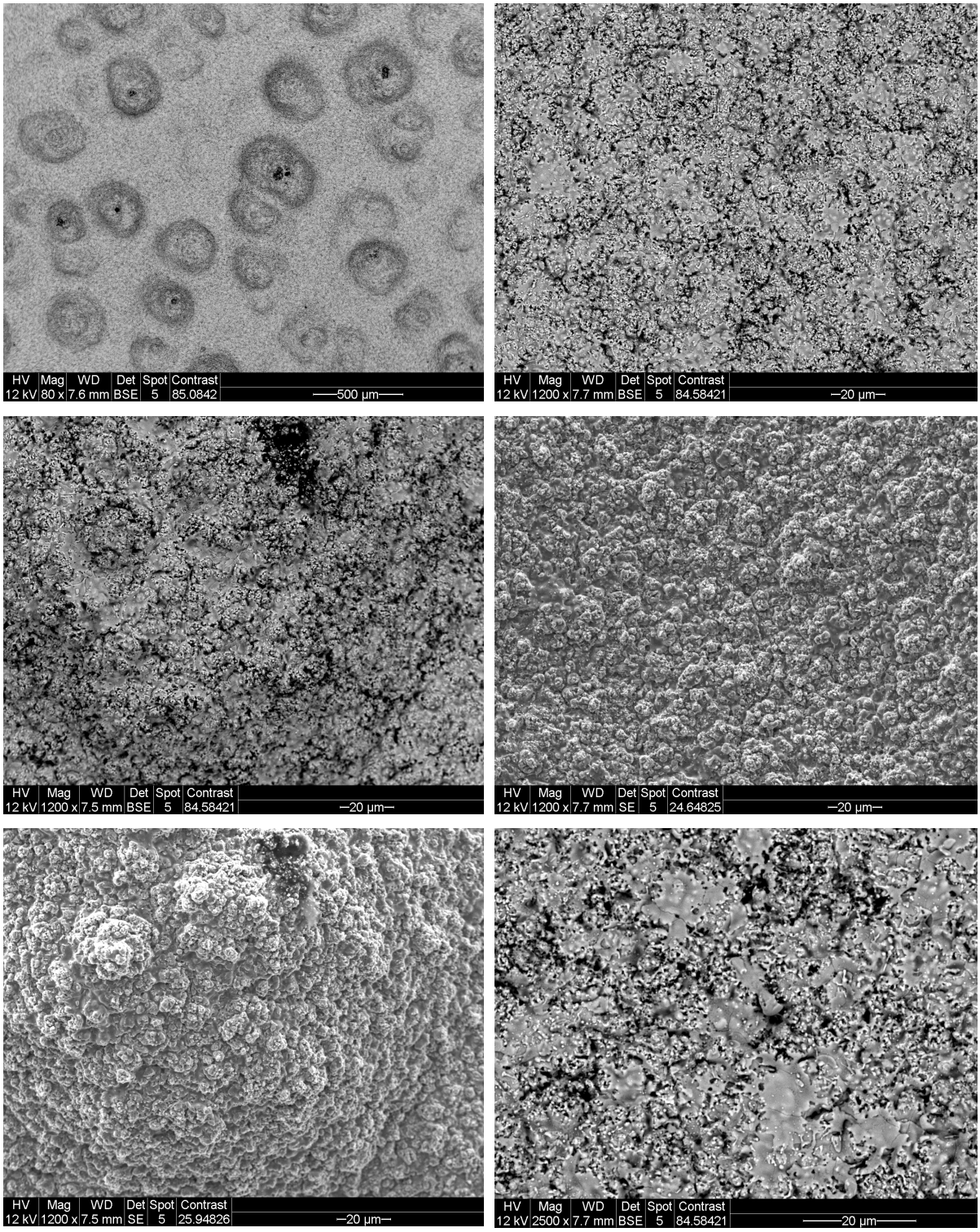

Figure 18. SEM topography images at different magnification and positions on Cr_2O_3 + 5% hBN sprayed at a 100 mm spray distance.

Appendix 5.2

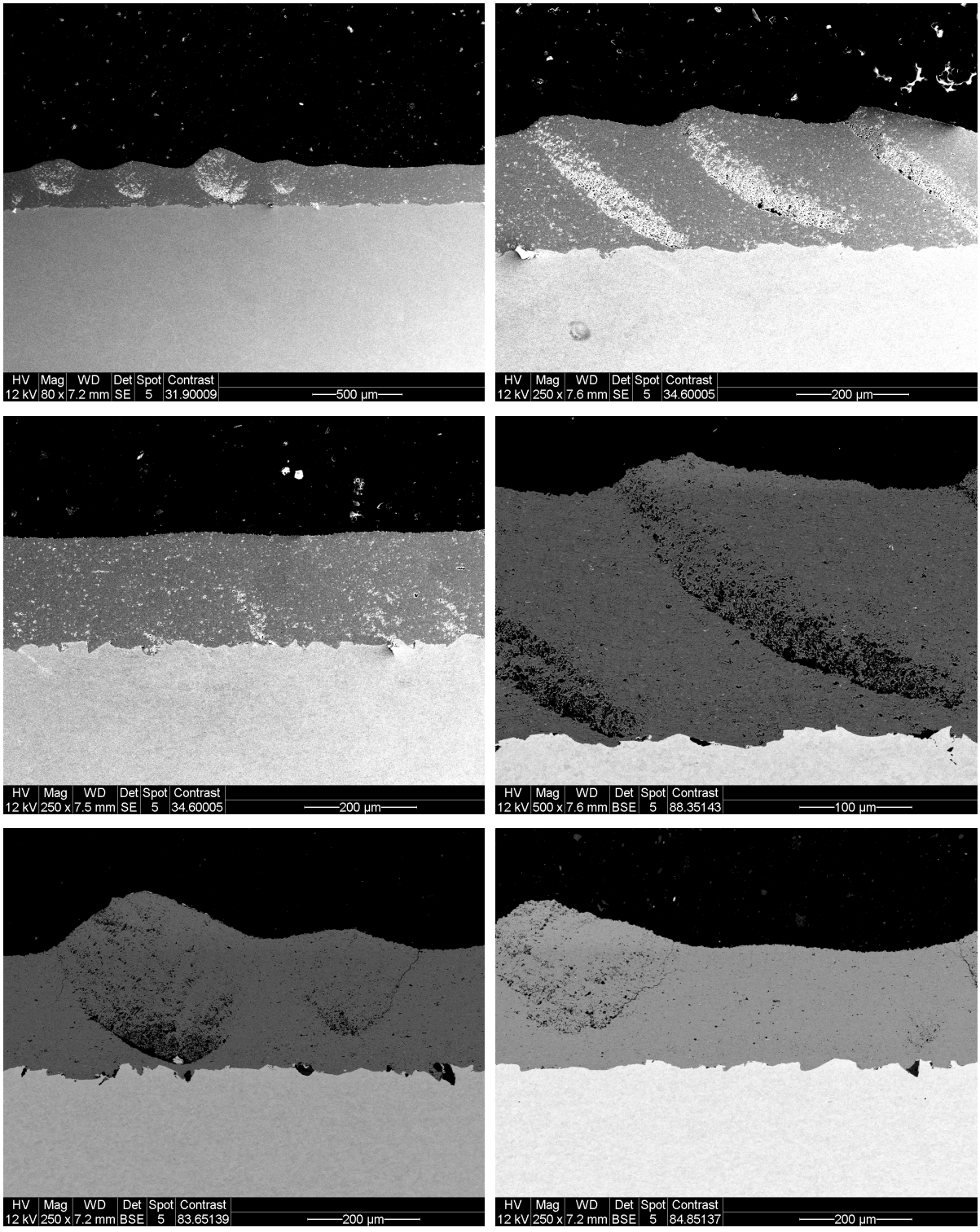
HV Mag WD Det Spot Contrast
12 kV 80 x 7.2 mm SE 5 31.90009
500 µm
HV Mag WD Det Spot Contrast
12 kV 250 x 7.6 mm SE 5 34.60005
200 µm
HV Mag WD Det Spot Contrast
12 kV 250 x 7.5 mm SE 5 34.60005
200 µm
HV Mag WD Det Spot Contrast
12 kV 500 x 7.6 mm BSE 5 88.35143
100 µm
HV Mag WD Det Spot Contrast
12 kV 250 x 7.2 mm BSE 5 83.65139
200 µm
HV Mag WD Det Spot Contrast
12 kV 250 x 7.2 mm BSE 5 84.85137
200 µm

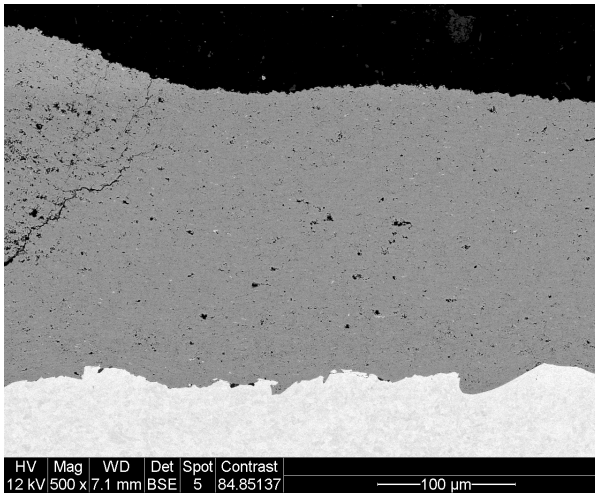
HV Mag WD Det Spot Contrast
12 kV 500 x 7.1 mm BSE 5 84.85137
100 µm

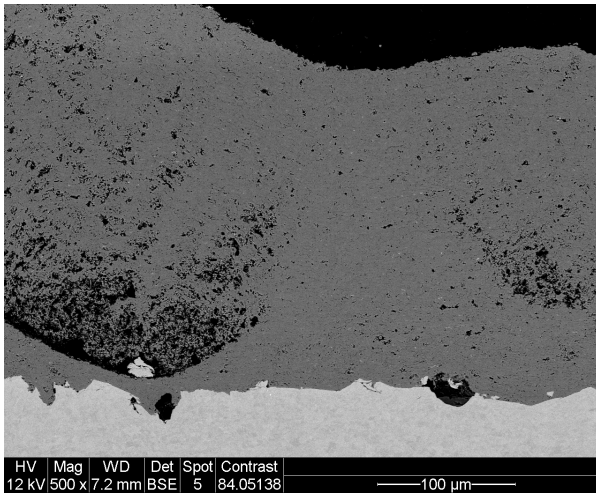
HV Mag WD Det Spot Contrast
12 kV 500 x 7.2 mm BSE 5 84.05138
100 µm

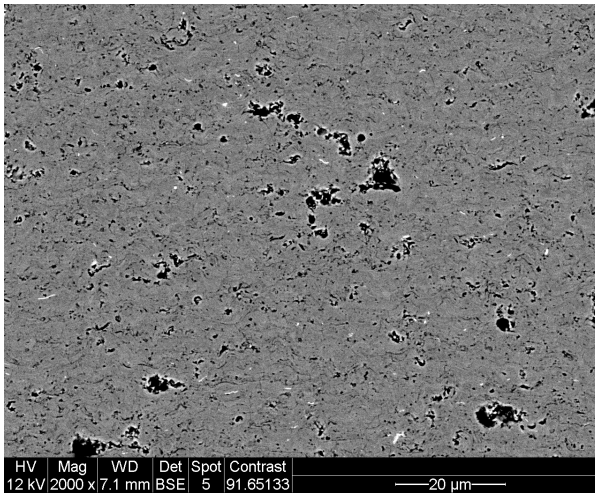
HV Mag WD Det Spot Contrast
12 kV 2000 x 7.1 mm BSE 5 91.65133
20 µm

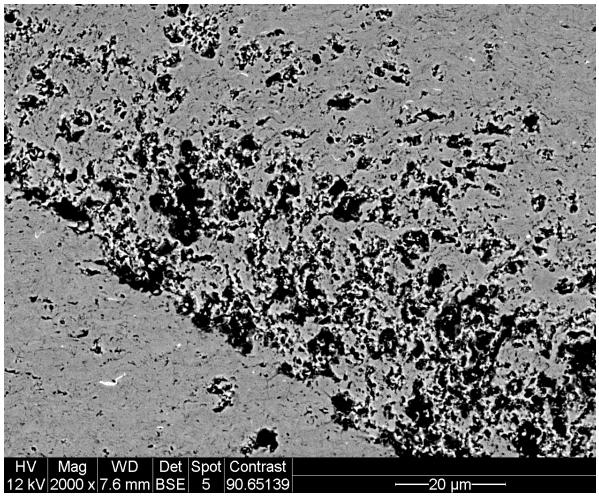
HV Mag WD Det Spot Contrast
12 kV 2000 x 7.6 mm BSE 5 90.65139
20 µm

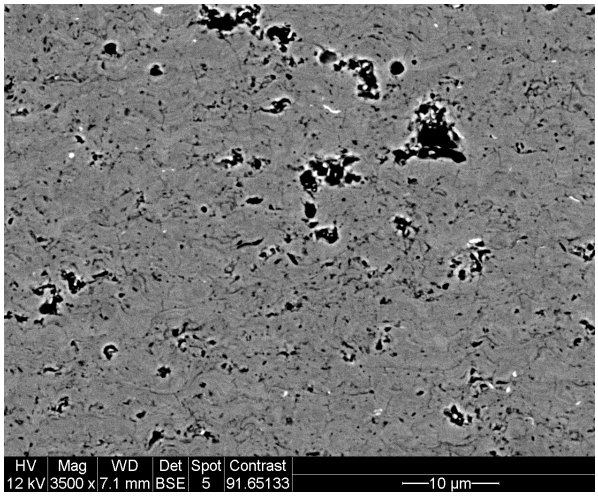
HV Mag WD Det Spot Contrast
12 kV 3500 x 7.1 mm BSE 5 91.65133
10 µm

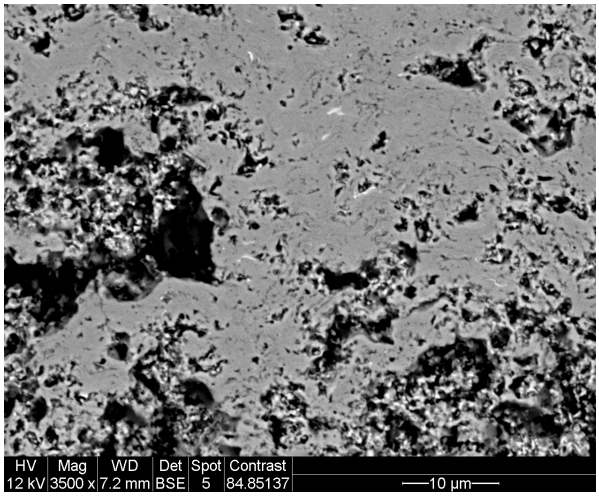
HV Mag WD Det Spot Contrast
12 kV 3500 x 7.2 mm BSE 5 84.85137
10 µm

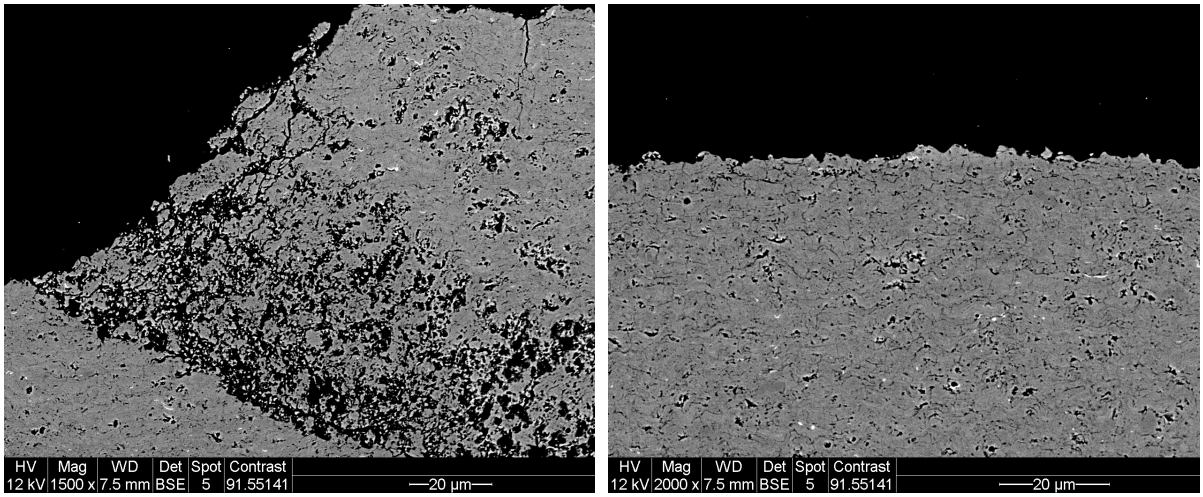

Figure 19. SEM cross section images at different magnification and positions on Cr_2O_3 + 5% hBN sprayed at a 100 mm spray distance.

Appendix 5.3

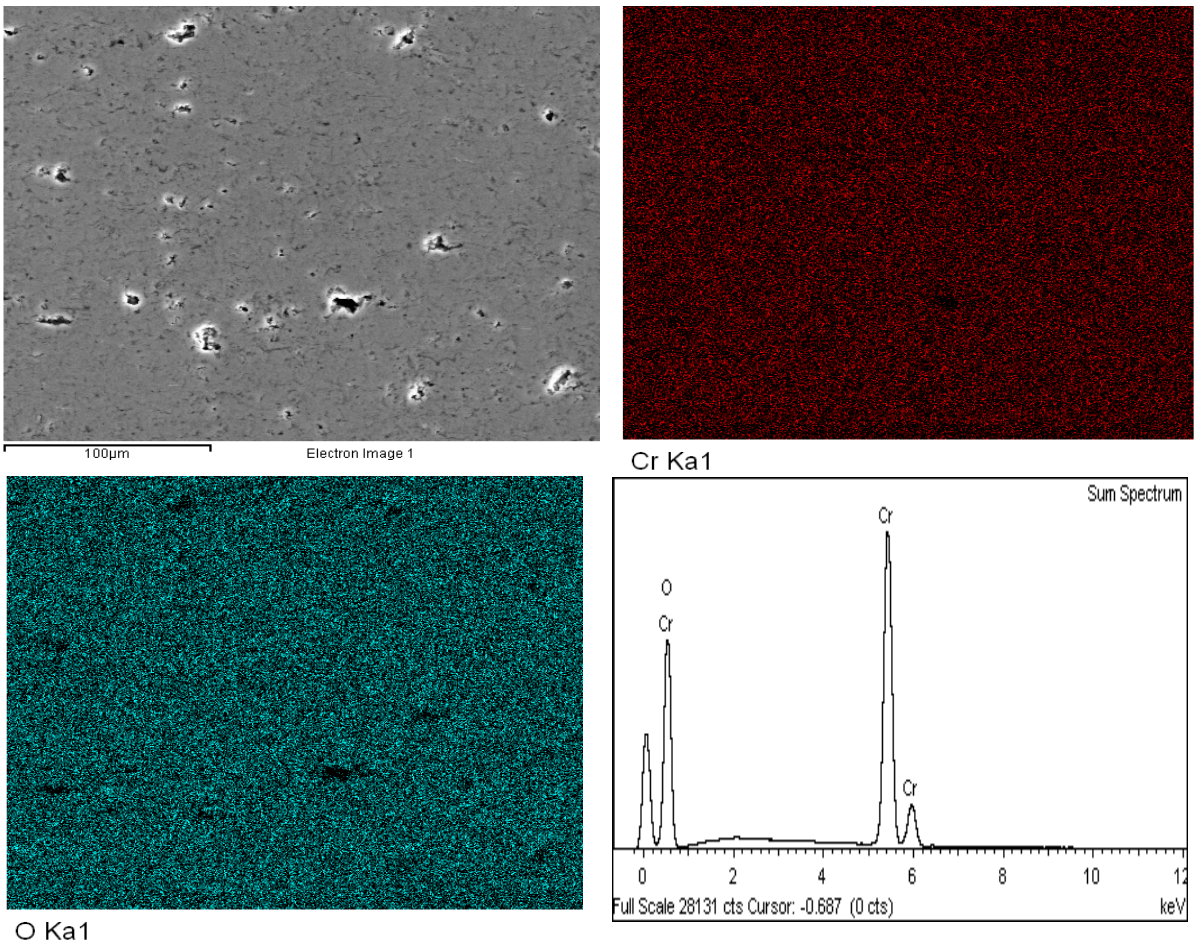

Figure 20. SE and EDS mapping images on the cross section of the Cr_2O_3 + 5% hBN coating (100 mm). The analyze was done with 20 keV and spot size 5.

Appendix 5.4

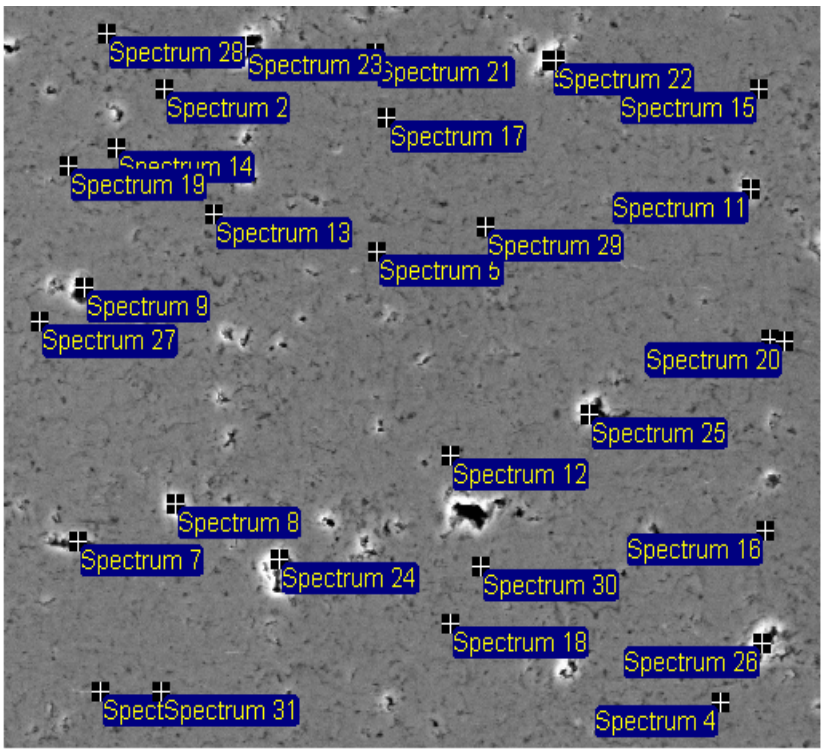

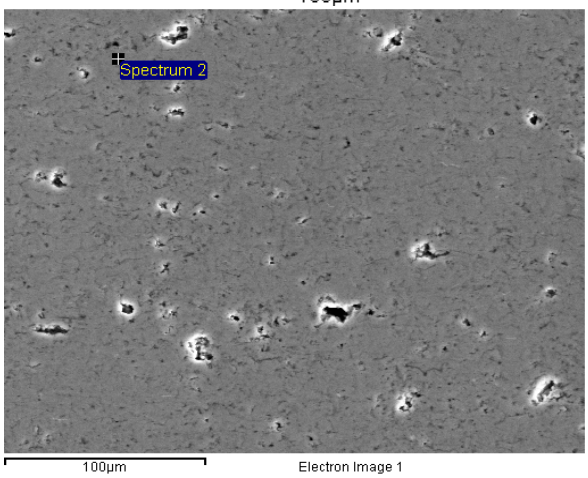

Electron Image 1

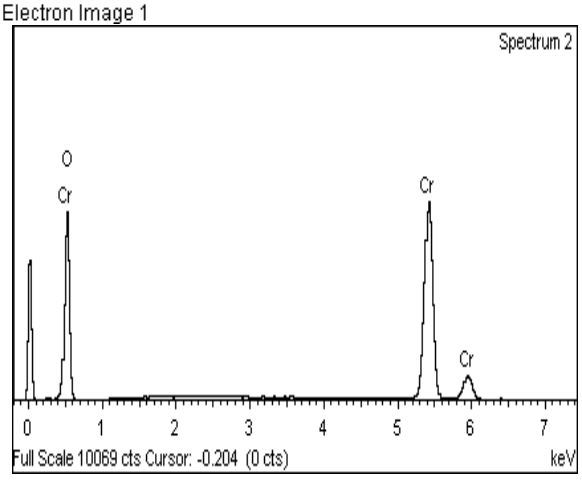

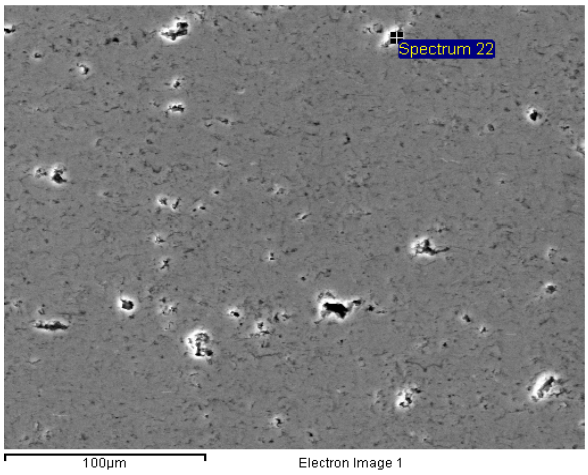

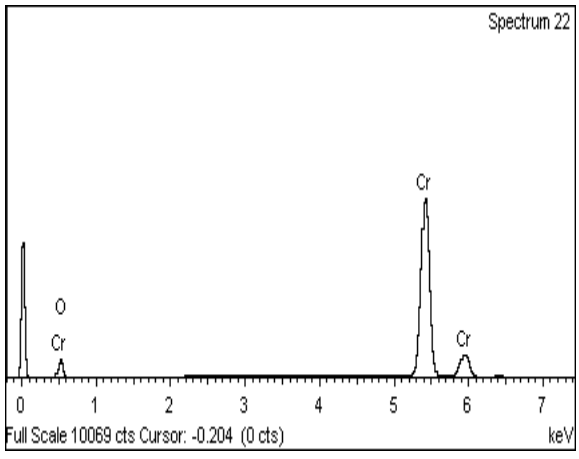

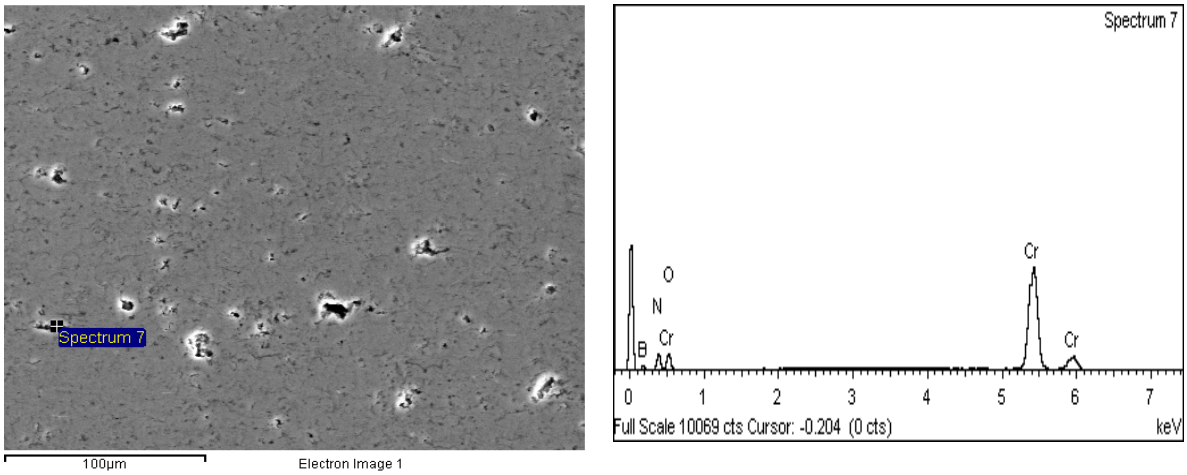

Figure 21. EDS spot analyses on the Cr_2O_3 + 5% hBN (100 mm) cross section at different locations. The analysis was done with 20 eV and spot size 5.

Table 6. List of elements and composition identified from the EDS spot analysis done on the Cr_2O_3 + 5% hBN (100 mm) cross section. All analyzed elements are normalized and are given in weight %. The position of all the spot analyzes can be seen in the EDS spot analysis image in Figure 21.

Spectrum	**B**	**C**	**N**	**O**	**Ca**	**Cr**	**Total**
Spectrum 2				33.27		66.73	100.00
Spectrum 3		1.40		33.71		64.89	100.00
Spectrum 4				34.07		65.93	100.00
Spectrum 5		1.39		32.74		65.87	100.00
Spectrum 6		1.29		33.42		65.29	100.00
Spectrum 7	21.66		19.71	10.81		47.81	100.00
Spectrum 8		2.02		23.12		74.86	100.00
Spectrum 9		2.41		34.35		63.24	100.00
Spectrum 10		1.12		10.32		88.56	100.00
Spectrum 11		2.62		22.26		75.12	100.00
Spectrum 12		1.71		34.04		64.25	100.00
Spectrum 13		1.60		34.40		64.00	100.00
Spectrum 14		1.13		33.60		65.28	100.00
Spectrum 15		1.26		32.14		66.60	100.00
Spectrum 16		1.40		32.65		65.95	100.00
Spectrum 17		1.31		33.30		65.39	100.00
Spectrum 18		1.41		33.85		64.74	100.00
Spectrum 19		1.58		34.20		64.22	100.00
Spectrum 20		1.28		34.35		64.38	100.00
Spectrum 21		1.28		33.42		65.30	100.00
Spectrum 22				5.87		94.13	100.00
Spectrum 23	12.03		8.17	14.23		65.57	100.00
Spectrum 24		2.91		36.14		60.95	100.00
Spectrum 25	9.17		4.45	12.69		73.69	100.00
Spectrum 26		1.90		21.88		76.22	100.00
Spectrum 27		1.59		34.28		64.13	100.00
Spectrum 28		1.35		31.22		67.43	100.00
Spectrum 29				24.03		75.97	100.00
Spectrum 30				32.96		67.04	100.00
Spectrum 31				33.64	0.96	65.40	100.00
Sum Spectrum				33.88		66.12	100.00
Max.	21.66	2.91	19.71	36.14	0.96	94.13	
Min.	9.17	1.12	4.45	5.87	0.96	47.81	

Appendix 5.5

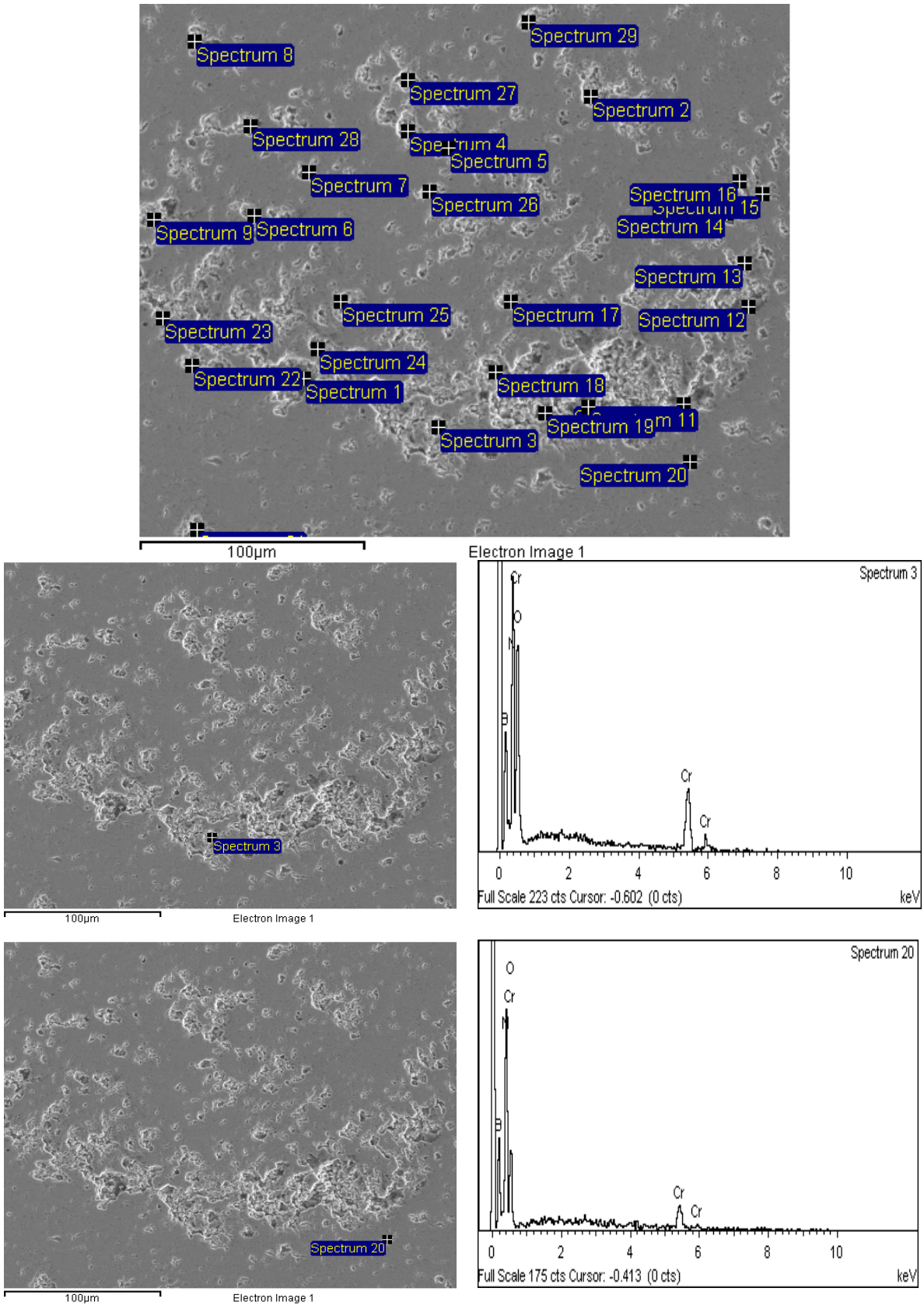

Figure 22. EDS spot analyses on the Cr_2O_3 + 5% hBN (100 mm) cross section at different locations. The analysis was done with 10 eV and spot size 4.

Table 7. List of elements and composition identified from the EDS spot analysis done on the Cr_2O_3 + 5% hBN (100 mm) cross section. All analyzed elements are normalized and are given in weight %. The position of all the spot analyzes can be seen in the EDS spot analysis image in Figure 22.

Spectrum	**B**	**C**	**N**	**O**	**Cr**	**Fe**	**Total**
Spectrum 1		37.15		33.51	29.34		100.00
Spectrum 2		11.16		73.50	15.34		100.00
Spectrum 3	33.78		40.15	23.15	2.92		100.00
Spectrum 4		9.13		72.56	18.31		100.00
Spectrum 5		14.55		40.75	44.71		100.00
Spectrum 6		24.93		55.03	20.04		100.00
Spectrum 7		9.97		69.52	20.51		100.00
Spectrum 8		10.77	7.24	67.69	14.30		100.00
Spectrum 9		6.21	5.38	69.66	18.76		100.00
Spectrum 10	22.89	9.15	46.64	13.71	7.61		100.00
Spectrum 11				18.37	49.44	32.19	100.00
Spectrum 12		51.48		43.42	1.35	3.75	100.00
Spectrum 13		31.89	6.85	53.83	4.39	3.05	100.00
Spectrum 14	27.09	9.70	43.59	16.52	3.10		100.00
Spectrum 15		24.04		65.96	4.40	5.60	100.00
Spectrum 16	15.16	8.47	9.03	59.85	7.49		100.00
Spectrum 17				51.64	48.36		100.00
Spectrum 18		11.61		40.19	48.20		100.00
Spectrum 19		11.58		53.29	35.12		100.00
Spectrum 20	34.07		47.71	16.63	1.59		100.00
Spectrum 21		6.37		70.35	23.27		100.00
Spectrum 22				33.27	66.73		100.00
Spectrum 23		7.69		72.50	19.81		100.00
Spectrum 24			13.01	47.11	39.88		100.00
Spectrum 25				41.31	58.69		100.00
Spectrum 26		8.75		52.37	38.88		100.00
Spectrum 27	26.23		17.26	50.12	6.39		100.00
Spectrum 28		27.05		58.32	14.64		100.00
Spectrum 29				27.30	72.70		100.00
Max.	34.07	51.48	47.71	73.50	72.70	32.19	
Min.	15.16	6.21	5.38	13.71	1.35	3.05	

Appendix 6.1

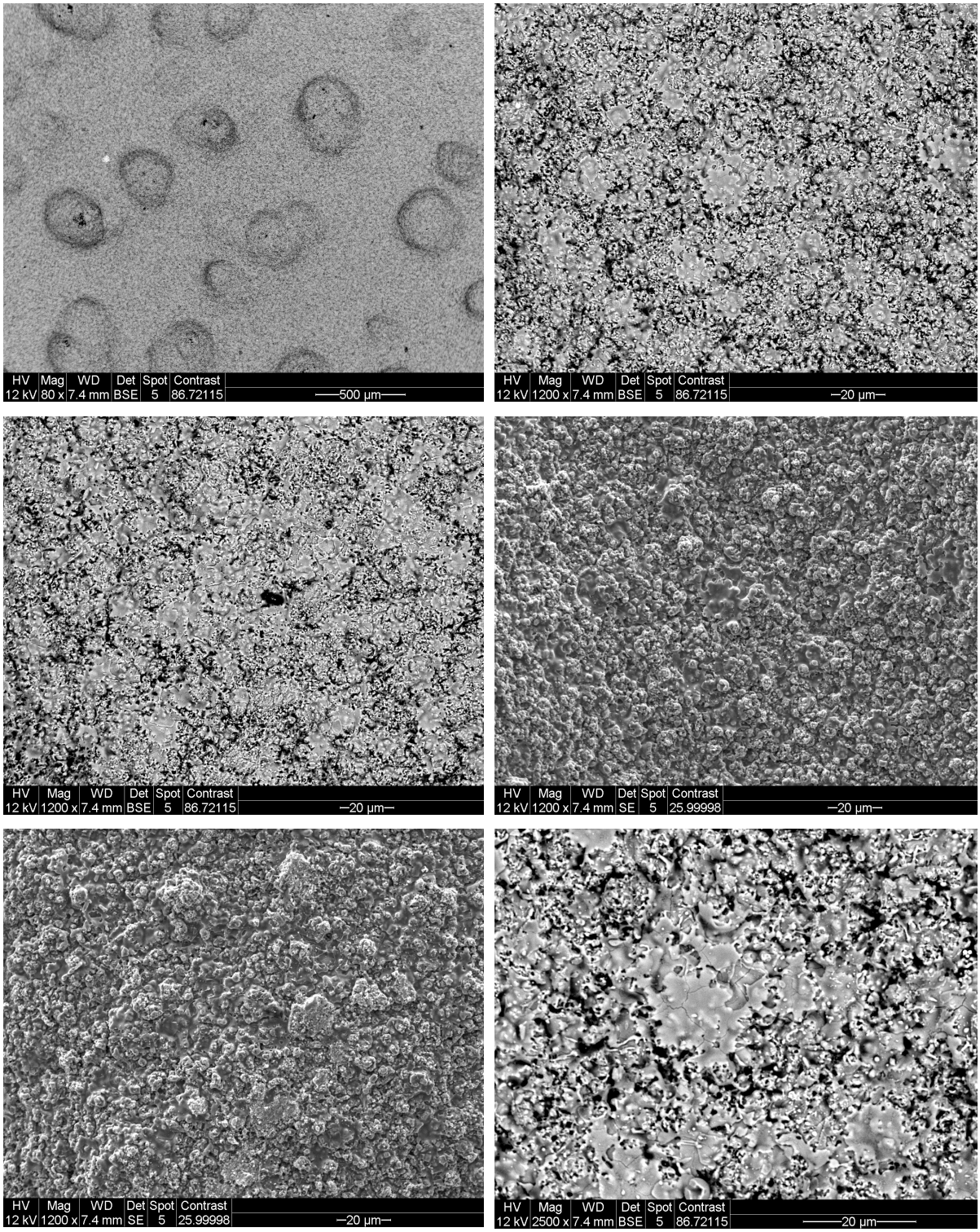

Figure 23. SEM topography images at different magnification and positions on Cr_2O_3 + 5% hBN sprayed at a 110 mm spray distance.

Appendix 6.2

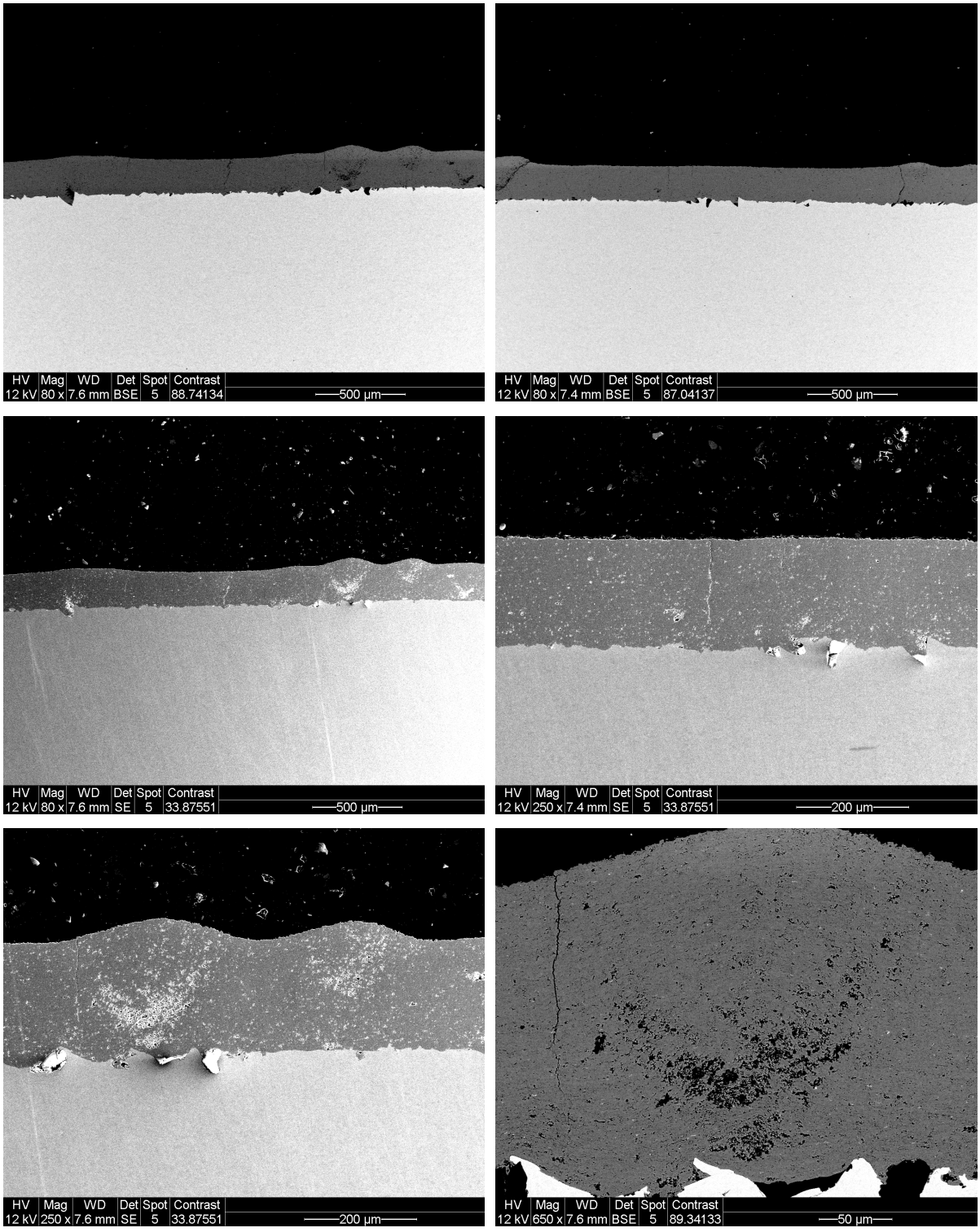
HV Mag WD Det Spot Contrast
12 kV 80 x 7.6 mm BSE 5 88.74134
500 µm
HV Mag WD Det Spot Contrast
12 kV 80 x 7.4 mm BSE 5 87.04137
500 µm
HV Mag WD Det Spot Contrast
12 kV 80 x 7.6 mm SE 5 33.87551
500 µm
HV Mag WD Det Spot Contrast
12 kV 250 x 7.4 mm SE 5 33.87551
200 µm
HV Mag WD Det Spot Contrast
12 kV 250 x 7.6 mm SE 5 33.87551
200 µm
HV Mag WD Det Spot Contrast
12 kV 650 x 7.6 mm BSE 5 89.34133
50 µm

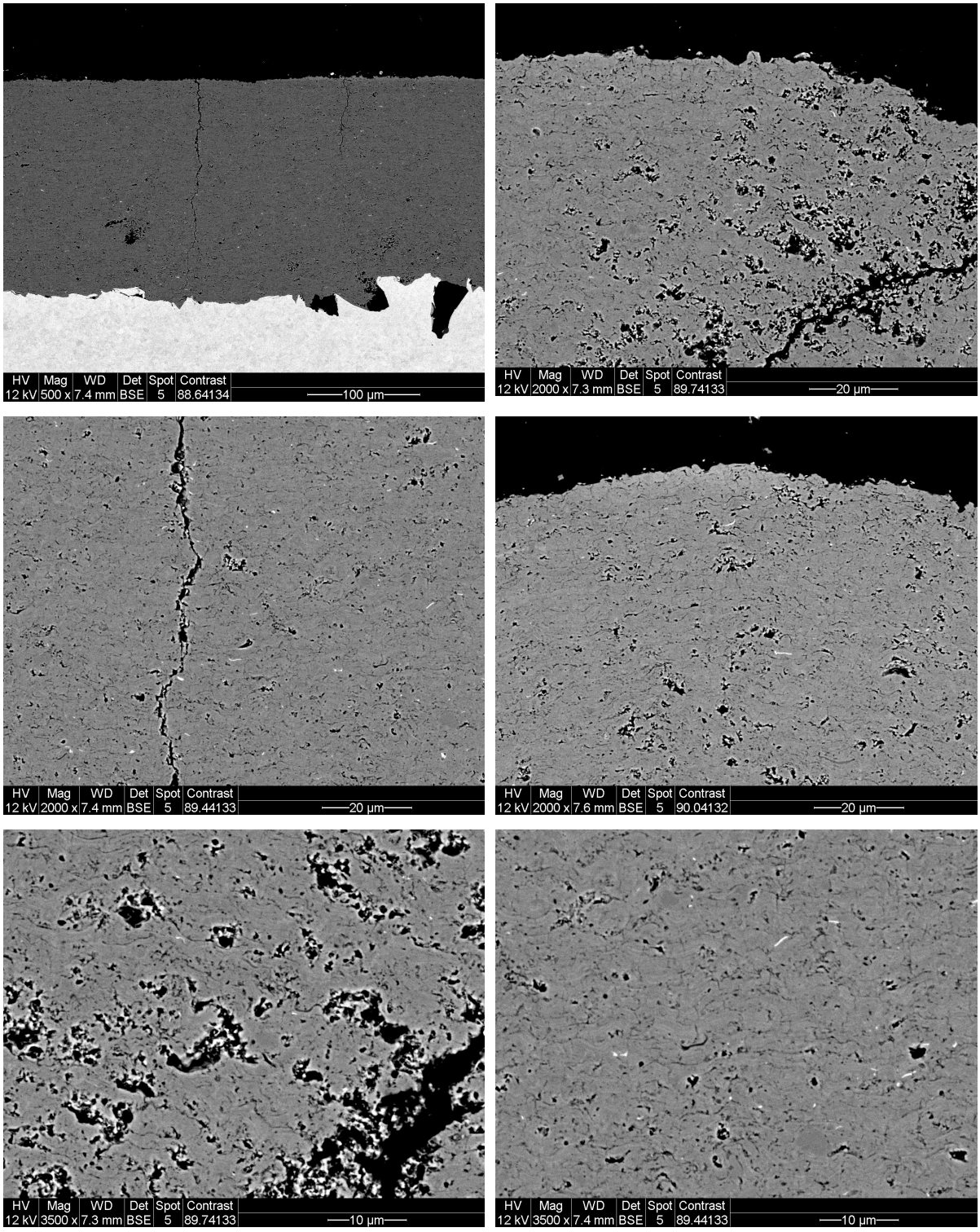

Figure 24. SEM cross section images at different magnification and positions on Cr_2O_3 + 5% hBN sprayed at a 110 mm spray distance.

Appendix 6.3

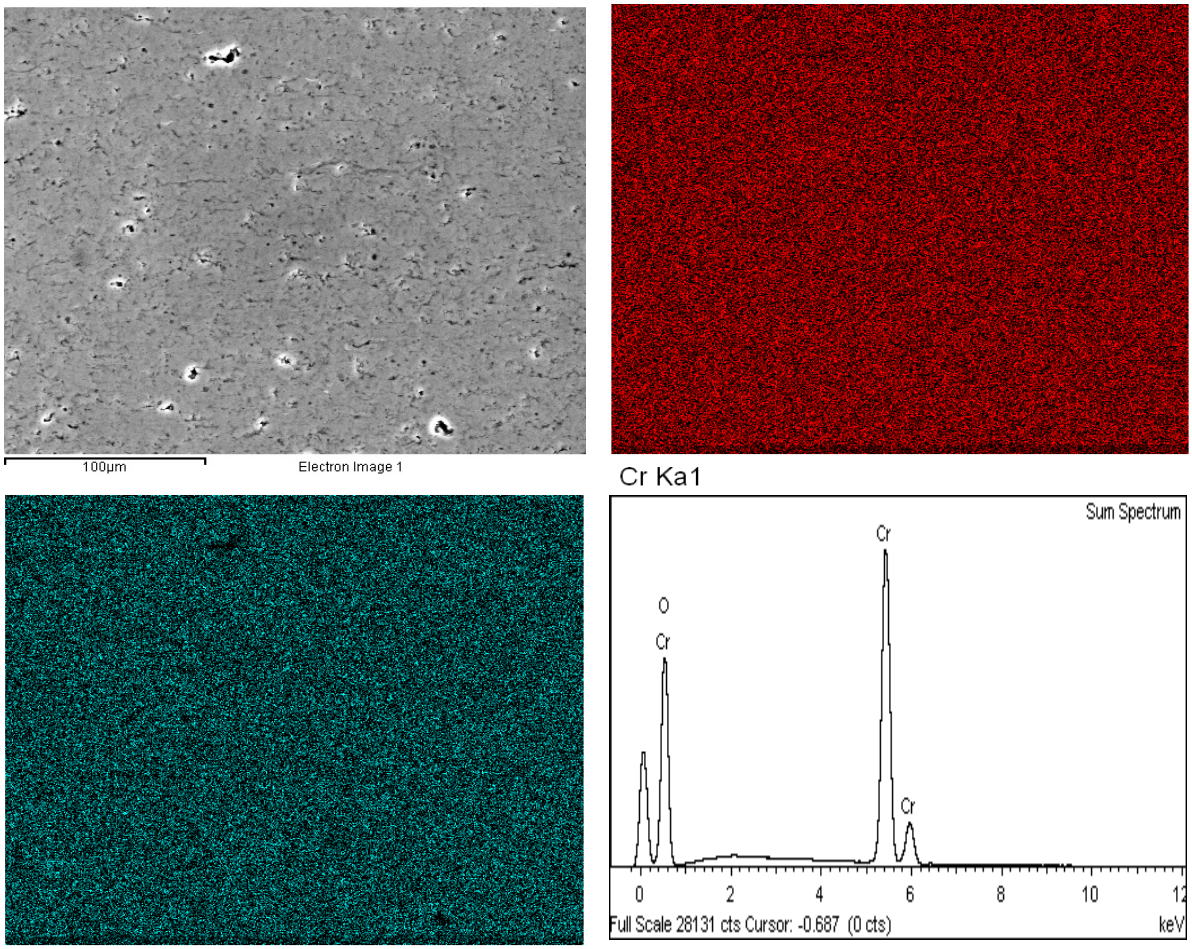

Figure 25. SE and EDS mapping images on the cross section of the Cr_2O_3 + 5%hBN (110 mm) and the sum spectra on corresponding analyzed area. Analysis was done with 20 keV and spot size 5.

Appendix 6.4

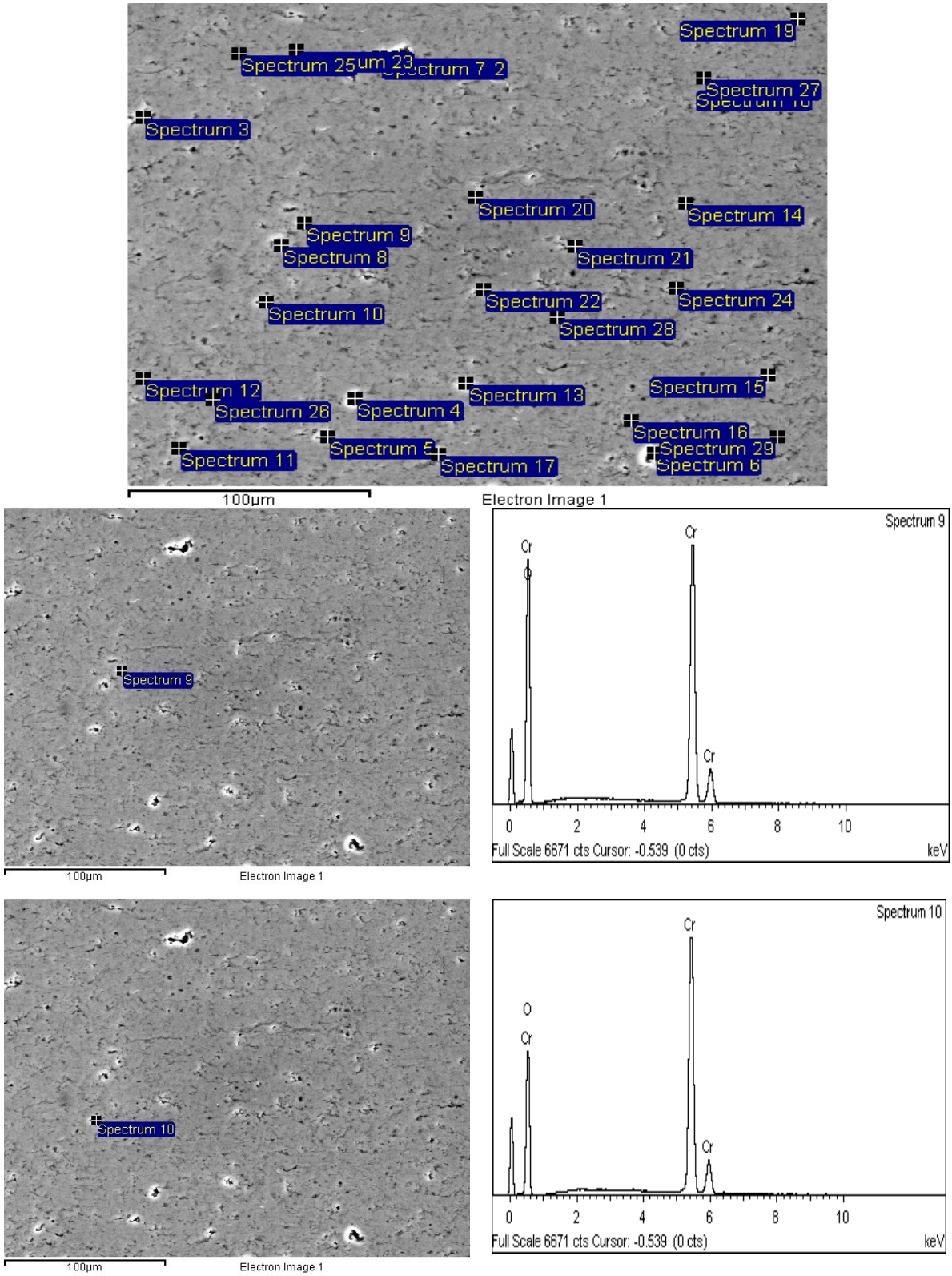

Figure 26. EDS spot analyses on the Cr_2O_3 + 5% hBN (110 mm) cross section at different locations. The analysis was done with 20 eV and spot size 5.

Table 8. List of elements and composition identified from the EDS spot analysis done on the Cr_2O_3 + 5% hBN (110 mm) cross section. All analyzed elements are normalized and are given in weight %. The position of all the spot analyzes can be seen in the EDS spot analysis image in Figure 26.

Spectrum	**B**	**C**	**N**	**O**	**Cr**	**Total**
Spectrum 2				18.31	81.69	100.00
Spectrum 3		2.33		27.46	70.20	100.00
Spectrum 4		2.97		21.49	75.54	100.00
Spectrum 5				29.32	70.68	100.00
Spectrum 6	16.80		9.04	12.83	61.33	100.00
Spectrum 7				8.56	91.44	100.00
Spectrum 8		3.82		35.08	61.10	100.00
Spectrum 9				35.62	64.38	100.00
Spectrum 10				26.57	73.43	100.00
Spectrum 11				24.99	75.01	100.00
Spectrum 12				35.61	64.39	100.00
Spectrum 13				24.50	75.50	100.00
Spectrum 14				33.35	66.65	100.00
Spectrum 15				34.09	65.91	100.00
Spectrum 16				35.05	64.95	100.00
Spectrum 17				33.99	66.01	100.00
Spectrum 18				34.81	65.19	100.00
Spectrum 19				28.18	71.82	100.00
Spectrum 20				29.47	70.53	100.00
Spectrum 21				35.03	64.97	100.00
Spectrum 22				33.61	66.39	100.00
Spectrum 23				35.49	64.51	100.00
Spectrum 24				33.77	66.23	100.00
Spectrum 25				35.04	64.96	100.00
Spectrum 26				36.03	63.97	100.00
Spectrum 27				34.91	65.09	100.00
Spectrum 28				34.99	65.01	100.00
Spectrum 29				36.00	64.00	100.00
Sum Spectrum				35.06	64.94	100.00
Max.	16.80	3.82	9.04	36.03	91.44	
Min.	16.80	2.33	9.04	8.56	61.10	

Appendix 6.5

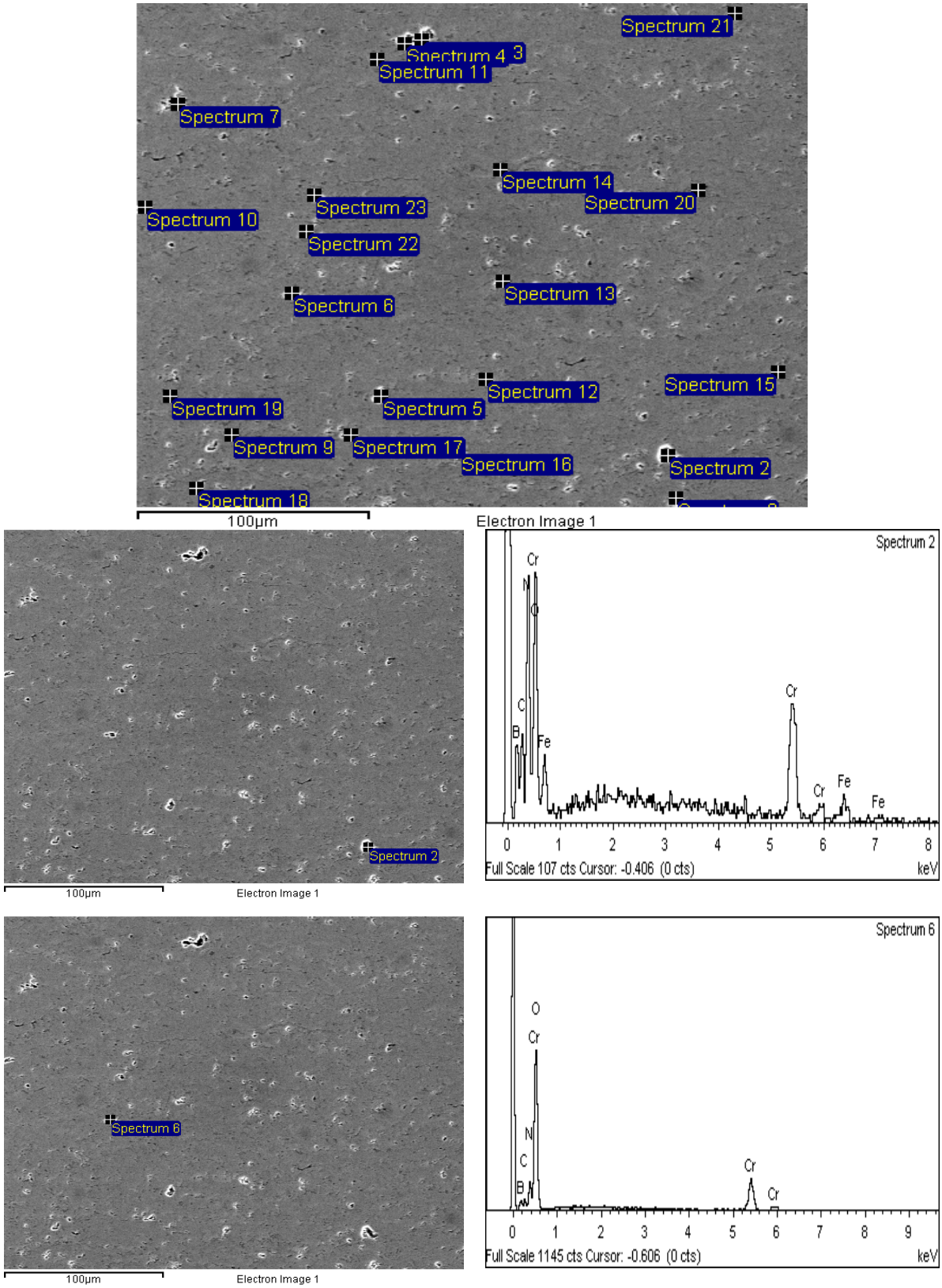

Figure 27. EDS spot analyses on the Cr_2O_3 + 5% hBN (110 mm) cross section at different locations. The analysis was done with 10 eV and spot size 4.

Table 9. List of elements and composition identified from the EDS spot analysis done on the Cr_2O_3 + 5% hBN (110 mm) cross section. All analyzed elements are normalized and are given in weight %. The position of all the spot analyzes can be seen in the EDS spot analysis image in Figure 27.

Spectrum	**B**	**C**	**N**	**O**	**Ca**	**Cr**	**Fe**	**Total**
Spectrum 2	23.60	11.59	34.63	23.97		5.19	1.03	100.00
Spectrum 3	21.16	8.91	26.96	36.65		6.31		100.00
Spectrum 4				69.48		30.52		100.00
Spectrum 5		9.31		65.51		25.19		100.00
Spectrum 6	18.77	7.81	16.29	49.87		7.26		100.00
Spectrum 7		7.75		57.60		34.66		100.00
Spectrum 8		5.05		71.75		23.19		100.00
Spectrum 9		5.69		72.90		21.41		100.00
Spectrum 10		5.14		71.55		23.31		100.00
Spectrum 11		3.56		73.68		22.75		100.00
Spectrum 12		4.82		72.69		22.49		100.00
Spectrum 13				72.37		27.63		100.00
Spectrum 14		4.99		72.93	2.56	19.53		100.00
Spectrum 15				70.48		29.52		100.00
Spectrum 16				67.54		32.46		100.00
Spectrum 17				71.56		28.44		100.00
Spectrum 18				71.21		28.79		100.00
Spectrum 19				72.13		27.87		100.00
Spectrum 20				71.89		28.11		100.00
Spectrum 21				73.75		26.25		100.00
Spectrum 22				74.99		25.01		100.00
Spectrum 23		5.48		73.98		20.54		100.00
Max.	23.60	11.59	34.63	74.99	2.56	34.66	1.03	
Min.	18.77	3.56	16.29	23.97	2.56	5.19	1.03	

.

Appendix 7.1

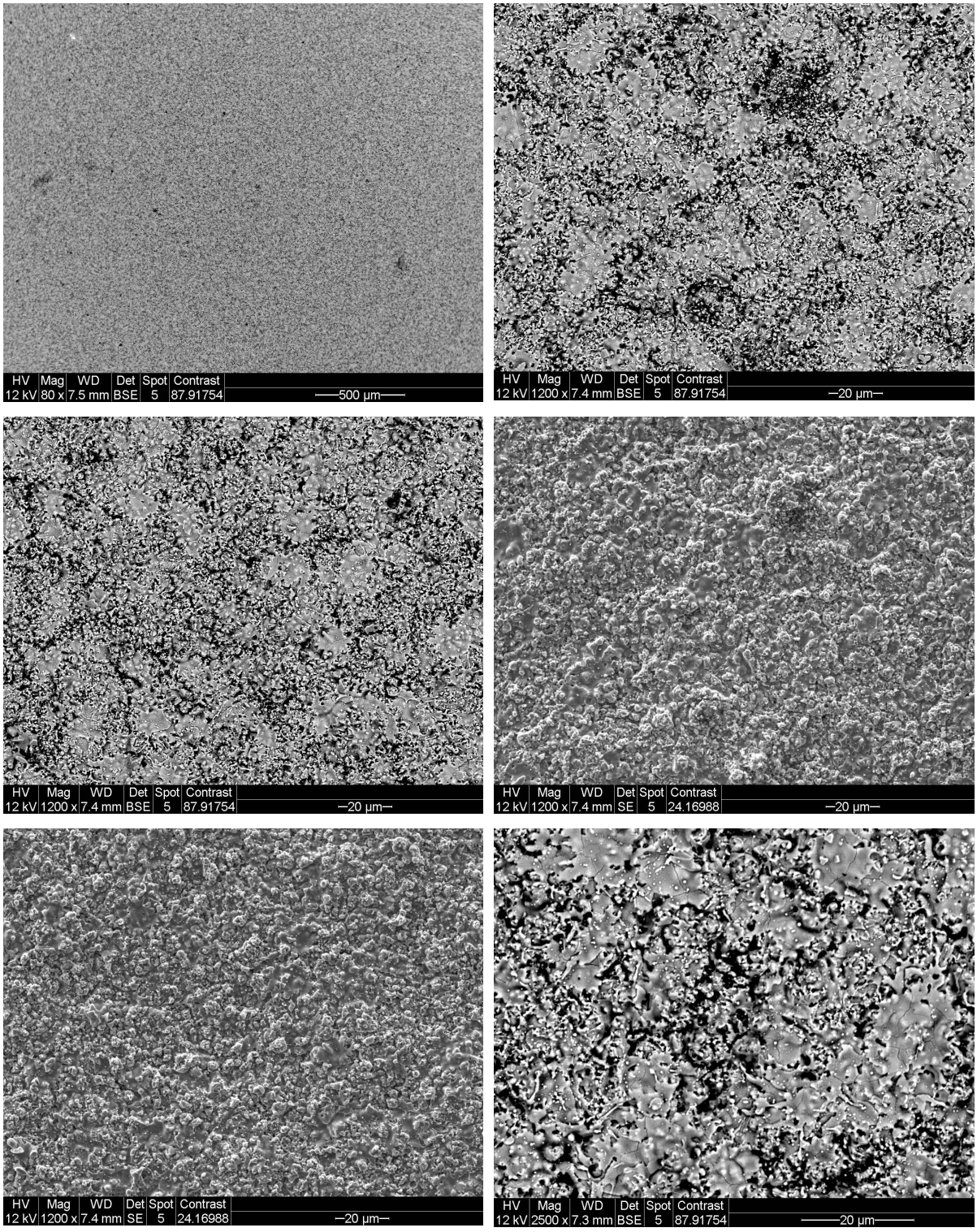

Figure 28. SEM topography images at different magnitudes and positions of Cr_2O_3 + 5% hBN sprayed at a 130 mm spray distance.

Appendix 7.2

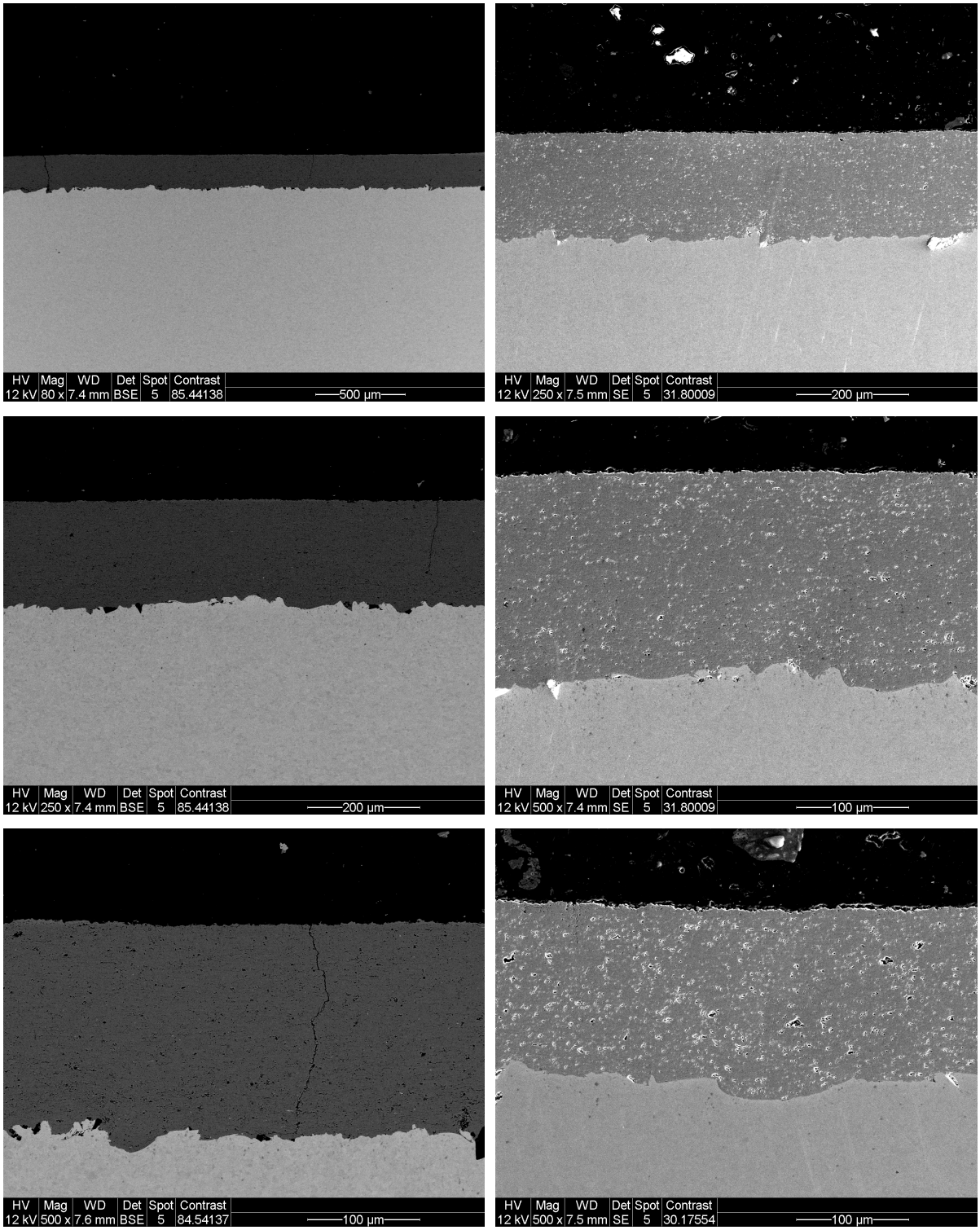
HV Mag WD Det Spot Contrast
12 kV 80 x 7.4 mm BSE 5 85.44138
500 µm
HV Mag WD Det Spot Contrast
12 kV 250 x 7.5 mm SE 5 31.80009
200 µm
HV Mag WD Det Spot Contrast
12 kV 250 x 7.4 mm BSE 5 85.44138
200 µm
HV Mag WD Det Spot Contrast
12 kV 500 x 7.4 mm SE 5 31.80009
100 µm
HV Mag WD Det Spot Contrast
12 kV 500 x 7.6 mm BSE 5 84.54137
100 µm
HV Mag WD Det Spot Contrast
12 kV 500 x 7.5 mm SE 5 30.17554
100 µm

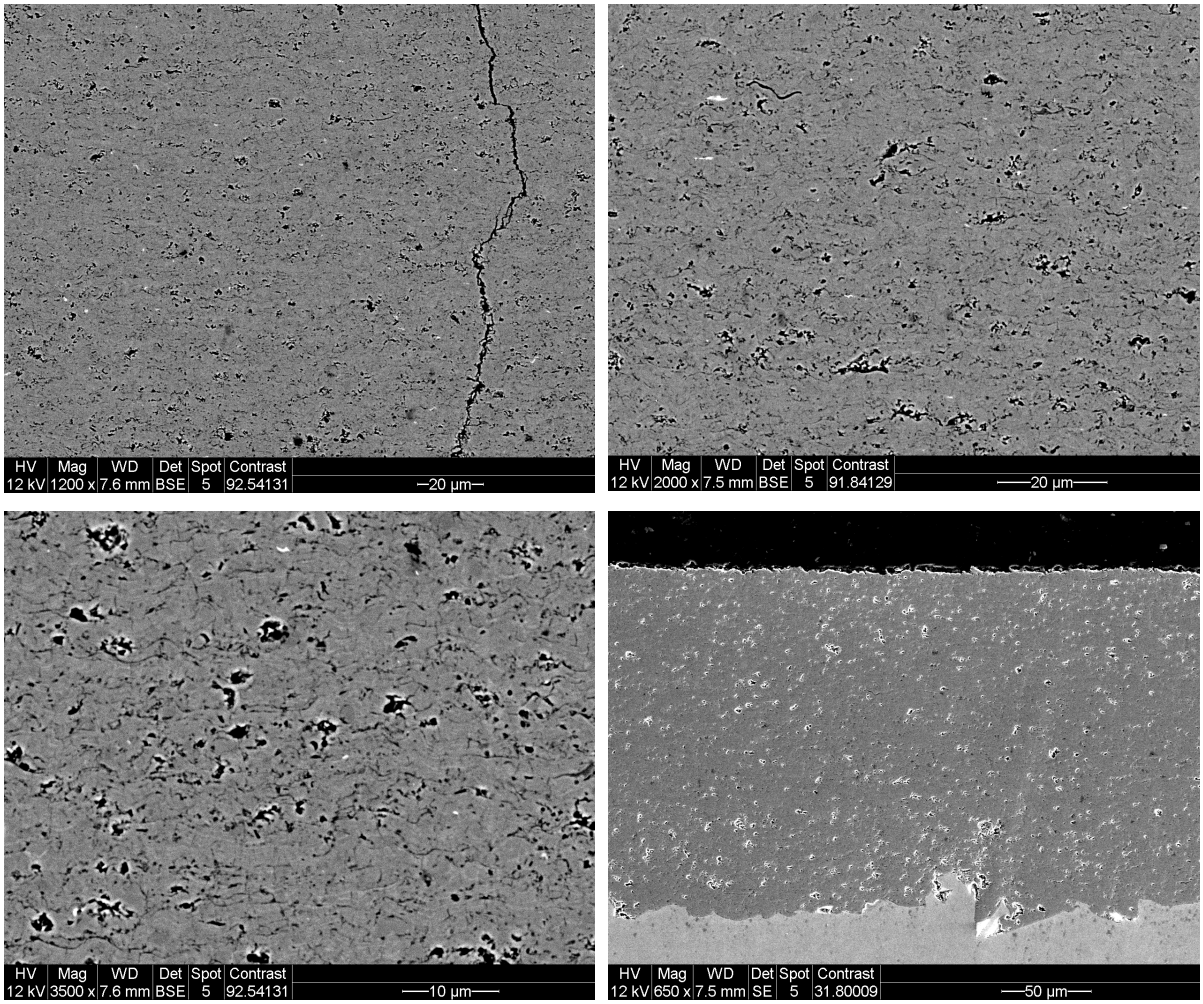

Figure 29. SEM cross section images at different magnification and positions on Cr_2O_3 + 5% hBN sprayed at a 130 mm spray distance.

Appendix 7.3

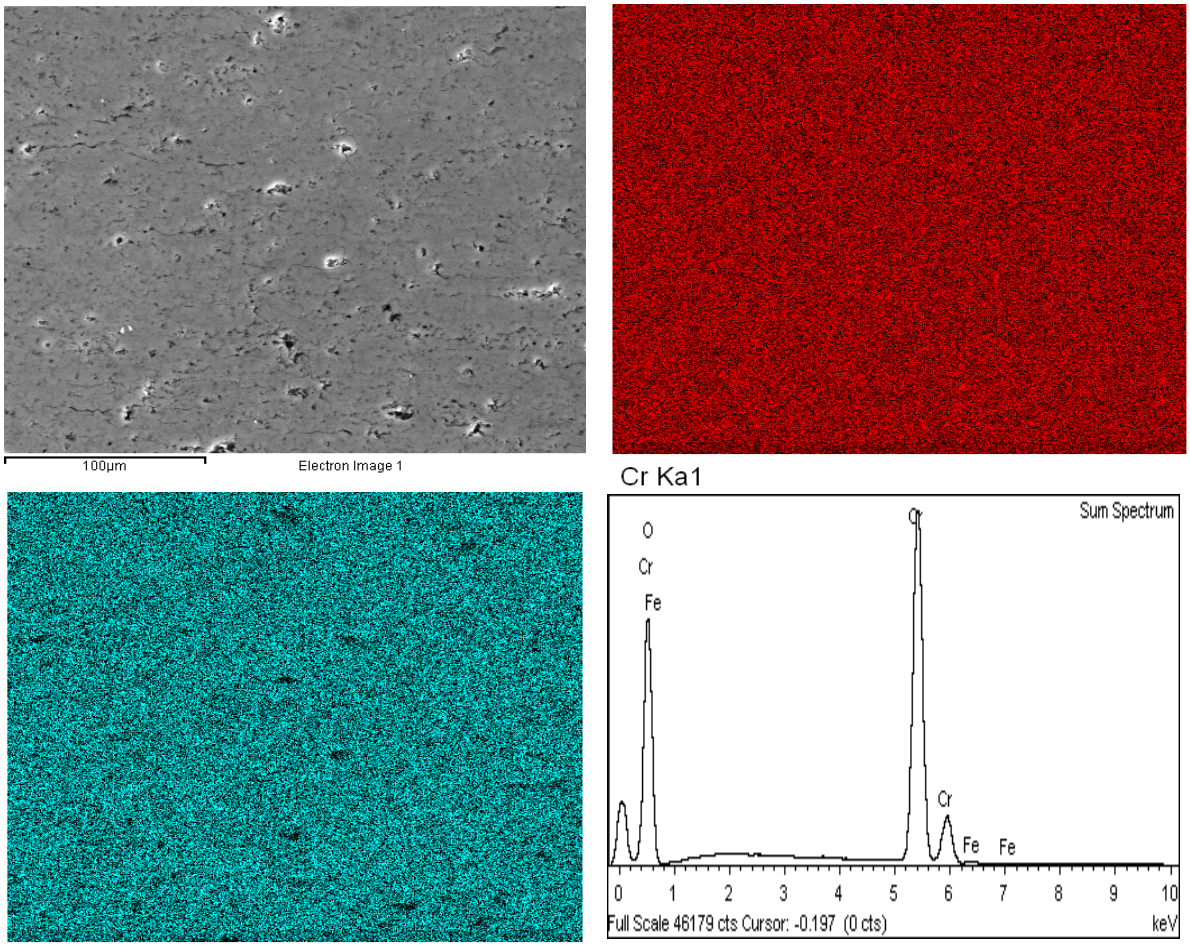

Figure 30. SE and EDS mapping images on the cross section of the Cr_2O_3 + 5%hBN (130 mm) coating together with the corresponding sum spectra on the analyzed area. Analysis was done with 20 keV and spot size 5.

Appendix 7.4

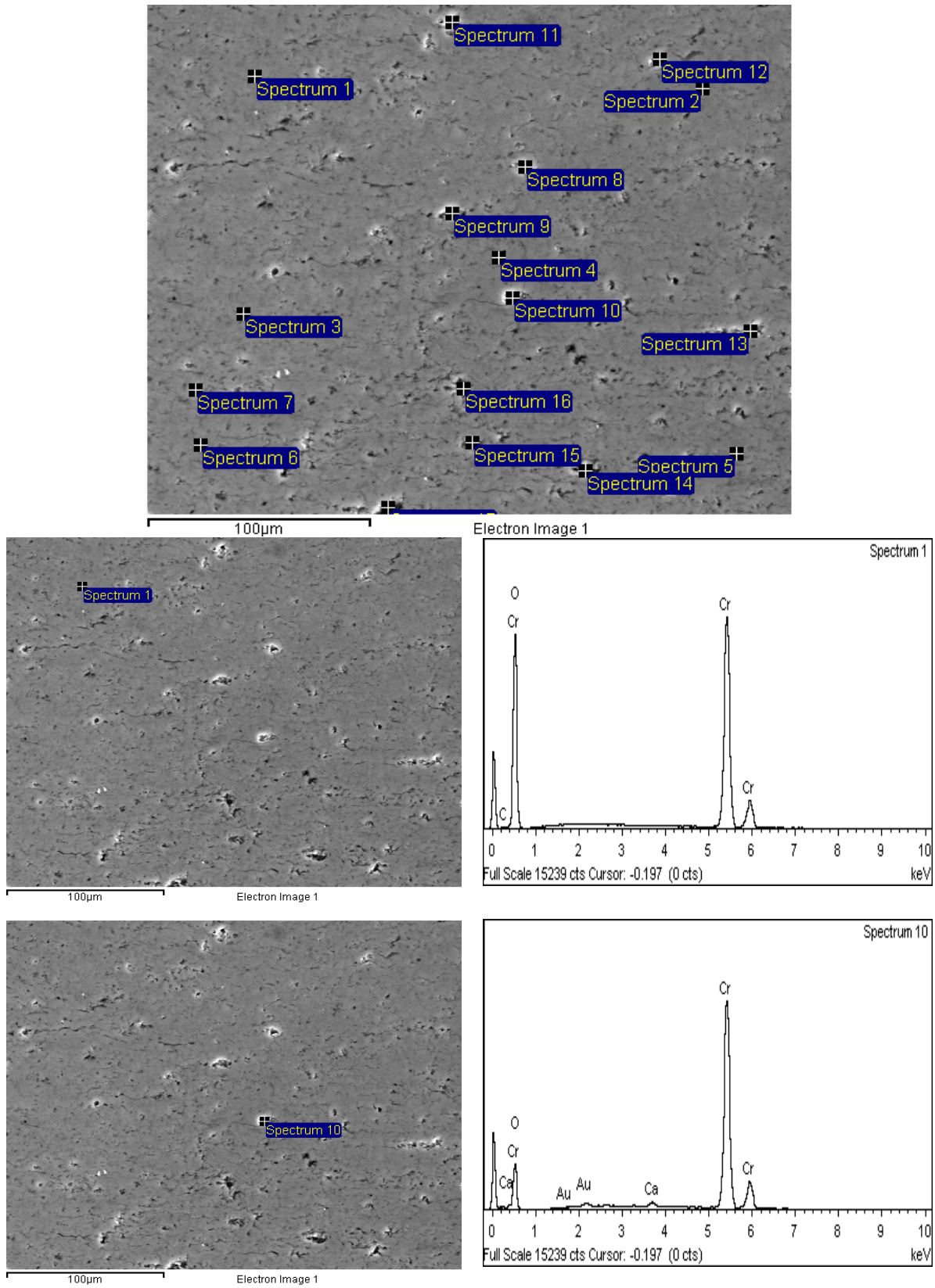

Figure 31. EDS spot analyses on the Cr_2O_3 + 5% hBN (130 mm) cross section at different locations. The analysis was done with 20 eV and spot size 5.

Table 10. List of elements and composition identified from the EDS spot analysis done on the Cr_2O_3 + 5% hBN (130 mm) cross section. All analyzed elements are normalized and are given in weight %. The position of all the spot analyzes can be seen in the EDS spot analysis image in Figure 31.

Spectrum	**C**	**O**	**Ca**	**Cr**	**Fe**	**Total**
Spectrum 1	2.03	46.73		51.24		100.00
Spectrum 2	2.22	46.24		51.54		100.00
Spectrum 3	2.58	47.59		49.83		100.00
Spectrum 4	3.14	46.40		50.46		100.00
Spectrum 5	2.65	47.42		49.65	0.28	100.00
Spectrum 6	2.01	46.82		51.17		100.00
Spectrum 7	5.14	47.88		46.98		100.00
Spectrum 8	5.24	37.29		56.99	0.48	100.00
Spectrum 9		26.28		73.28	0.45	100.00
Spectrum 10		19.85	0.78	79.37		100.00
Spectrum 11	6.88	45.56		47.10	0.46	100.00
Spectrum 12	4.92	46.61		47.99	0.48	100.00
Spectrum 13	5.48	47.16		46.98	0.38	100.00
Spectrum 14	5.46	23.28		69.92	1.34	100.00
Spectrum 15	6.85	48.31	0.55	44.29		100.00
Spectrum 16	7.60	38.15		53.51	0.74	100.00
Spectrum 17	7.75	47.30		44.15	0.80	100.00
Sum Spectrum		45.54		54.23	0.23	100.00
Max.	7.75	48.31	0.78	79.37	1.34	
Min.	2.01	19.85	0.55	44.15	0.23	

Appendix 7.5

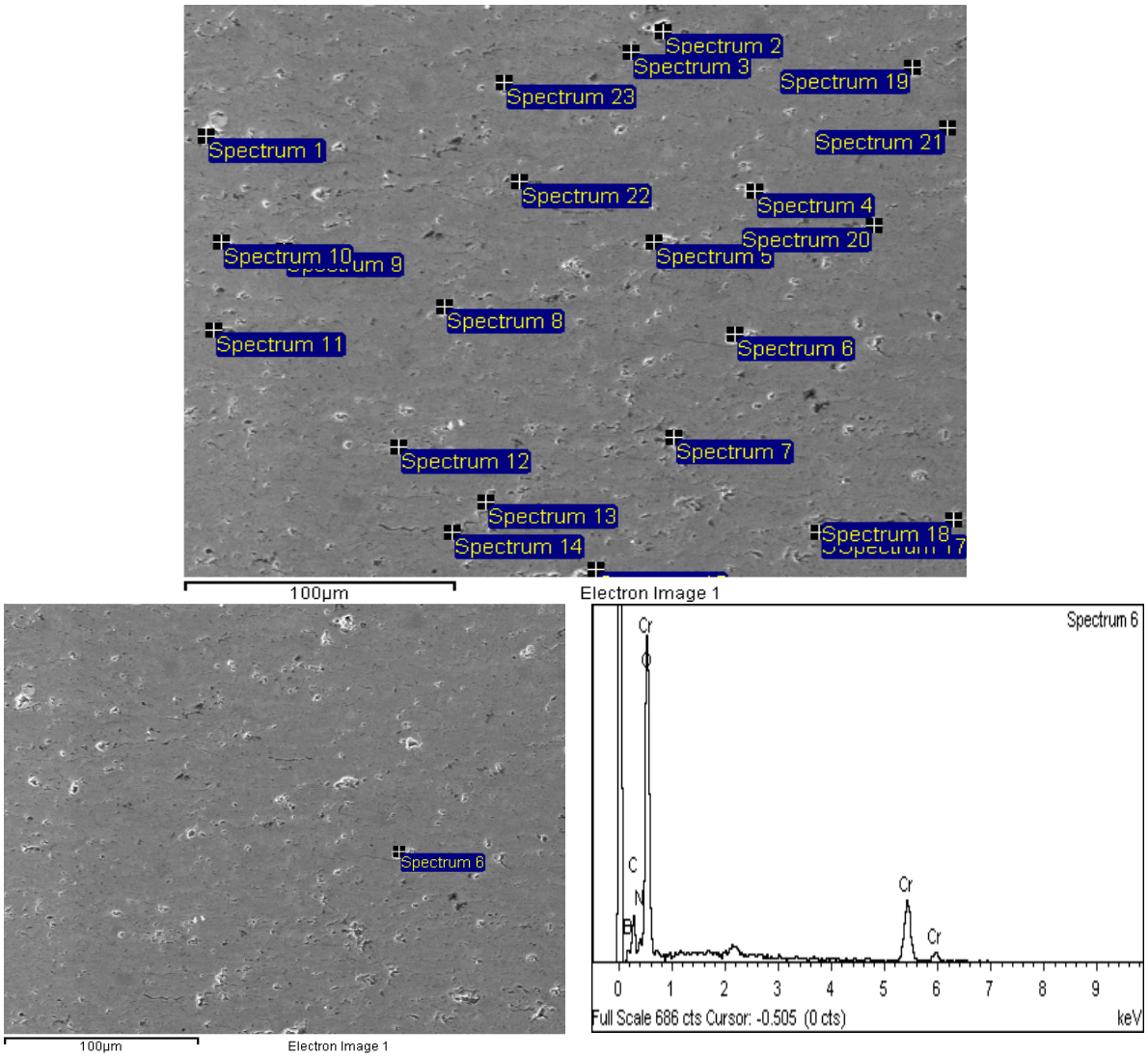

Figure 32. EDS spot analyses on the Cr_2O_3 + 5% hBN (130 mm) cross section at different locations. The analysis was done with 10 eV and spot size 4.

Table 11. List of elements and composition identified from the EDS spot analysis done on the Cr_2O_3 + 5% hBN (130 mm) cross section. All analyzed elements are normalized and are given in weight %. The position of all the spot analyzes can be seen in the EDS spot analysis image in Figure 32.

Spectrum	B	C	N	O	Cr	Fe	Total
Spectrum 1		7.19		78.87	13.94		100.00
Spectrum 2		12.73		72.09	12.46	2.72	100.00
Spectrum 3		5.94		80.29	13.77		100.00
Spectrum 4				55.73	39.40	4.87	100.00
Spectrum 5		19.13		69.20	11.67		100.00
Spectrum 6	11.99	19.34	10.02	53.77	4.87		100.00
Spectrum 7		22.53		70.02	7.45		100.00
Spectrum 8		31.01		64.14	4.30	0.55	100.00
Spectrum 9		10.36		64.50	18.27	6.87	100.00
Spectrum 10		13.39		76.13	10.48		100.00
Spectrum 11		21.89		68.13	9.98		100.00
Spectrum 12		8.56		78.69	12.75		100.00
Spectrum 13		9.97		74.20	15.83		100.00

Spectrum 14		11.94		75.61	12.45		100.00
Spectrum 15		22.79		68.45	6.13	2.63	100.00
Spectrum 16		20.13		68.98	10.89		100.00
Spectrum 17		31.36		57.83	8.55	2.25	100.00
Spectrum 18		16.73		69.32	13.95		100.00
Spectrum 19		12.57		75.98	11.46		100.00
Spectrum 20		16.92		72.80	10.28		100.00
Spectrum 21		15.23		75.89	8.89		100.00
Spectrum 22		15.59		69.68	14.73		100.00
Spectrum 23		6.10		80.46	13.44		100.00
Max.	11.99	31.36	10.02	80.46	39.40	6.87	
Min.	11.99	5.94	10.02	53.77	4.30	0.55	

Appendix 8.1

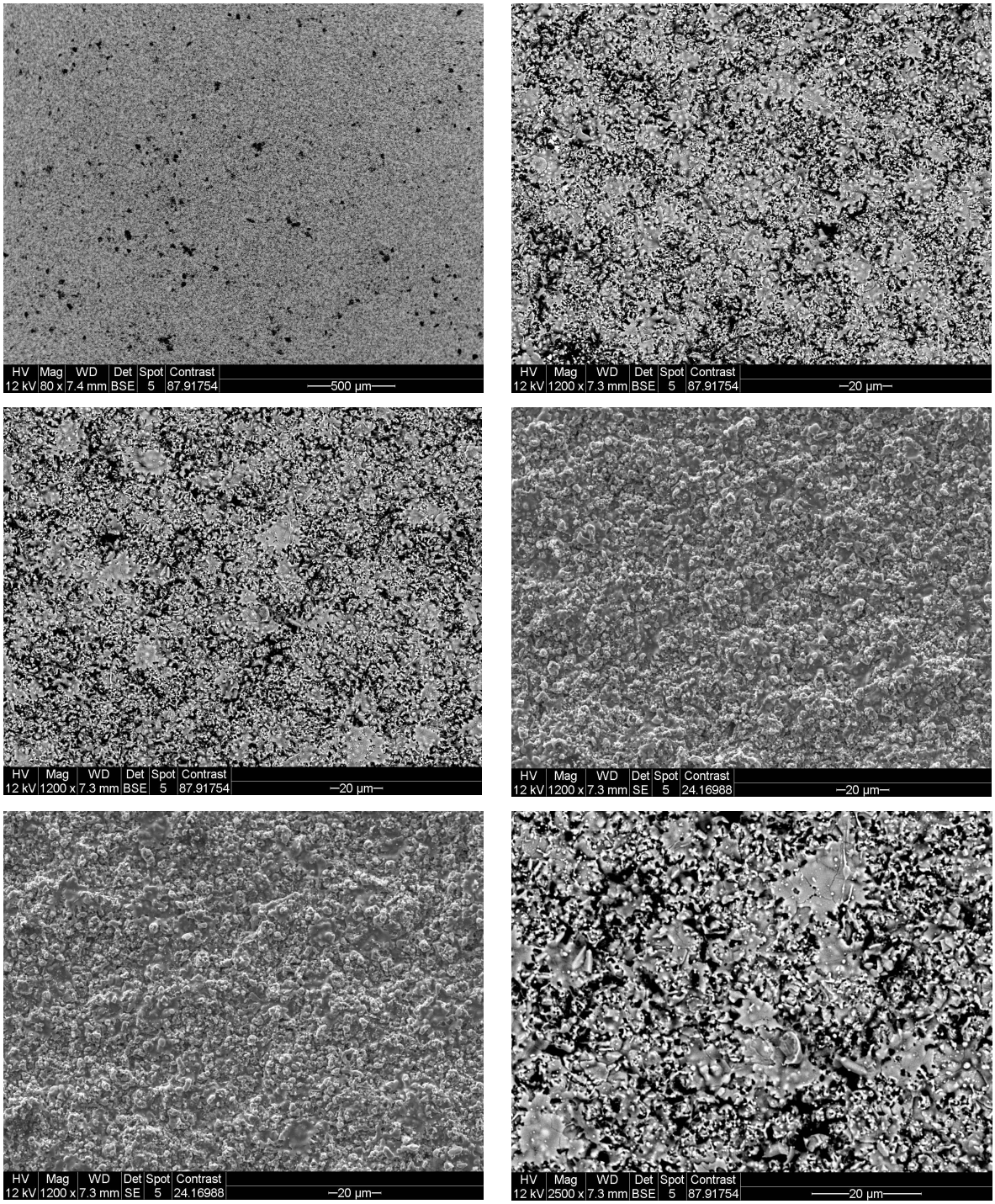

Figure 33. SEM topography images at different magnification and positions on Cr_2O_3 + 10% hBN sprayed at a 130 mm spray distance.

Appendix 8.2

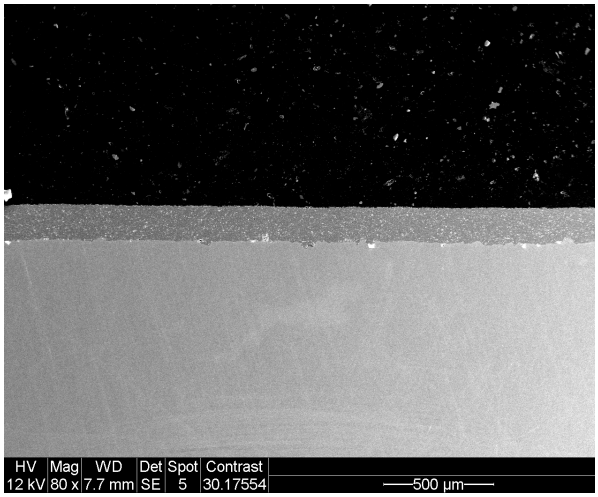
HV Mag WD Det Spot Contrast
12 kV 80 x 7.7 mm SE 5 30.17554
500 µm

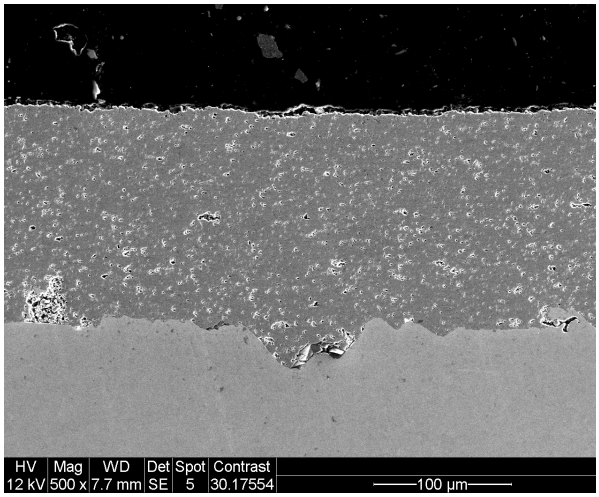
HV Mag WD Det Spot Contrast
12 kV 500 x 7.7 mm SE 5 30.17554
100 µm

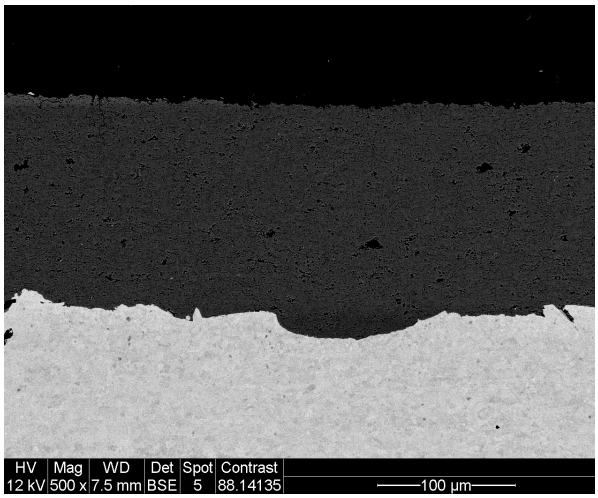
HV Mag WD Det Spot Contrast
12 kV 500 x 7.5 mm BSE 5 88.14135
100 µm

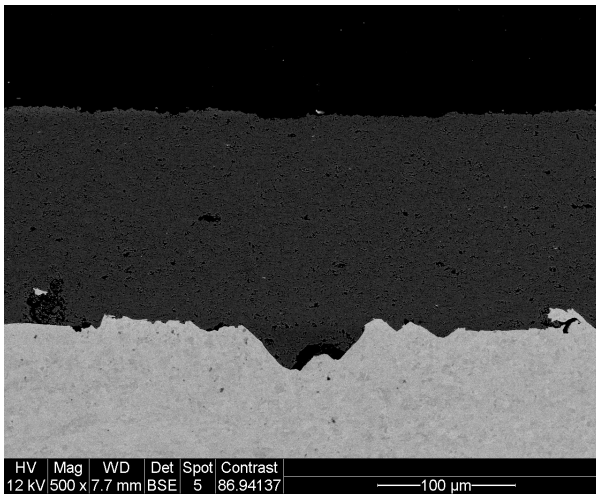
HV Mag WD Det Spot Contrast
12 kV 500 x 7.7 mm BSE 5 86.94137
100 µm

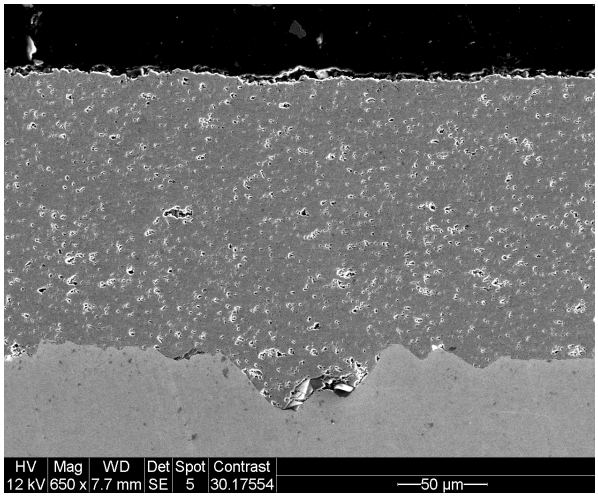
HV Mag WD Det Spot Contrast
12 kV 650 x 7.7 mm SE 5 30.17554
50 µm

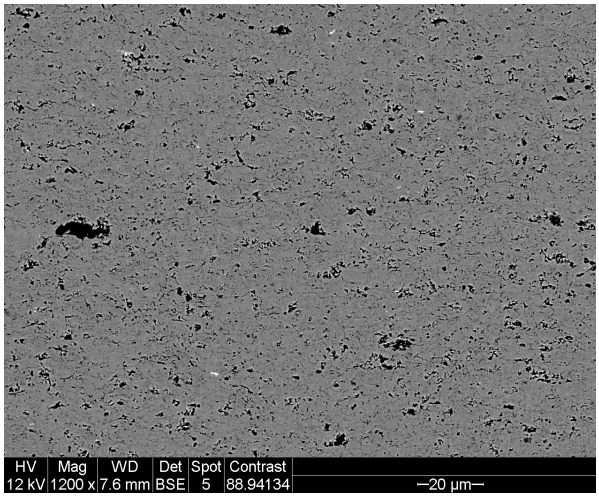
HV Mag WD Det Spot Contrast
12 kV 1200 x 7.6 mm BSE 5 88.94134
20 µm

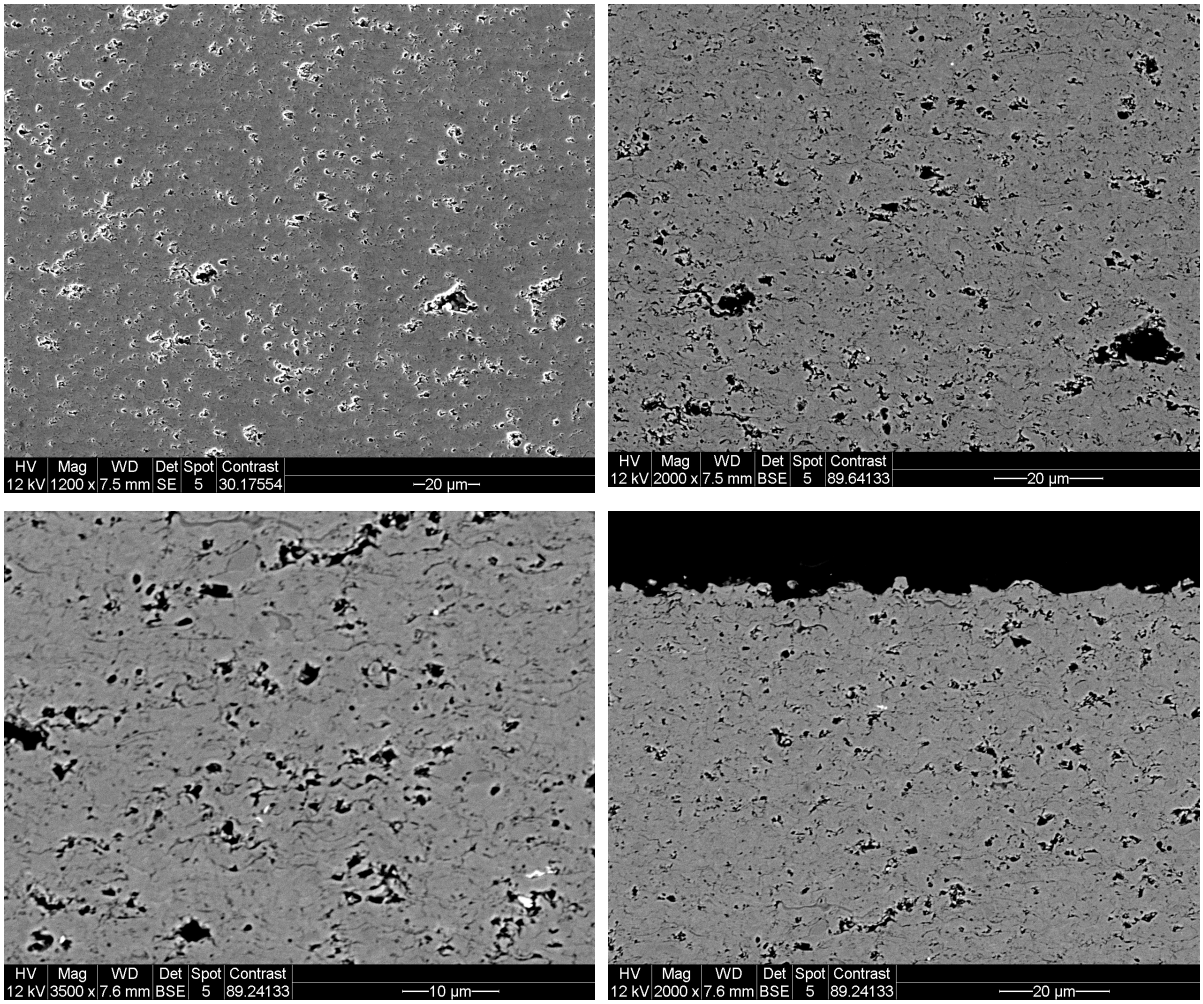

Figure 34. SEM cross section images at different magnification and positions on Cr_2O_3 + 10% hBN sprayed at a 130 mm spray distance.

Appendix 8.3

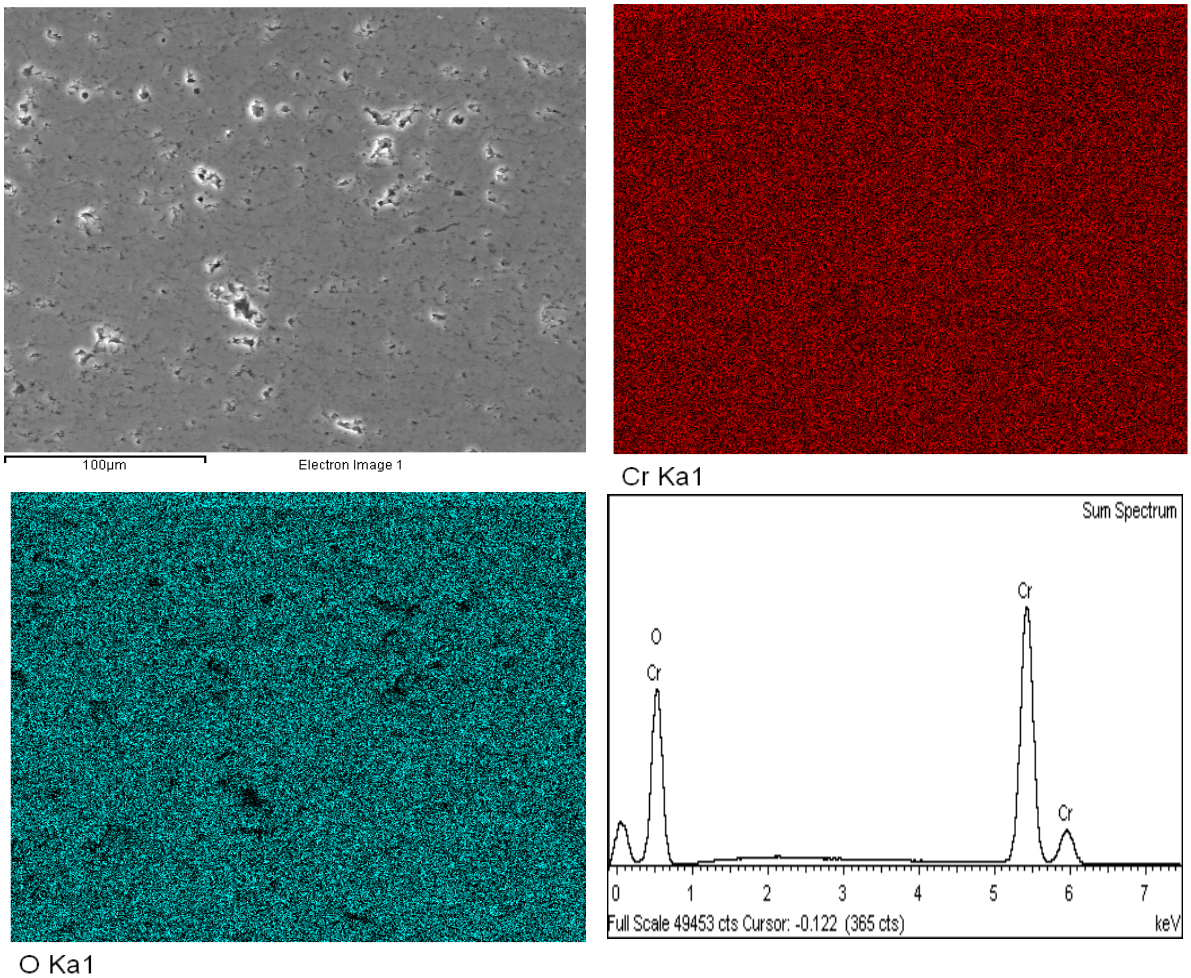

Figure 35. SE and EDS mapping images on the cross section of the Cr_2O_3 + 10%hBN (130 mm) coating together with the corresponding sum spectra on the analyzed area. Analysis was done with 20 keV and spot size 5.

Appendix 8.4

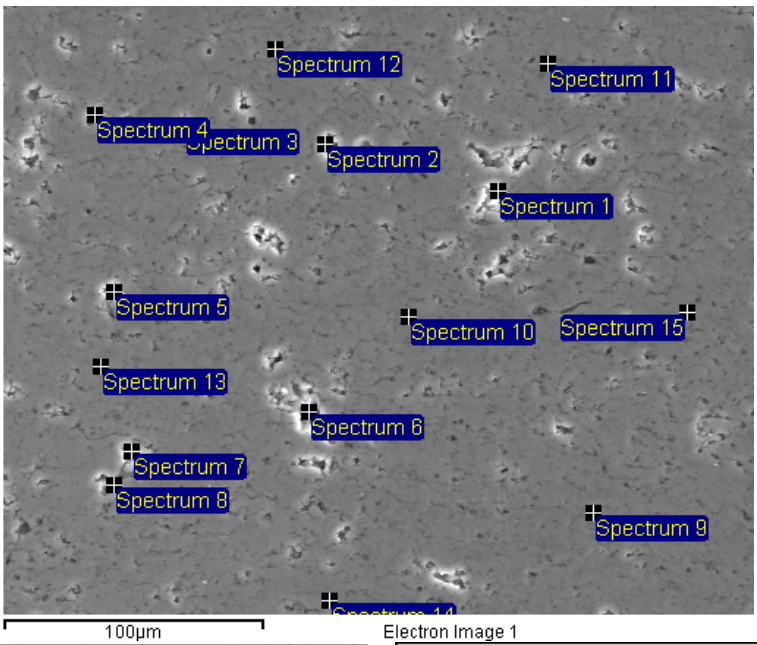
Spectrum 12
Spectrum 11
Spectrum 4
Spectrum 3
Spectrum 2
Spectrum 1
Spectrum 5
Spectrum 10
Spectrum 15
Spectrum 13
Spectrum 6
Spectrum 7
Spectrum 8
Spectrum 9
100µm
Electron Image 1

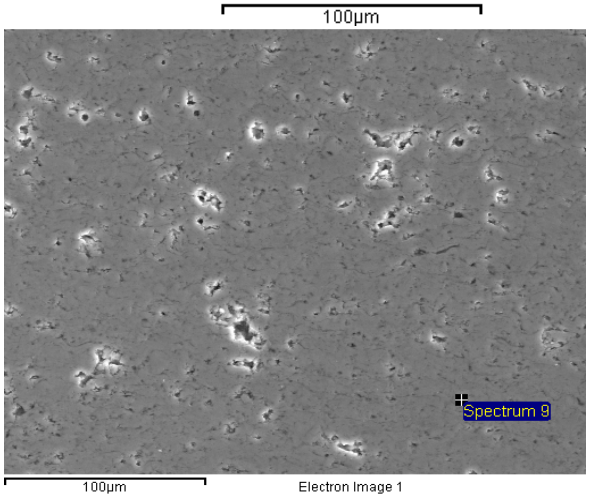
Spectrum 9
100µm
Electron Image 1

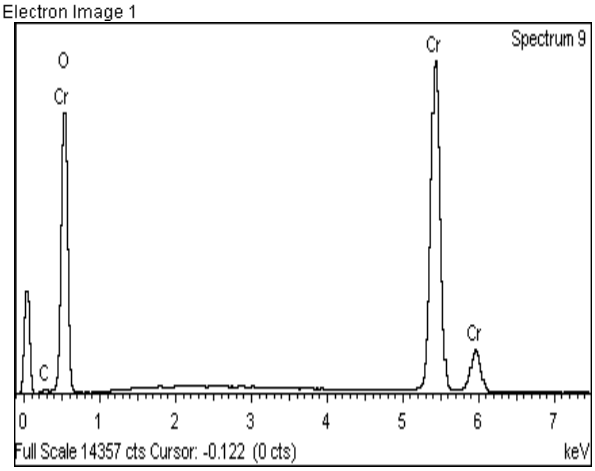
Spectrum 9
O
Cr
Cr
C
Cr
0
1
2
3
4
5
6
7
Full Scale 14357 cts Cursor: -0.122 (0 cts)
keV

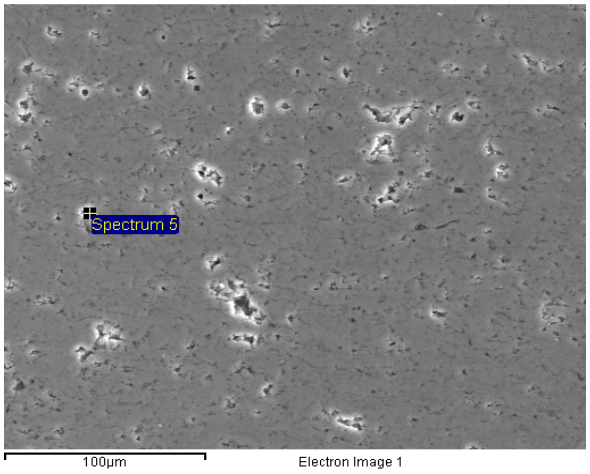
Spectrum 5
100µm
Electron Image 1

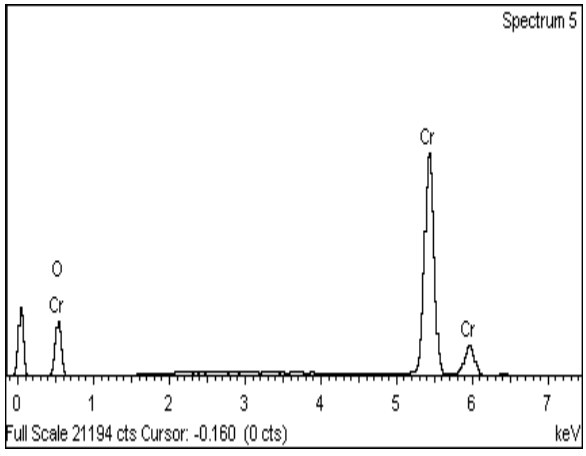
Spectrum 5
Cr
O
Cr
Cr
0
1
2
3
4
5
6
7
Full Scale 21194 cts Cursor: -0.160 (0 cts)
keV

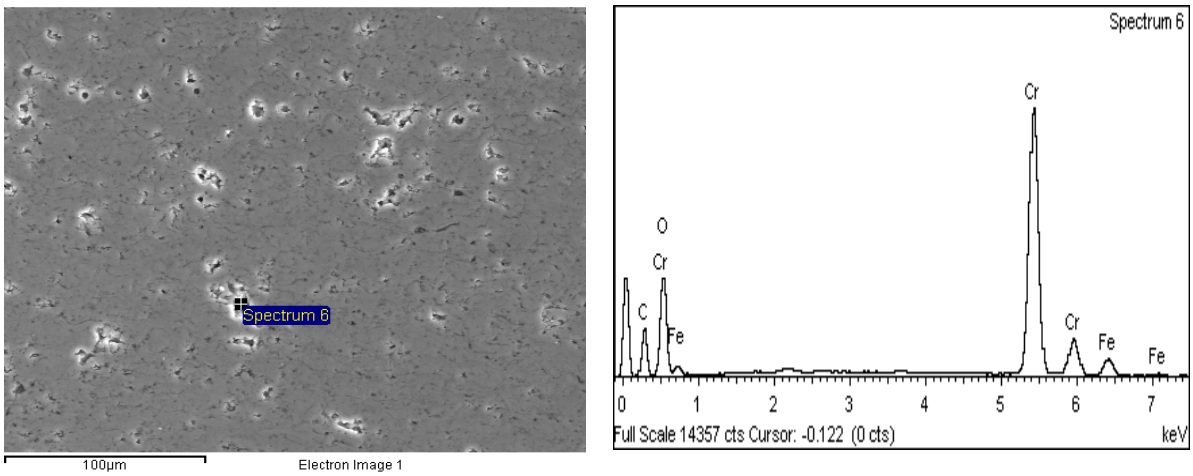

Figure 36. EDS spot analyses on the Cr_2O_3 + 10% hBN (130 mm) cross section at different locations. The analysis was done with 20 eV and spot size 5.

Table 12. List of elements and composition identified from the EDS spot analysis done on the Cr_2O_3 + 10% hBN (130 mm) cross section. All analyzed elements are normalized and are given in weight %. The position of all the spot analyzes can be seen in the EDS spot analysis image in Figure 36.

Spectrum	**C**	**O**	**Cr**	**Fe**	**Total**
Spectrum 1	5.03	41.74	53.24		100.00
Spectrum 2	5.26	44.85	49.88		100.00
Spectrum 3	13.45	20.64	64.79	1.13	100.00
Spectrum 4	3.44	36.79	59.77		100.00
Spectrum 5		21.34	78.66		100.00
Spectrum 6	28.34	29.31	38.76	3.59	100.00
Spectrum 7	6.28	40.15	53.14	0.43	100.00
Spectrum 8	2.90	20.27	75.68	1.15	100.00
Spectrum 9	2.70	44.85	52.45		100.00
Spectrum 10	2.34	46.66	51.00		100.00
Spectrum 11	2.59	46.57	50.84		100.00
Spectrum 12	2.10	46.89	51.01		100.00
Spectrum 13	2.10	46.95	50.95		100.00
Spectrum 14	1.98	47.25	50.77		100.00
Spectrum 15	2.51	46.29	51.20		100.00
Sum Spectrum		45.14	54.86		100.00
Max.	28.34	47.25	78.66	3.59	
Min.	1.98	20.27	38.76	0.43	

Appendix 8.5

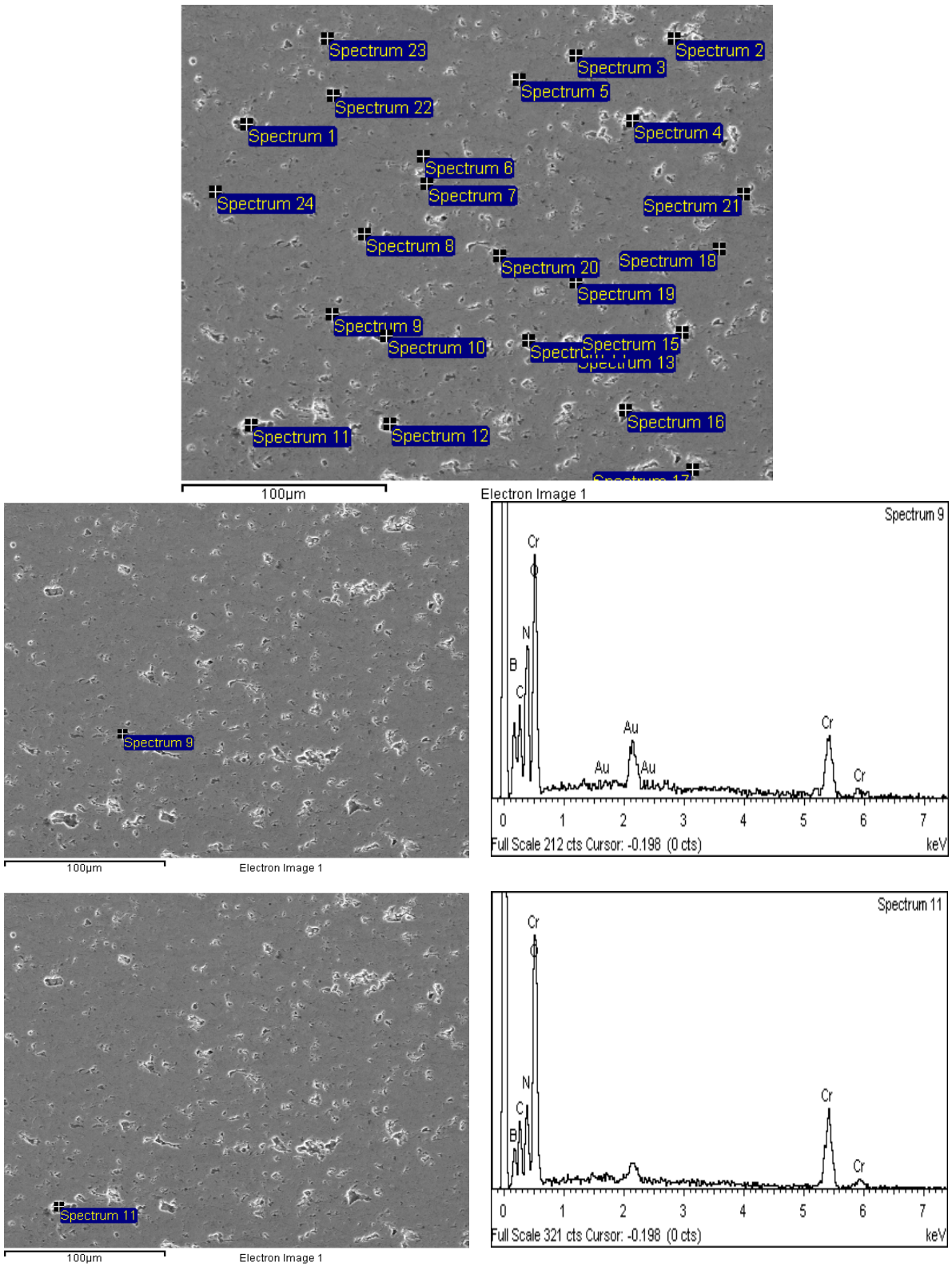

Figure 37. EDS spot analyses on the Cr_2O_3 + 10% hBN (130 mm) cross section at different locations. The analysis was done with 10 eV and spot size 4.

Table 13. List of elements and composition identified from the EDS spot analysis done on the Cr_2O_3 + 10% hBN (130 mm) cross section. All analyzed elements are normalized and are given in weight %. The position of all the spot analyzes can be seen in the EDS spot analysis image in Figure 37.

Spectrum	**B**	**C**	**N**	**O**	**Cr**	**Total**
Spectrum 1		23.09		45.31	31.60	100.00
Spectrum 2		10.42		66.03	23.55	100.00
Spectrum 3		13.84		67.89	18.27	100.00
Spectrum 4		6.77		80.58	12.65	100.00
Spectrum 5		17.03		70.43	12.54	100.00
Spectrum 6		12.97		66.42	20.61	100.00
Spectrum 7		7.79		75.53	16.69	100.00
Spectrum 8		25.04		65.84	9.12	100.00
Spectrum 9	20.73	16.58	33.73	27.30	1.65	100.00
Spectrum 10		6.39		80.24	13.37	100.00
Spectrum 11	18.89	17.50	25.28	35.59	2.73	100.00
Spectrum 12		19.23		69.52	11.26	100.00
Spectrum 13		14.06		74.57	11.37	100.00
Spectrum 14		12.77		76.95	10.28	100.00
Spectrum 15				83.40	16.60	100.00
Spectrum 16		16.56		74.49	8.94	100.00
Spectrum 17		14.16		75.35	10.49	100.00
Spectrum 18				83.45	16.55	100.00
Spectrum 19				83.07	16.93	100.00
Spectrum 20				82.00	18.00	100.00
Spectrum 21				82.75	17.25	100.00
Spectrum 22				83.58	16.42	100.00
Spectrum 23		9.24		77.06	13.70	100.00
Spectrum 24				82.41	17.59	100.00
Max.	20.73	25.04	33.73	83.58	31.60	
Min.	18.89	6.39	25.28	27.30	1.65	